

**EVALUATION OF RC WALL AND FRAME SYSTEMS UNDER BEYOND
DESIGN ACCELERATIONS INCLUDING AGING EFFECTS**

by

Adrián Argente del Castillo Garrido

Thesis submitted in partial fulfillment
of the requirements for the degree of

MASTER OF SCIENCE
in
CIVIL ENGINEERING

UNIVERSITY OF PUERTO RICO
MAYAGÜEZ CAMPUS
2018

Approved by:

Luis E. Suárez, Ph.D.
Member, Graduate Committee

Date

Luis A. Montejo-Valencia, Ph.D.
Member, Graduate Committee

Date

Ricardo R. López-Rodríguez, Ph.D.
Member, Graduate Committee

Date

Aidcer L. Vidot-Vega, Ph.D.
President, Graduate Committee

Date

Ismael Pagán-Trinidad, M.S.C.E.
Chairperson of the Department

Date

Sylvia Rodríguez Abudo, Ph.D.
Graduate School Representative

Date

Abstract

Nuclear power plants and other civil structures in the world have recently experienced strong ground motions exceeding the original design values. The evaluation of the capacity of structural systems in a nuclear power plant and other civil structures under beyond design accelerations is important to address the level of seismic damage that they can safely manage. This thesis evaluates the impact of beyond design earthquake accelerations in the response of typical RC buildings with and without considering aging effects of the reinforcing steel. Typical RC buildings are composed of frames and walls that are designed to resist the lateral loads during a seismic event. Nonlinear dynamic analyses of RC dual wall-frame systems are performed under the effects of beyond design seismic accelerations using OpenSees. Walls are modeled using the cyclic shear-flexure interaction model and the reinforced concrete elements in the frame are modeled using the beam with hinges element and constitutive relationships for concrete and reinforcing steel available in OpenSees. Dynamic analyses of the RC wall-frame dual system with and without aging effects are performed under different earthquake scenarios. Displacement capacities, shear strengths, displacement limit states are evaluated for different earthquake magnitudes. It was found that the stiffness of the structure degrades more significantly as the design condition is exceeded. The initial stiffness of the system has the most pronounced change as the moment magnitude increases. Moreover, the degradation in peak shear capacity follows a constant pattern and does not precisely depend on the exceedance of the design condition. Finally, the model including the reduction in steel due to aging presents higher deformations, less stiffness and more nonlinearity, affecting more the shear strengths at limit states.

Resumen

Las plantas nucleares y otras estructuras civiles en el mundo han experimentado aceleraciones sísmicas excediendo los valores de diseño originales. La evaluación de la capacidad de los componentes estructurales en los edificios que componen una planta nuclear u otras estructuras bajo aceleraciones que exceden la de diseño es importante para poder tener un panorama completo del nivel de daño que estas pueden manejar seguramente después del rango lineal. Esta tesis evalúa el impacto de las aceleraciones que exceden la de diseño en la respuesta de edificios típicos de hormigón reforzado con y sin considerar los efectos de deterioro en el acero de refuerzo. Edificios típicos de hormigón reforzado están compuestos de pórticos y paredes que son diseñadas para resistir las cargas laterales durante un evento sísmico. Análisis dinámicos non-lineares de sistemas pórtico-pared de hormigón reforzado se realizan usando OpenSees. Las paredes se modelan usando un modelo que acopla la interacción entre cortante y flexión y los elementos del pórtico son modelados usando un elemento en el cual se agrupa la plasticidad en los extremos de este. Relaciones constitutivas para el hormigón y acero se utilizan para modelar de las disponibles en OpenSees. Los análisis dinámicos del sistema dual de pared-pórtico de hormigón reforzado con y sin considerar los efectos de deterioro del acero se realizan bajo distintos escenarios de sismos. Se encontró que la rigidez de la estructura se degrada más significativamente cuando la condición de diseño ha sido excedida. La rigidez inicial presenta un cambio más pronunciado según la magnitud de momento del sismo aumenta. Además, la degradación en la capacidad a cortante pico sigue un patrón constante y no depende precisamente de cuando se excede la condición de diseño. Finalmente, el modelo incluyendo la reducción en acero debido al deterioro presenta mayores deformaciones, una rigidez menor y mayor no-linealidad, afectando más los cortantes en un límite de daño en particular.

TABLE OF CONTENTS

Chapter 1. Introduction.....	1
1.1 Research Significance and Motivation	1
1.2 Research Objectives and Scope.....	2
1.3 Literature review	3
1.3.1 Seismic concern -events that exceeded design accelerations	3
1.3.1.1 Nuclear Power Plants (NPPs).....	3
1.3.1.2 Civil Structures.....	5
1.3.2 Structural aging	8
1.3.2.1. <i>Higgins and Farrow III, 2006</i>	10
1.3.2.2. <i>Bourahla et al., 2008</i>	10
1.3.2.3. <i>Ghosh et al. 2010</i>	11
1.3.2.4. Hanjari et al., 2011	13
1.3.2.5. Mohammed et al., 2011.....	14
1.4 Research Methodology	16
1.5 Organization of Thesis.....	18
Chapter 2. Modeling and Methodology.....	19
2.1 Introduction.....	19
2.2 RC frame and wall models.....	19
2.2.1 SMART project 2008.....	29
2.2.2 RC Frame structure.....	30
2.2.3 RC frame -wall dual system	31
2.3 Materials	34
2.3.1 Frame sections	35
2.3.2 Wall sections	37
2.4 Element Modeling	40
2.5 Model analysis.....	41
Chapter 3. Evaluation of beyond design seismic accelerations	43
Dynamic analyses	43
3.1 Analysis Parameters	48
3.2 Stiffness Degradation	49
3.3 Strength Degradation.....	51
3.4 Displacement/strain limit states	53
3.5 Summary of Results.....	59

Chapter 4. Evaluation of beyond design seismic accelerations considering aging effects	61
4.1 Aging effects considerations	61
4.2 Analysis Parameters	63
4.3 Stiffness Degradation	64
4.4 Strength Degradation	66
4.5 Displacement/strain limit states	68
4.6 Summary of Results.....	72
4.7 Comparison of Results.....	73
Chapter 5. Conclusions.....	82
5.1 Summary	82
5.2 Conclusions.....	82
5.3 Recommendations for future works	84
6. References.....	85
Appendix 1 (OpenSees code)	92
Appendix 2 (Pushover results)	118

LIST OF TABLES

TABLE 1. 1 DESCRIPTORS OF LOGNORMAL RANDOM VARIABLES AFFECTING THE CORROSION DETERIORATION. (GHOSH ET AL. 2010)	12
TABLE 2. 1 FRAME PARAMETERS FOR CONCRETE AND STEEL REINFORCEMENT	37
TABLE 2. 2 WALL PARAMETERS FOR CONCRETE AND STEEL REINFORCEMENT	39
TABLE 3. 1 SEED EARTHQUAKE RECORDS SELECTED FOR THE ANALYSIS.	45
TABLE 3. 2 CASES COMPLETED AFTER APPLYING SEISMIC LOAD AND PUSHOVER ANALYSIS (MAXIMUM DRIFT).....	48
TABLE 3. 3 STIFFNESS FOR PUSHOVER ANALYSES AFTER DYNAMIC ANALYSES FOR DIFFERENT SEISMIC MAGNITUDES.....	50
TABLE 3. 4 STIFFNESS RATIO FOR PUSHOVER ANALYSES AFTER DYNAMIC ANALYSES FOR DIFFERENT SEISMIC MAGNITUDES	50
TABLE 3. 5 STRENGTH FOR PUSHOVER ANALYSES AFTER DYNAMIC ANALYSES FOR DIFFERENT SEISMIC MAGNITUDES.....	53
TABLE 3. 6 STRENGTH RATIO FOR PUSHOVER ANALYSES AFTER DYNAMIC ANALYSES FOR DIFFERENT SEISMIC MAGNITUDES	53
TABLE 3. 7 SEQUENCE OF STRAIN LIMITS IN THE PUSHOVER ANALYSIS BEFORE SEISMIC LOADS.....	58
TABLE 3. 8 STRAIN LIMITS FOR PUSHOVER ANALYSES AFTER DYNAMIC ANALYSES FOR DIFFERENT SEISMIC MAGNITUDES.....	58
TABLE 3. 9 STRAIN RATIO FOR PUSHOVER ANALYSES AFTER DYNAMIC ANALYSES FOR DIFFERENT SEISMIC MAGNITUDES.....	58
TABLE 4. 1 CASES COMPLETED AFTER APPLYING SEISMIC LOAD AND PUSHOVER ANALYSIS (MAXIMUM DRIFT).....	64
TABLE 4. 2 STIFFNESS FOR PUSHOVER ANALYSES AFTER DYNAMIC ANALYSES FOR DIFFERENT SEISMIC MAGNITUDES.....	65
TABLE 4. 3 STIFFNESS RATIO FOR PUSHOVER ANALYSES AFTER DYNAMIC ANALYSES FOR DIFFERENT SEISMIC MAGNITUDES.....	65
TABLE 4. 4 STRENGTH FOR PUSHOVER ANALYSES AFTER DYNAMIC ANALYSES FOR DIFFERENT SEISMIC MAGNITUDES.....	67
TABLE 4. 5 STRENGTH RATIO FOR PUSHOVER ANALYSES AFTER DYNAMIC ANALYSES FOR DIFFERENT SEISMIC MAGNITUDES	67
TABLE 4. 6 SEQUENCE OF STRAIN LIMITS IN THE PUSHOVER ANALYSIS BEFORE SEISMIC LOADS.....	70
TABLE 4. 7 STRAIN LIMITS FOR PUSHOVER ANALYSES AFTER DYNAMIC ANALYSES FOR DIFFERENT SEISMIC MAGNITUDES	71
TABLE 4. 8 STRAIN RATIO FOR PUSHOVER ANALYSES AFTER DYNAMIC ANALYSES FOR DIFFERENT SEISMIC MAGNITUDES	71

LIST OF FIGURES

FIGURE 1. 1 LOCATION OF 2011 MINERAL, VA EARTHQUAKE AND THE NORTH ANNA NUCLEAR POWER PLANT. (LI AND MANOLY, 2012)	4
FIGURE 1. 2 LEFT: INCLINED CRACK ON THE INTERIOR WALL. RIGHT: HORIZONTAL CRACKS DEVELOPED FROM CONSTRUCTION JOINTS BETWEEN LIFTS (LI AND MANOLY, 2012).....	5
FIGURE 1. 3 MAP OF SOUTH ICELAND SHOWING THE EVENTS OCCURRED.(BESSASON AND BJARNASON 2016)	6
FIGURE 1. 4 TYPICAL CHILEAN “FISH-BONE” PLAN BUILDING.(JÜNEMANN ET AL. 2015)	8
FIGURE 1. 5 DISTRIBUTION OF NORMALIZED TIME-VARIANT AREA OF THE COLUMN REINFORCEMENT. (GHOSH ET AL. 2010)	13
FIGURE 1. 6 CORROSION MODEL (A) PIT CONFIGURATION AND (B) UNIFORM CORROSION.(FROM MOHAMMED ET AL., 2011).....	15
FIGURE 2. 1 RC FRAME SPECIMEN (BECHTOULA ET. AL 2006)	20
FIGURE 2. 2 DISTRIBUTION OF THE ELEMENTS OF THE STRUCTURE.....	21
FIGURE 2. 3 BEAM WITH HINGES ELEMENT (SCOTT AND FENVES, 2006)	21
FIGURE 2. 4 CONCRETE 01 AND REINFORCING STEEL CONSTITUTIVE RELATIONSHIP FOR FRAME ELEMENTS	22
FIGURE 2. 5 SHEAR VS DRIFT RC FRAME SPECIMEN	22
FIGURE 2. 6 MODEL DISCRETIZATION: A) PLAN VIEW, B) CROSS-SECTION (KOLOZVARI ET. AL., 2014).....	23
FIGURE 2. 7 IMPLEMENTATION OF RC PANEL BEHAVIOR INTO MVLEM: (A) ORIGINAL MVLEM; (B) RC PANEL ELEMENT; AND (C) SFI-MVLEM.	24
FIGURE 2. 8 FSAM FOR CONVERTING IN-PLANE STRAINS TO IN-PLANE SMEARED STRESSES ON A RC PANEL ELEMENT (TOP). DOWEL ACTION OF REINFORCEMENT (BOTTOM). ((KOLOZVARI, ET. AL 2015)	25
FIGURE 2. 9 A) SFI_MVLEM ELEMENT, B) RC PANEL ELEMENT (NDMATERIAL FSAM) (SFI-MVLEM, KOLOZVARI ET AL., 2015).....	26
FIGURE 2. 10 ELEMENT DEFORMATIONS OF THE MVLEM ELEMENT (VULCANO ET AL. 1988).....	27
FIGURE 2. 11 WALL RESPONSES: A) LOAD VERSUS TOP DISPLACEMENT BEHAVIOR	28
FIGURE 2. 12 STRESS-STRAIN BEHAVIOR FOR VERTICAL (Y) STEEL.....	28
FIGURE 2. 13 STRESS-STRAIN BEHAVIOR FOR CONCRETE STRUT 1 MODEL.....	29
FIGURE 2. 14 PLAN VIEW AND ELEVATION OF THE SMART2008 SPECIMEN (LERMITTE, CHAUDAT, AND PAYEN 2008)	30
FIGURE 2. 15 FRAME GEOMETRY	31
FIGURE 2. 16 DESIGN SPECTRUM	31
FIGURE 2. 17 GEOMETRY AND DIMENSIONS OF THE RC WALL AND FRAME SYSTEM	32
FIGURE 2. 18 WALL REINFORCEMENT DETAILS.....	33
FIGURE 2. 19 NODAL DISTRIBUTION AND SAP2000 MODAL ANALYSIS.	34
FIGURE 2. 20 CONCRETE 01 CONSTITUTIVE RELATIONSHIP (OPENSEES 2014).....	35
FIGURE 2. 21 REINFORCING STEEL CONSTITUTIVE RELATIONSHIP FOR FRAME ELEMENTS (CHANG AND MANDER 1994)	36
FIGURE 2. 22 HYSTERETIC CONSTITUTIVE MODEL FOR CONCRETE BY CHANG AND MANDER (1994) AND COMPRESSION AND TENSION ENVELOPE CURVES	38
FIGURE 2. 23 CONSTITUTIVE MODEL FOR STEEL (MENEGOTTO AND PINTO, 1973)	39
FIGURE 2. 24 FRAME NODAL DISTRIBUTION	40
FIGURE 2. 25 PUSHOVER ANALYSIS FOR EACH MODEL: FRAME, WALL AND DUAL SYSTEM.	41
FIGURE 2. 26 CYCLIC ANALYSIS FOR EACH MODEL: FRAME, WALL AND DUAL SYSTEM	42
FIGURE 3. 1 TARGET AND DESIGN SPECTRA.....	44
FIGURE 3. 2 EARTHQUAKE SEEDS FOR THE ANALYSIS	46
FIGURE 3. 3 MAXIMUM DISPLACEMENT FOR DYNAMIC ANALYSIS (IN MM).	47
FIGURE 3. 4 RESIDUAL DISPLACEMENT FROM DYNAMIC ANALYSIS (IN MM).....	47

FIGURE 3. 5 STIFFNESS RATIO AS FUNCTION OF THE SEISMIC MOMENT MAGNITUDE.....	51
FIGURE 3. 6 PUSHOVER CURVES BEFORE AND AFTER SEISMIC LOAD.....	53
FIGURE 3. 7 PUSHOVER STATE LIMITS ANALYSIS FOR THE FRAME SPECIMEN.....	55
FIGURE 3. 8 PUSHOVER STATE LIMITS ANALYSIS FOR THE WALL SPECIMEN.....	56
FIGURE 3. 9 PUSHOVER STATE LIMITS ANALYSIS FOR THE DS SPECIMEN.....	56
FIGURE 3. 10 STRAIN RATIO AS FUNCTION OF THE SEISMIC MOMENT MAGNITUDE	59
FIGURE 4. 1 PUSHOVER BEFORE AND AFTER APPLYING AGING EFFECTS.	62
FIGURE 4. 2 STIFFNESS RATIO AS FUNCTION OF THE SEISMIC MOMENT MAGNITUDE.....	66
FIGURE 4. 3 PUSHOVER CURVES BEFORE AND AFTER SEISMIC LOAD.....	67
FIGURE 4. 4 PUSHOVER STATE LIMITS ANALYSIS FOR THE FRAME	69
FIGURE 4. 5 PUSHOVER STATE LIMITS ANALYSIS FOR THE WALL SPECIMEN	69
FIGURE 4. 6 PUSHOVER STATE LIMITS ANALYSIS FOR THE DUAL SYSTEM.	70
FIGURE 4. 7 STRAIN RATIO AS FUNCTION OF THE SEISMIC MOMENT MAGNITUDE	72
FIGURE 4. 8 PUSHOVER BEFORE AND AFTER APPLYING AGING EFFECTS.	74
FIGURE 4. 9 DESIGN SPECTRUM	74
FIGURE 4. 10 COMPARISON OF THE INITIAL STIFFNESS DEGRADATION	76
FIGURE 4. 11 COMPARISON OF THE STIFFNESS DEGRADATION AT 60%VU MAXIMUM.....	76
FIGURE 4. 12 COMPARISON OF THE STIFFNESS DEGRADATION AT VU MAXIMUM	77
FIGURE 4. 13 COMPARISON OF THE CHANGES IN STIFFNESS DEGRADATION WITH (LEFT) AND WITHOUT (RIGHT) AGING EFFECTS.....	77
FIGURE 4. 14 CHANGE OF CAPACITY	78
FIGURE 4. 15 COMPARISON OF THE YIELDING STRAIN RATIO AS FUNCTION OF THE SEISMIC MOMENT MAGNITUDE.....	80
FIGURE 4. 16 COMPARISON OF THE SERVICEABILITY STRAIN RATIO AS FUNCTION OF THE SEISMIC MOMENT MAGNITUDE.....	80
FIGURE 4. 17 COMPARISON OF THE DAMAGE CONTROL STRAIN RATIO AS FUNCTION OF THE SEISMIC MOMENT MAGNITUDE	81

Chapter 1. Introduction

1.1 Research Significance and Motivation

Nuclear power plants (NPPs) and other civil structures in the US and Japan have recently experienced strong ground motions exceeding the original design values. In 2011, the Mineral-Virginia earthquake imposed ground accelerations to the North Anna nuclear power plant exceeding the design basis earthquake (DBE) and causing the initiation of safety shutdown procedures. After extensive evaluation of the plant's structures, systems and components (SSCs), some minor damage was found but deemed not significant (Li and Manoly, 2012.). According to Li and Manoly (2012), horizontal and inclined hairline cracks were found on interior walls of non-safety-related structures. The horizontal cracks were found to occur in pre-existing weaker interfaces such as in construction joints between concrete pour lifts. Other documented events involving NPPs are the Fukushima Daiichi NPP during the 2011 Tohoku earthquake and the Kashiwazaki-Kariwa NPP struck by the 2007 Niigata Earthquake, with this last one inducing seismic accelerations at the base of the reactor building exceeding twice its design level considerations (Takada, 2012). In general, these plants had experienced relatively good performance under unexpectedly large ground motions mainly due to the implicit conservatism in the seismic design procedures, requiring the structure to perform in the linear (elastic) range and thus, providing a considerable safety margin. These incidents, and the need to account for newly available seismic data, triggered a program that requires site seismic hazard re-evaluation for all US operating NPPs and that may require some plants to perform a seismic risk analysis to determine if the plant's seismic design provides adequate seismic margin (Li and Manoly, 2012, EPRI, 2013).

It is of vital importance to evaluate the capacity of structural components in the buildings that compose a nuclear power plant to have a reliable idea of the level of seismic damage after linear range that they can safely manage. In addition, according to the Nuclear Energy Agency (NEA, 2002), the average age of existing NPPs is constantly increasing while the number of new NPP constructions is still limited. Many of the existing NPPs are more than twenty years old, and some have a design life of forty years or more. The original operating licenses for commercial nuclear power plants are valid for 40 years from the issuance date (US-NRC, 2007). By 2007, 48 applications to renew this original license for an additional 20 years were approved and renewal applications for 14 plants were under review. Currently, there are plants that are still under revision. With this panorama, it becomes apparent that the aging of reinforced concrete components combined with the effect of cyclic loading are significant and need to be further studied. This proposal presents a research plan to evaluate the impact of beyond design earthquake accelerations in the response of RC structural components of auxiliary buildings found in NPPs and in civil structures. The effects of aging-related degradation in the reinforcing steel will be also considered in the analyses.

1.2 Research Objectives and Scope

The scope of this study is limited to the analytical modeling of a RC frame-wall dual system that constitutes a typical auxiliary building found in NPPs and in civil structures under seismic accelerations and reinforcing steel degradation effects. The main objective of this research is: to evaluate the impact of beyond design earthquake accelerations in the response of a RC dual frame-wall system with and without aging-related reinforcing steel degradation effects.

The specific research objectives of this study can be summarized as follows:

1. Evaluate different nonlinear modeling approaches using OpenSees to model a typical RC building with walls and frames representing a dual system used mainly in auxiliary buildings in NPPs and other civil structures.
2. Determine the effects of beyond earthquake accelerations in the seismic response, base shear capacity, stiffness and limit states of a RC dual wall-frame system.
3. Determine the effects of beyond earthquake accelerations in the seismic response, base shear capacity, stiffness and limit states of a RC dual wall-frame system introducing aging effects in the reinforcing steel.

1.3 Literature review

1.3.1 Seismic concern -events that exceeded design accelerations

1.3.1.1 Nuclear Power Plants (NPPs)

Recently, some important seismic events have occurred near NPPs. The most noticed earthquake triggered the Fukushima NPP incident (Takada, 2012). In March 11 of 2011, the Great East Japan Earthquake occurred with a moment magnitude of 9.0. This earthquake and tsunami generated a great disaster in Japan and produced heavy damage to the Fukushima Daiichi NPP resulting in an environmental damage of unexpected proportions (Takada, 2008). In this case the major damage was caused by the tsunami flood, which damaged the emergency power supply subsequently interrupting the operation of the cooling system.

In contrast, there are cases that show nuclear power plants survive larger earthquakes than those considered in the seismic design (Katona, 2012). In July 16 of 2007, the Kashiwazaki-Kariwa NPP, which is located in Niigata, was struck by the Niigata-ken Chuetsu-oki earthquake. In this case, all the components of the plant survived (safety classified structures, systems and components) without damage and loss of function. The earthquake records show that the design

parameters were clearly exceeded. From the base-mat record obtained, it was noted that in the reactor building, it was exceeded the seismic acceleration design level by twice or more, but even in this circumstance, the plant presented an excellent performance against an unexpectedly seismic excitation. The reason for the good performance of NPPs under unexpectedly large ground motions is thought to be due to the implicit conservatism in the seismic design procedures, requiring the structure to perform in the linear (elastic) range and thus, providing a considerable safety margin.

Another earthquake event that impacted a NPP was the 2011 Mineral, VA Earthquake. Li and Manoly (2012) performed a study about the impact over the North Anna NPP of the 2011 Virginia earthquake. Figure 1 shows the location of the plant and the earthquake's epicenter. The earthquake had a 5.8 magnitude with several aftershocks, including the largest aftershock of 4.5 magnitude. Furthermore, the largest historical earthquake (1875) known to have occurred in the zone of the plant before this event had an estimated magnitude of 4.8.

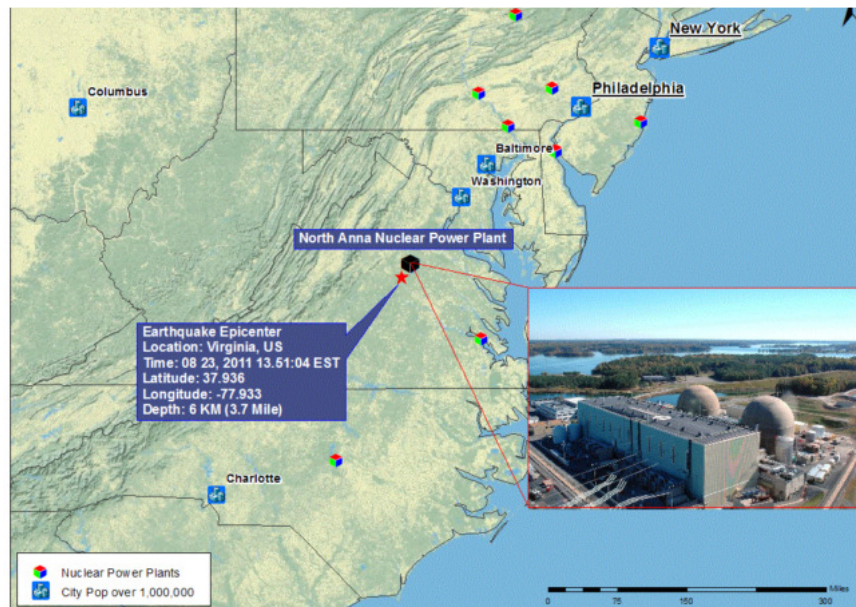


Figure 1. 1 Location of 2011 Mineral, VA Earthquake and the North Anna nuclear power plant. (Li and Manoly, 2012)

Despite that the operating basis earthquake and the design basis earthquake were exceeded, no significant structural damage was observed. The plant's structures, systems and components did not suffer significant damage. Figure 1.2 shows some examples of the damage presented in some walls and construction joints.



Figure 1. 2 Left: Inclined crack on the interior wall. Right: Horizontal cracks developed from construction joints between lifts (Li and Manoly, 2012).

On walls, two typical types of cracks in terms of their orientation were presented; inclined and horizontal, both were generally hairline cracks. For example, the horizontal cracks were typically developed from pre-existing weaker interfaces such as construction joints between lifts and in some cases between the ceiling and the wall (Figure 1.2). Moreover, the damage observed were cracks on interior walls and occurred mostly inside non-safety structures. There cracks did not affect the structure functionality.

1.3.1.2 Civil Structures

There are some studies in the literature that carry out assessments from several seismic events that exceeded the design accelerations and had impacted RC buildings in different ways.

Between June 2000 and May 2008, three significant events occurred in South Iceland. An extensive study of the seismic vulnerability of low-rise residential buildings based on damage data from the three earthquakes was carried out by Bessason and Bjarnason (2015). This zone presents high seismic activity, and even there is evidence of historical destructive earthquakes back to the 11th century AD. Figure 1.3 shows the location of these 3 recent events in the map of Iceland.

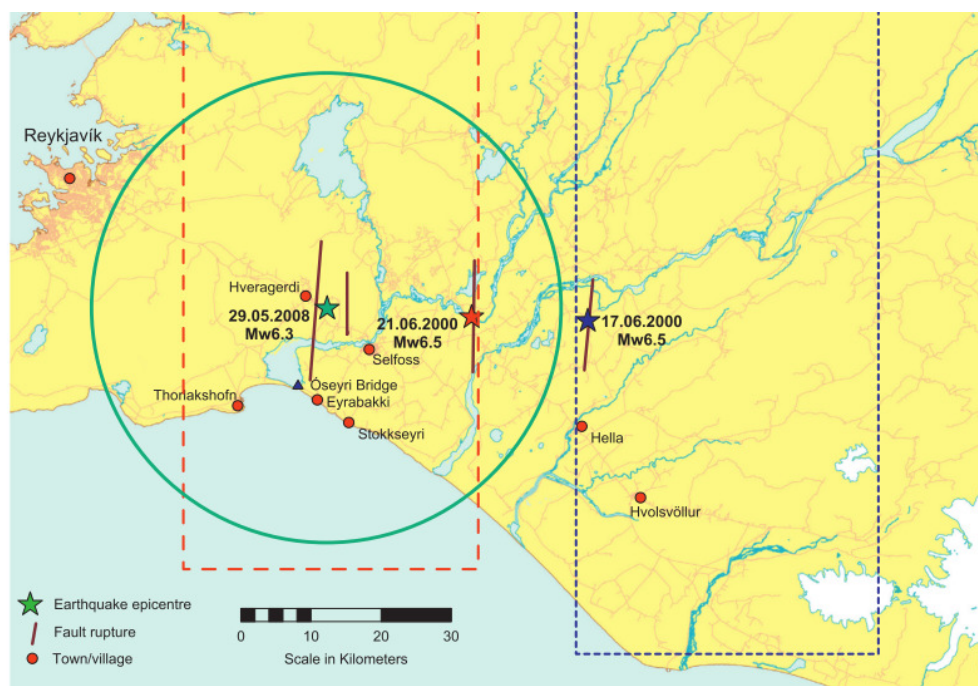


Figure 1. 3 Map of South Iceland showing the events occurred. (Bessason and Bjarnason 2016)

A deep assessment of the damage of buildings was performed. All the buildings existing in Iceland are registered in an official database. Detailed information is available about the type of occupation, date of construction, number of stories, building material, and geographical location. The area affected is mostly composed of low-rise building between 1-3 stories. The study was focused on the damage produced in buildings constructed using the new and the older codes. From the study, it was concluded that most residential buildings suffered damage, but a few were classified as totally damaged by the heavy damage they suffered.

Buildings constructed using the new code were significantly less damaged than older buildings. This circumstance shows the importance of implementing the seismic requirements in the building codes. Response spectra from two stations located on rock, exceeded the maximum value of the Eurocode 8 response spectrum (0.4 g), valid at the time that the earthquake struck the area.

Further, Verderame et al. (2012) performed an assessment of the damage scenario in the region of Emilia (Italy) after the 2012 Emilia Earthquake. Many of the buildings located in the area are masonry buildings, with 2 stories and constructed before 1981 (around 85%) and the rest are RC buildings. It can be said that most of the buildings located in the area struck by Emilia earthquake were only designed for gravity loads. The main earthquake had a magnitude of 6.0. Most of the damage was registered on masonry buildings. RC buildings were affected by slight and moderate damage although only in rare situations structural collapse was observed. The opening in walls as well the partial infills were prone to the occurrence of brittle failures. These studies showed the importance of the seismic design and the need to a better understanding of the response of buildings beyond design accelerations.

In 2010, an earthquake impacted Chile. The Maule earthquake that occurred in 2010 had a 8.8 magnitude and it was one of the strongest ground shaking ever measured. Jünemann et al. (2015) performed an analysis of RC walls damaged during the Chile earthquake in 2010. Jünemann et al. (2015) focused the research in the structural damage found in the inventory composed of Chilean “fish-bone” type buildings, as it is shown in Figure 1.4 which relies almost exclusively on a system of RC walls to resist both, gravity and lateral loads. The typical building is taller than 9 stories. There was a total of 46 buildings that presented moderate or severe damage during the earthquake, of which 36 cases presented completed information. The observations show that the damage occurred mainly in RC walls

located in the first few stories. In general, the nature of the damage presented was brittle.

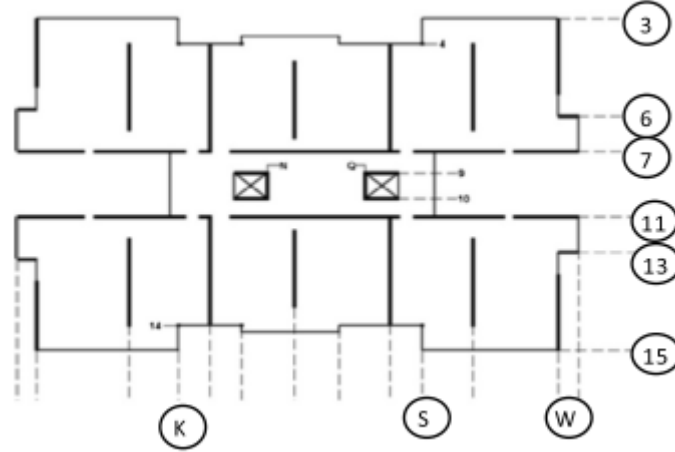


Figure 1. 4 Typical Chilean “fish-bone” plan building.(Jünemann et al., 2015)

Reduction in wall thickness in newer designed buildings had a negative impact on the seismic response of the buildings. According to these authors, to improve the cyclic behavior of the walls, an increase of the wall thickness could reduce damage on walls during earthquake events. Furthermore, experiments have shown the importance of the axial load ratio (ALR) of the RC walls in controlling the damage of shear walls. Finally, it could be summarized that the damage presented on the RC buildings presents three critical aspects. These aspects are: the smaller thickness, the larger axial loads and the significantly large vertical irregularities. It should be noted that these aspects were not common in buildings affected by the earlier Chile earthquake in 1985.

1.3.2 Structural aging

The importance of the aging-related degradation of concrete components and structures in NPPs lies in that they are commonly used to house the reactors and other importance equipment, guard their safety against large natural disasters

such as earthquakes, and contain and mitigate the postulated release of radioactive materials (BNL, 2009). As the nuclear power plants age, degradation incidences are starting to occur at an increasing rate, primarily due to environmental-related factors. One fourth of all containments have experienced corrosion, and nearly half of the concrete containments have reported degradation related to either the reinforced concrete or post-tensioning system (US-NRC, 1995). The observed and reported degradations were more severe at coastal plants than those observed in inland plants because of brackish and sea water (US-NRC, 2012). Although the vast majority of these structures will continue to meet their functional and performance requirements during their initial and extended licenses, it is reasonable to assume that with the increasing age of the operation some of these structures may not exhibit the desired durability without some form of rehabilitation.

A series of tests on RC shear walls with no degraded and degraded reinforcing steel (with various levels of steel corrosion) subjected to static cyclic loading were performed in Japan (Yamakawa, 1995). These tests are one of the few tests found in literature that study the effects of aging in RC walls subjected to cyclic loads. Specimens were degraded by mixing salt in the concrete, and then the corrosion of the reinforcement was accelerated by using the electrolytic corrosion method or by exposing specimens to oceanic environment for several years. They found out that the ultimate strength and ductility of the degraded specimens decrease when compared with the non-degraded specimens. The failure mode and crack pattern varied considerably between the degraded and non-degraded walls. In general, during these tests the degraded walls failed by fracture of the main reinforcement at the location of large deformation, meanwhile non-degraded specimens failed by buckling of the reinforcement. The results from these tests also indicated that the seismic performance is dependent of the

location/orientation of existing aging related cracks with respect to the applied seismic stresses. The orientation of cracks in concrete shear walls will determine whether cracks affect the seismic capacity of components. For example, cracks will affect the shear capacity if they coincide with the cracks caused by applied seismic loads or when they altered the failure mode (Yamakawa, 1995 and Park, 1998).

Other investigations of RC structural elements found in buildings with effects of aging-related degradation and some including cyclic or seismic considerations are highlighted next.

1.3.2.1. Higgins and Farrow III (2006)

This research focused in the understanding of shear behavior of corrosion damaged beams to assess the corrosion damage effect on the shear capacity of RC beams and girders. Large size specimens were constructed, and the embedded stirrups were subjected to accelerated corrosion and tested in four-point bending. Corrosion of the stirrups produced non-uniform section loss along the length of the stirrups. Significant local pitting damage was observed, particularly at higher corrosion damage states. The locally reduced areas on stirrups lead to localized yielding and reduced ductility. Fractures of stirrups occurred at severely corroded locations, thereby limiting strength and deformation capacity. Corrosion damage reduced the ability of the stirrups to constrain diagonal cracks upon initiation. Impact of cyclic loads was not considered.

1. 3.2.2. Bourahla et al. (2008)

In this study, a model for predicting the evolution in time using damage factors were introduced to assess the reduction of stiffness, strength capacity and hysteresis parameters of RC elements in a prototype bridge. The results obtained

showed significant changes in energy dissipation capacity and displacement of RC elements at different time intervals. They concluded that it was needed to have better ways to include the progressive effect of damage due to aging of the materials and changes in the hysteresis characteristics in the analyses of RC elements. The relationship between the aging damage level and the cyclic strength decay, the stiffness degradation and the slip-bond effect need also to be fully understand.

1.3.2.3. Ghosh et al. (2010)

This paper provides a framework for time-dependent fragility analysis of corroded bridges performance in seismic events, illustrating the impact of aging on component and system reliability. They concluded that it is required to evaluate the effect of aging on system response and fragility, considering not only the vulnerability of multiple components but also their simultaneous aging. Due to corrosion and subsequent area loss of reinforcing steel, the load carrying capacity and yield curvature of the RC columns undergo a significant reduction.

The diameter reduction function was presented as:

$$D(t) = D_i - r_{corr} * (t - T_i) \quad (1.1)$$

where D_i is the initial diameter, r_{corr} is the rate of corrosion, t is the elapsed time in years and T_i is the corrosion initiation time which is expressed with the following formula:

$$T_i = \frac{x^2}{4D_c} \left[\text{erf}^{-1} \left(\frac{C_0 - C_{cr}}{C_0} \right) \right]^{-2} \quad (1.2)$$

where C_0 is the equilibrium chloride concentration at the concrete surface, C_{cr} is the critical chloride concentration that causes dissolution of the protective passive film around the reinforcement and initiates corrosion and erf is the Gaussian error

function. The authors presented mean values for these parameters which are shown in Table 1.1 (adapted from Ghosh et al. (2010)).

*Table 1. 1 Descriptors of lognormal random variables affecting the corrosion deterioration.
(Ghosh et al. 2010)*

Descriptor	Unit	Mean	COV ^a
Cover depth (x)	cm	3.81	0.2
Diffusion coefficient (D_c)	cm ² /year	1.29	0.1
Surface chloride concentration (C_0)	wt % concrete ^b	0.1	0.1
Critical chloride concentration (C_{cr})	wt % concrete ^b	0.04	0.1
Rate of corrosion (r_{corr})	mm/year	0.127	0.3

^aCOV = coefficient of variation

^bwt % chloride = percent by weight of concrete

Figure 1.5 presents the reduction in steel cross-sectional area over time due to the combined effect of initial reinforcement diameter variability, rate of corrosion and corrosion initiation time.

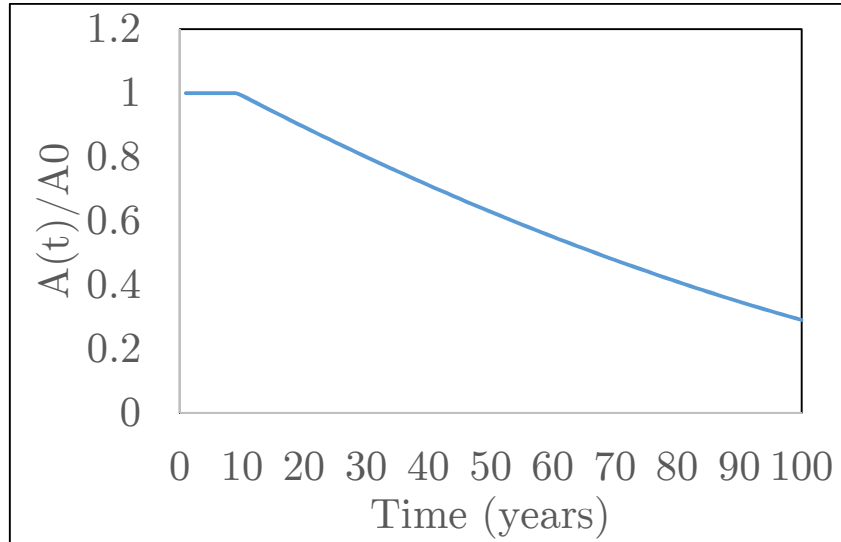


Figure 1. 5 Distribution of normalized time-variant area of the column reinforcement. (Ghosh et al., 2010)

1.3.2.4. Hanjari et al. (2011)

This research presents a methodology to analyze the mechanical behavior and remaining load-carrying capacity of corroded reinforced concrete (RC) structures. They determined that the main uncertainties in the available models were the determination of the ductility reduction of the corroded reinforcing bar and the variability of pitting corrosion in terms of when and where it takes place. It was assumed that the effect of corrosion can be modeled as a change in geometry and material properties of the concrete, the reinforcement, and the interface.

The effect of corrosion in the reinforcement steel bar is represented by changing of the cross-section area and changing of reinforcement ductility. The reduction of the effective reinforcement area is done as follows:

$$D = D_i - 2x \quad (1.3)$$

where D is the remaining diameter of the reinforcement, D_i is the original diameter and x is the corrosion penetration. Also, a change in the material properties is

recommended by these researchers. Although the strength ratio and the elastic modulus of the steel are not significantly affected by uniform corrosion, the ultimate strain change is presented by the following function:

$$\varepsilon_{su} = (1 - \alpha_i A_{cor}) \varepsilon_{su0} \quad (1.4)$$

where ε_{su} is the ultimate strain of corroded bars, α_i is an empirical coefficient valued in 0.01, A_{cor} is the average cross-sectional loss and ε_{su0} is the ultimate strain of non-corroded reinforcement steel bars.

1.3.2.5. Mohammed et al. (2011)

The study includes the development of a comprehensive methodology to evaluate the seismic performance, the residual strength and deformation capacity of aging RC bridge columns suffering from reinforcement corrosion. A nonlinear elasto-plastic numerical model to simulate bridge columns under the combined effects of reinforcement corrosion and seismic excitation was presented. Corrosion-induced damage was simulated by assuming a steel mass loss. The reduction of the concrete cross section due to spalling of the concrete cover and the reduction in the ductility of reinforcing bars were also considered. Corrosion of the longitudinal reinforcement results in significant degradation of the ultimate flexural capacity of the column and its capability to dissipate energy.

Mohammed proposed a reduction of the rebar cross-sectional area over time using the Faraday's law for the loss of reinforcement steel section due to the corrosion effect. The thickness reduction $x(t)$ is calculated according to:

$$x(t) = \frac{M}{zF\rho_s} * i_{corr} * t \quad (1.5)$$

where M is the metal molar mass (55.85 g/mol), z is the valence of the ion formed as a result of iron oxidation, F is Faraday's constant ($F=96.485$ C/mol), ρ_s is the density of iron (7.85 g/cm³), i_{corr} is the corrosion current density, and finally, t

is the time elapsed since corrosion started. Figure 1.6 shows the uniform corrosion and pit configuration of a corroded bar. Mohammed also proposed to modify the ductility of the reinforcing bars. The Lay and Schiebl (2003) and Cairns et al. (2005) empirical equations were recommended to evaluate the residual ductility due to corrosion:

$$f_y(t) = (1.0 - \alpha_y * A_s(t))f_y \quad (1.6)$$

$$f_u(t) = (1.0 - \alpha_u * A_s(t))f_u \quad (1.7)$$

where $f_y(t)$ and $f_u(t)$ are the yield strength at time t and the ultimate tensile strength at time t , respectively, f_y and f_u are the yield and ultimate tensile strengths of a non-corroded bar, respectively, α_y , α_u are regression coefficients proposed by Lay and Schiebl (2003), and $A_s(t)$ is the cross section loss function.

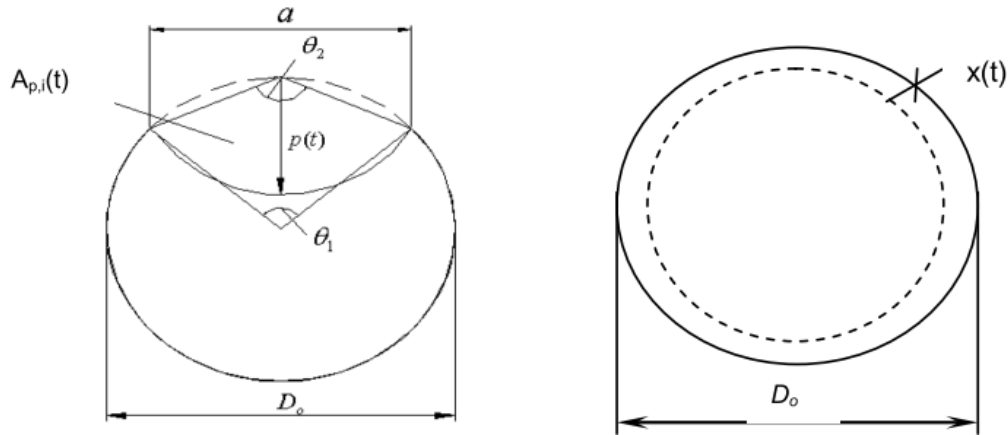


Figure 1. 6 Corrosion model (a) pit configuration and (b) uniform corrosion.(from Mohammed et al., 2011)

In summary, many researchers have studied aging-related problems in RC structural elements with special emphasis in corrosion of the steel reinforcement. Reinforcement corrosion in RC elements has a marked effect on the flexural load capacity, deflection, and ductility of RC elements (Ting and Nowak, 1991, Du et al., 2007, Mullard and Stewart, 2011). Others have focused on the cracking of concrete during aging (Braverman, 2001, Coronelli, 2002). The orientation of

cracks in concrete affects the response of the structure depending on the applied loading. Naus (2007) provided an extensive and in-depth review of important factors that contribute to concrete degradation, with emphasis on factors that apply to NPP environment. Durability of concrete can be affected by adverse performance of either its cement-paste matrix or aggregate materials under chemical or physical attack. Chemical attack may occur in several forms: efflorescence or leaching, sulfate attack, attack by acids and bases, salt crystallization, and alkali-aggregate reactions. Physical attack mechanisms for concrete include freeze/thaw cycling, thermal exposure/thermal cycling, abrasion/erosion/cavitation, irradiation, and fatigue or vibration. Degradation of mild steel reinforcing materials can occur as a result of corrosion, irradiation, elevated temperature, or fatigue effects (Naus, 2007).

These researchers have undoubtedly performed great contributions to the study of aging-related problems in RC structures. A few of them have focused on the understanding of the response of RC elements subjected to seismic ground motions with combined effects of aging related degradation. It is deemed important to combine the effects of rebar aging in the study of the seismic response of RC building during events exceeding design considerations to understand in detail changes in stiffness and strength in the structural members under these circumstances.

1.4 Research Methodology

In order to achieve the proposed objectives, the following tasks will be performed:

- Model the system components of the RC dual frame and wall independently using available nonlinear models and modeling schemes used for quasi-static cyclic lateral and dynamic loads in OpenSees. This program is an

open source software for developing applications to simulate the performance of structural and geotechnical systems subjected to earthquakes (<http://opensees.berkeley.edu/>)

- First, structural members of a RC frame (e.g. a cantilever column) will be studied using different modeling approaches, under monotonic, lateral cyclic loads and dynamic excitations to get familiar with the program and its capabilities.
- Second, a RC frame will be modeled from experimental tests available in literature (e.g. Bechtoula et al. 2006). The model proposed is a two-story frame that represent an 11-story RC frame building to assess nonlinear modeling capabilities of OpenSees of more complex systems.
- Third, available models for RC walls will be evaluated to find a model capable to reproduce the cyclic response of these structural systems. The wall models will be validated using also experimental tests found in literature.
- Develop a model of a 2D RC building with walls and frames representing a typical auxiliary building found in nuclear power plants and other structures.
- Dynamic analyses will be performed to the selected RC frame-wall model using spectrum compatible records for different magnitude scenarios. The objective of these analyses will be to evaluate available capacity and ductility after the structure is subjected to different intensities of seismic action. The analyses will be complemented with pushover analyses after the dynamic analyses to assess available shear strength capacities, stiffness changes and displacement limits states.

- The final step will be to include aging effects in the reinforcing steel and perform the dynamic analyses to establish differences in the seismic behavior of RC dual wall frame systems with and without aging effects.

1.5 Organization of Thesis

This thesis includes five chapters. Chapter 1 presents the motivation, objectives, scope and methodology of the conducted research as well as a discussion on seismic events exceeding design accelerations in NPPs and civil structures and studies of aging related effects in RC elements. Chapter 2 describes in detail the methodology and modeling scheme used in the analyses. Chapter 3 presents the results of the analyses without the consideration of aging related effects. Chapter 4 presents the results of the analyses with the consideration of aging related effects. Chapter 5 summarizes the key findings and conclusions. Also provides recommendations for future studies.

Chapter 2. Modeling and Methodology

2.1 Introduction

This chapter describes the modeling techniques and methodology used to perform the analyses in this thesis. All the models were developed in OpenSees, which is a software framework for developing applications to simulate the performance of structural and geotechnical systems subjected to earthquakes (McKenna et. al 2000). An exhaustive study of the different models available in OpenSees for reinforced concrete (RC) elements was done. The modeling process started by analyzing a RC cantilever column and move forward to the modeling of a RC frame, a RC wall and then the final RC dual frame-wall system was developed and analyzed. For sake of brevity, only the results obtained for the analysis of the RC frame, RC wall and final RC dual frame-wall system will be shown in the next sections.

2.2 RC frame and wall models

A RC frame specimen was modeled to identify an appropriate modeling approach for the final RC frame-dual system model. A RC frame specimen from the experimental tests performed by Bechtoula et al. (2006) was modeled. Bechtoula et al. (2006) tested two 2-story frames with one bay representing the lower two stories of an 11-story RC frame building subjected to cyclic loading (Fig 2.1). The two reinforced concrete frames were designed with seismic considerations according to the Japanese standards and were tested to investigate the shear force distribution of columns under cyclic loading of the lower part of an entire frame. Figure 2.1 presents the geometry, dimensions and reinforcement steel of the RC frame tested by these researchers.

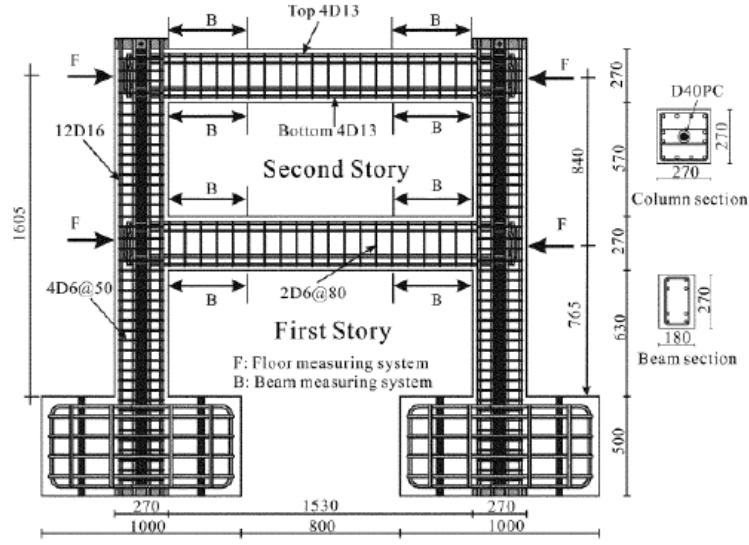


Figure 2. 1 RC frame specimen (Bechtoula et al., 2006)

The structural elements were modeled using the element “Beam with hinges” (Scott and Fenves, 2006). The elements in the interface of the beam and column were modeled as elastic elements. These elastic elements were extended from each joint half of the beam or column height to obtain a better response at joint by having a linear elastic section with the beam or column elastic stiffness (Priestley et al., 2007). When a beam with hinges element is used, it is considered that the plasticity of the element is concentrated at a specified hinge length at the element ends. The plastic hinge length for each element was calculated using equations 2.1-2.2 (Priestley et al. 1996). In these equations, L_p is the equivalent plastic hinge length, L_{sp} is the strain penetration length, L_c is the length from the critical section to the point of contraflexure, f_s is the tension stress in the longitudinal bars, f_y is the longitudinal bars yielding stress, and d_{bl} is the longitudinal bar diameter.

$$L_p = kL_c + L_{sp} \leq 2L_{sp} \quad (2.1)$$

$$L_{sp} = 0.022f_s d_{bl}; \quad f_s \leq f_y \quad (2.2)$$

$$k = 0.2 \frac{f_{su}}{f_y} - 1 \leq 0.08 \quad (2.3)$$

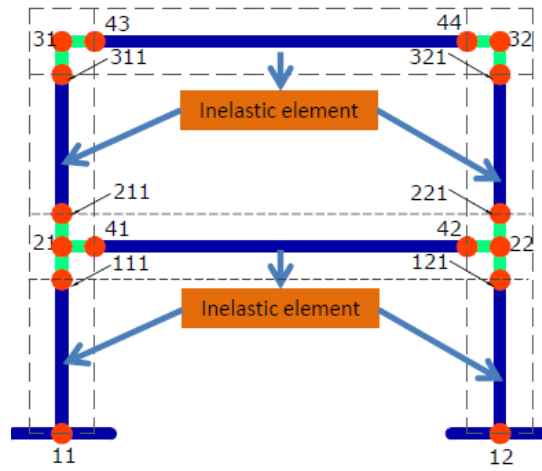


Figure 2. 2 Distribution of the elements of the structure.

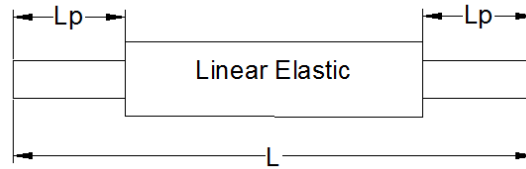


Figure 2. 3 Beam with Hinges element (Scott and Fennes, 2006)

The concrete was modeled using the Kent-Scott and Park concrete model (Kent and Park, 1971). The constitutive relationship used in OpenSees based on the Kent and Park (1971) model for the concrete model is named Concrete01. This presents unloading/reloading linear degradation of the stiffness according to the work of Karsan-Jirsa (1969) and no tensile strength is assumed. The reinforcing steel was modeled using the model developed by Moehle and Kunnath (2006). The Moehle and Kunnath (2006) steel constitutive model is based on the steel model proposed by Chang and Mander (1994). The model can be used to account for isotropic hardening, diminishing yield plateau and degrading strength and stiffness due to cyclic reversals. Figure 2.4 shows the concrete and reinforcing steel constitutive relationship for frame elements. The results obtained from the model developed in OpenSees show good agreement with the experimental results.

Figure 2.5 shows the shear vs drift cyclic response obtained from the analyses and the backbone obtained from the test.

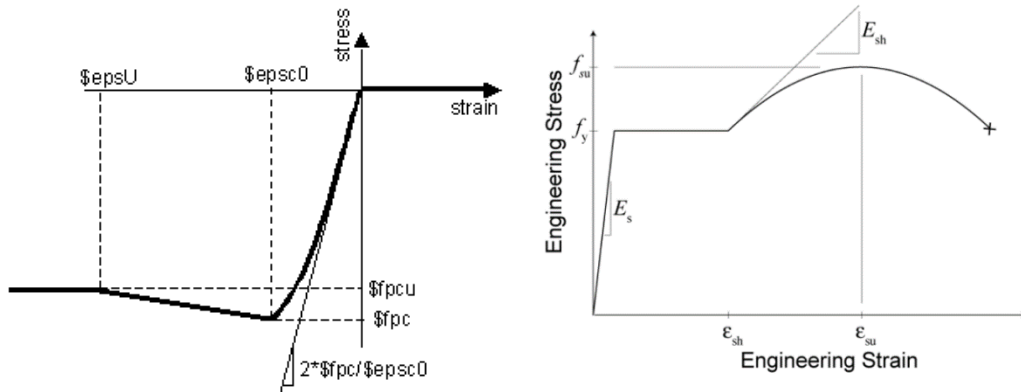


Figure 2. 4 Concrete 01 and Reinforcing steel constitutive relationship for frame elements

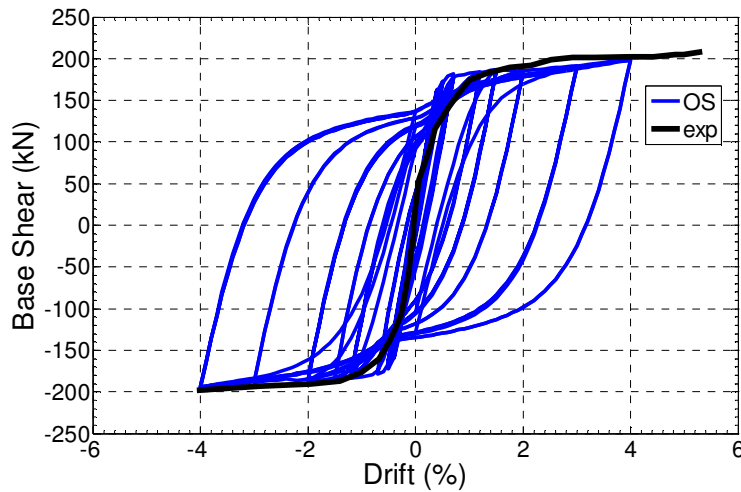


Figure 2. 5 Shear vs Drift RC frame specimen

The second model that was developed was a RC wall specimen. The RC wall has a height of 72 in, with dimensions and geometry shown in Figure 2.6. The reinforcement steel is also shown in this figure. The objective of this model is to select a modeling approach that appropriately captures the response of a RC wall under constant axial load and cyclic lateral loads. The specimen selected was tested by Tran and Wallace (2012) under axial load and cyclic lateral displacement applied at the top of the wall.

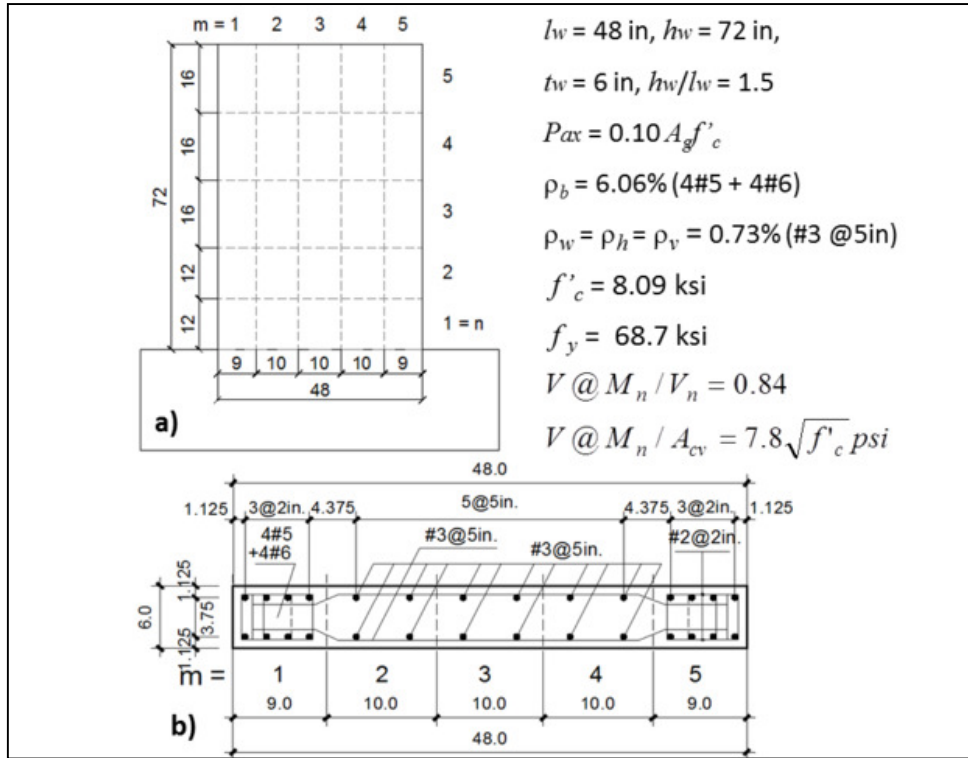


Figure 2. 6 Model discretization: a) Plan view, b) Cross-section (Kolozvari et al., 2014)

In order to perform the analyses of this wall, the Shear Flexure Interaction Multiple-Vertical-Line-Element-Model (SFI MVLEM) developed by Kolozvari et al. (2014) was used. This element was developed by modifying the original MVLEM proposed by Vulcano et al. (1988) and later extended by Orakcal et al. (2004). The model is composed by a series of RC panel elements connected at their top and bottom level by rigid beams. The flexural response is captured by the axial deformation of the RC panels in the vertical direction and the shear deformation by imposing shear strain on each RC panel at the height ch . The shear and the flexural/axial behavior at the panel level is coupled through the interaction between the flexure/axial and shear deformations and forces at the model level. The behavior of the RC panel elements is modeled using the Fixed-Strut-Angle-Model (FSAM). The fixed strut-angle concept is introduced in OpenSees using the command `nDMaterial FSAM`. It was developed by Kolozvari et al. (2015) and it is based in a plane-stress constitutive model inspired in the

RC panel elements under in-plane, reversed-cyclic loading conditions proposed by Ulugtekin (2010) and Orakcal et al. (2012). Figure 2.7 shows the RC panel model. The strain fields are assumed to be equal to each other between concrete and reinforcement steel, assuming a perfect bond between the reinforced steel bars and the concrete. The reinforcing ratio in horizontal and vertical directions (ρ_{uX} and ρ_{uY}), the friction coefficient (μ) and the dowel action stiffness parameter (α_{fadow}) are required as input parameters in this model. The dowel action of the reinforcing bars is modeled according to Kolozvari (2013). The dowel resistance of the vertical reinforcement is modeled using a simple linear-elastic constitutive model ($\tau_{sxy} = \alpha E_s \gamma_{xy}$) implemented in the RC panel model to simulate the contribution of reinforcement dowel action to shear resistance (Figure 2.8). τ_{sxy} is the resulting shear stress on the RC panel due to the dowel action of the vertical reinforcement, γ_{xy} is the shear strain acting on the panel in the horizontal plane of the wall and E_s is elastic steel modulus.

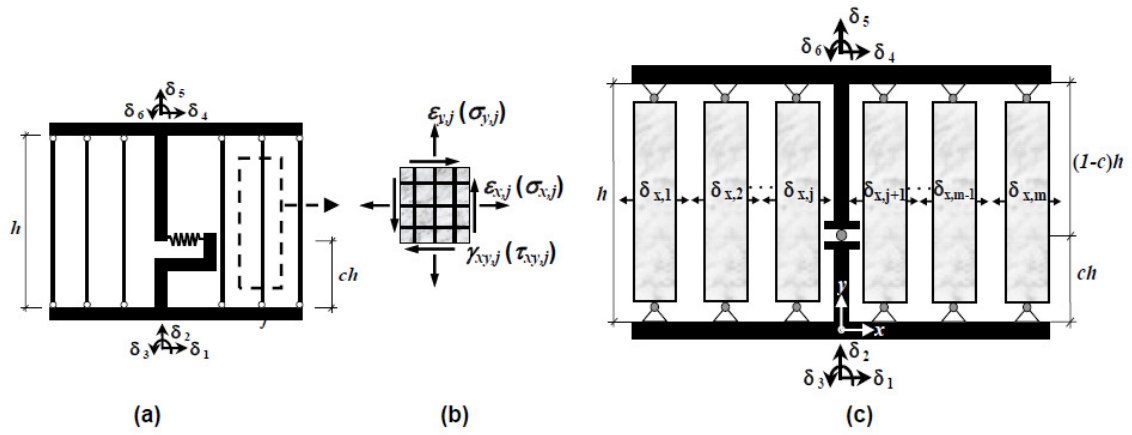


Figure 2. 7 Implementation of RC panel behavior into MVLEM: (a) original MVLEM; (b) RC panel element; and (c) SFI-MVLEM.

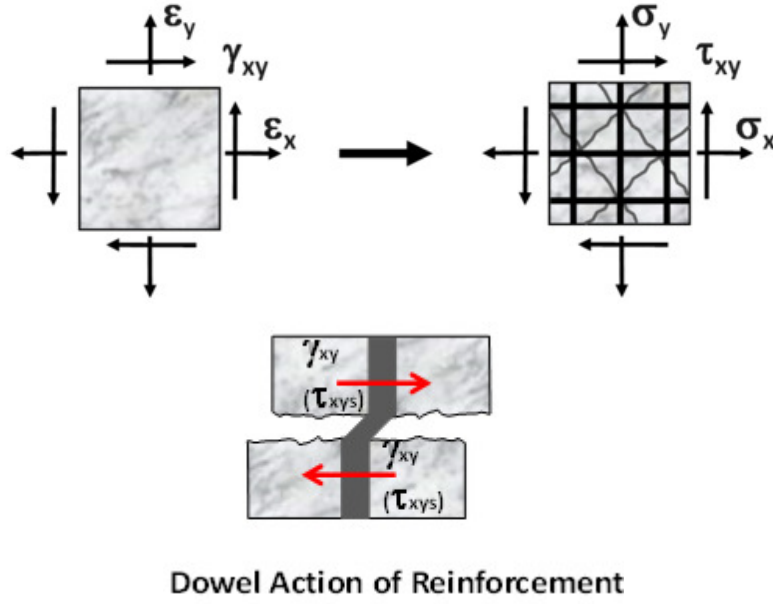


Figure 2. 8 FSAM for Converting In-Plane Strains to In-Plane Smeared Stresses on a RC Panel Element (Top). Dowel action of reinforcement (Bottom). (Kolozvari et al., 2015)

The model has six external DOFs situated at the top and bottom of the element nodes (displacements and rotation). The deformation at these DOFs are used to obtain the shear strain $\gamma_{xy,j}$ and the normal strain in the vertical direction $\epsilon_{y,j}$ for each j RC panel element. Furthermore, an internal DOF for each panel is defined to capture the normal strain in the horizontal direction, $\delta_{x,n}$. Figure 2.9 shows the DOFs distribution. The total DOFs of a model composed by SFI-MVLEM elements is obtained as:

$$TotalDOFS = (3 * n + 3) + m * n \quad (2.4)$$

where n is the number of SFI-MVLEM elements and m is the number of total panels in the SFI-MVLEM element.

The stiffness matrix for each SFI-MVLEM element has the following form:

$$[K_e] = \begin{bmatrix} [K_e]_N & [0] \\ [0] & [K_e]_x \end{bmatrix}$$

where $[K_e]_N$ is the element stiffness matrix relative to the external DOFs, which is derived based on the deformation of extension and the relative rotation at the top and the bottom of each SFI-MVLEM element (Orakcal et al. 2004) and $[K_e]_X$ is the element stiffness matrix associated with the internal DOFs. Figure 2.10 shows these deformations. The internal element stiffness DOFs' matrix is a diagonal matrix because each panel is independent of the others and its elements have the stiffness in the horizontal direction of each RC panel. Rotations and resulting lateral displacements are calculated based on the wall curvature and shear deformations coupled at the model element level, derived from the section and material properties of RC panel elements, respectively, corresponding to the bending moment and shear force at relative height ch of each element.

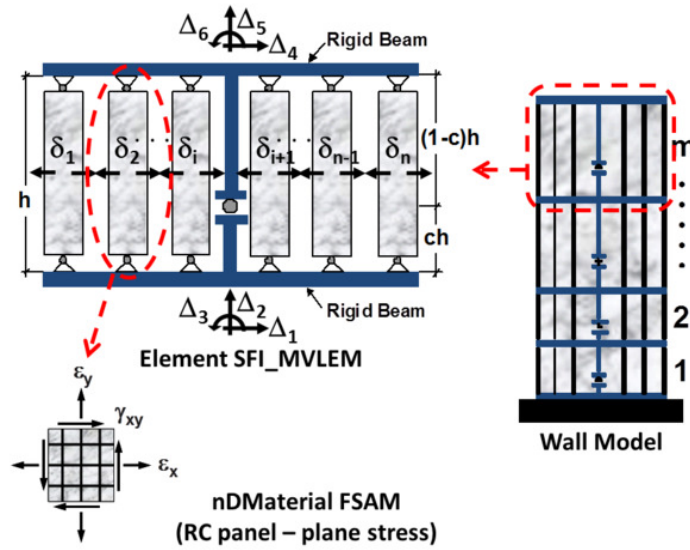


Figure 2. 9 a) SFI_MVLEM Element, b) RC Panel Element (nDMaterial FSAM) (SFI-MVLEM) (Koložvari et al., 2015)

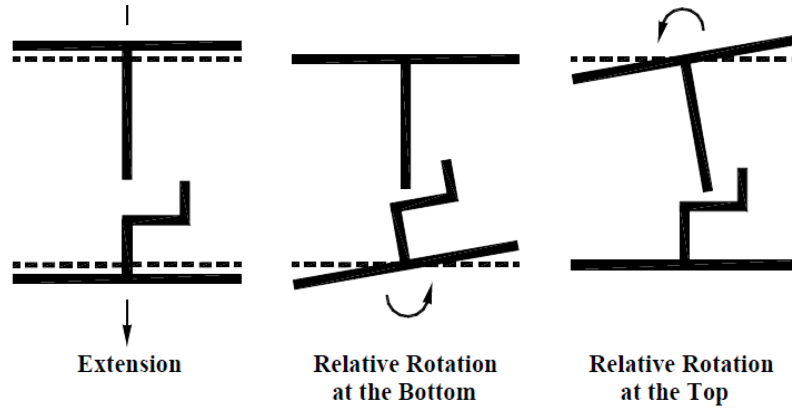


Figure 2. 10 Element deformations of the MVLEM element (Vulcano et al., 1988)

The concrete of the wall was modeled using the uniaxial material ConcreteCM (Kolosvari et al. 2015). The material is a uniaxial hysteretic constitutive model for concrete developed by Chang and Mander (1994). This model will be described in detail next. Figure 2.11 shows the lateral behavior under a cyclic load comparing the analytical response with an experimentally obtained backbone curve. The analytical response obtained with OpenSees is close to the experimental results which means that this model appropriately predicts the behavior of the RC wall under cyclic loads. Figures 2.12 and 2.13 show the stress-strain response obtained for the concrete and the reinforcing steel bars, respectively. The results are compared with the backbone results obtained by Tran and Wallace (2012). In both cases, the stress-strain curve for the concrete and the vertical reinforcing steel bars are in good agreement with the experimental envelope curve obtained by Tran and Wallace (2012).

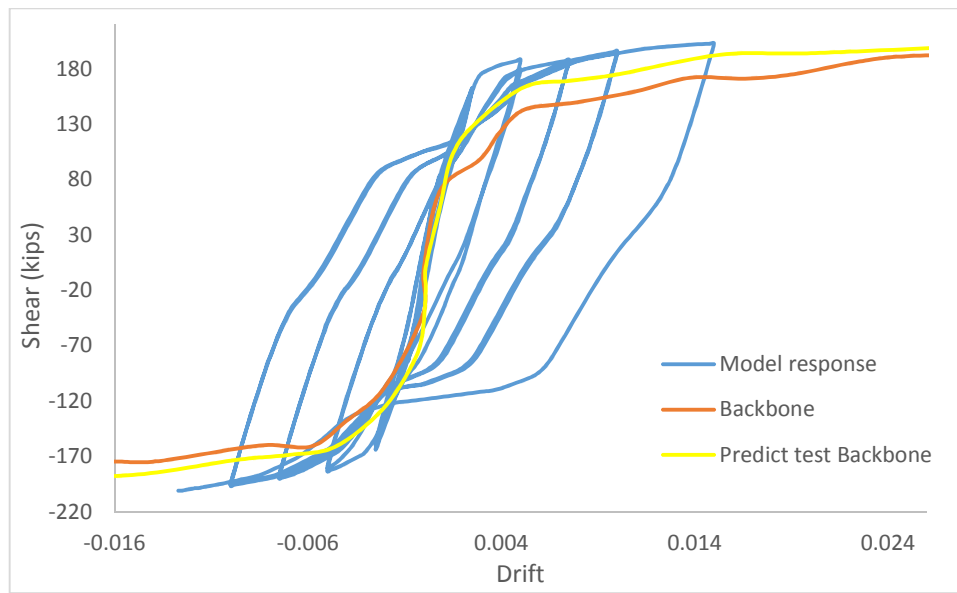


Figure 2. 11 Wall responses: a) Load versus Top Displacement Behavior

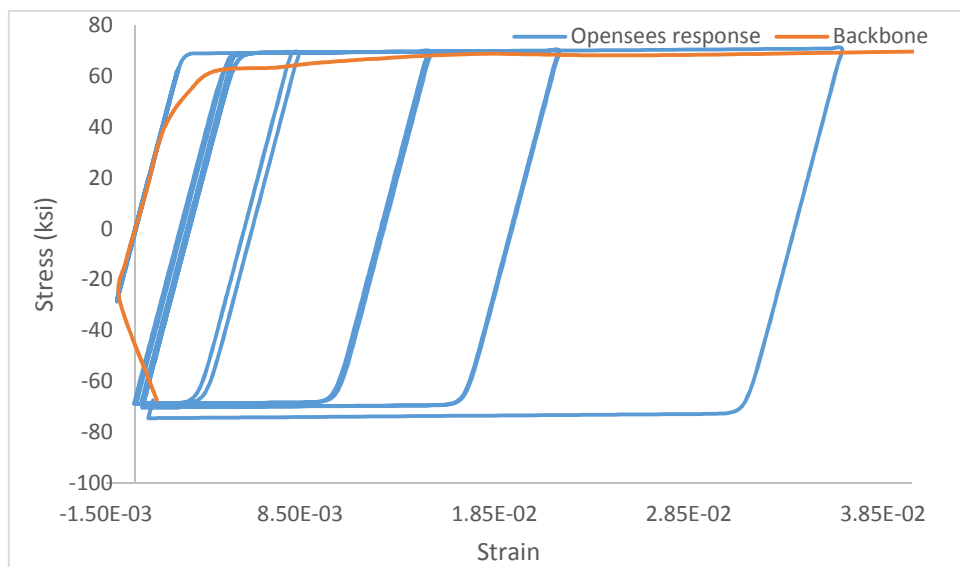


Figure 2. 12 Stress-Strain Behavior for Vertical (Y) Steel

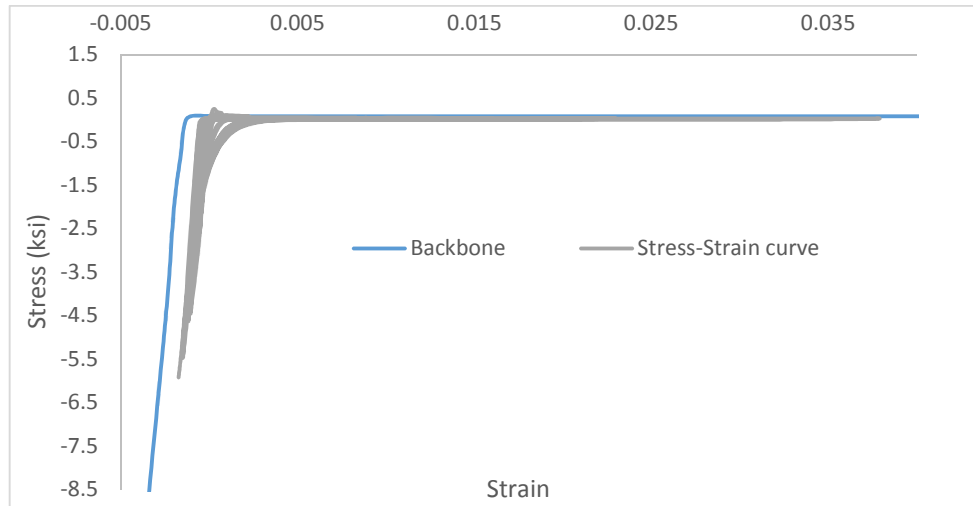


Figure 2. 13 Stress-Strain Behavior for Concrete Strut 1 Model

A model of a reinforced concrete frame-wall dual system was analyzed to accomplish the objectives of this research. The objective is to simulate a typical auxiliary building found in a nuclear power plant. The European experiment named SMART was used as base to develop the RC wall model. The frame was designed to accommodate the RC wall inspired from the SMART test using gravity loads. The lateral loads are supposed to be resisted by the wall.

2.2.1 SMART project 2008

The SMART project tested a reduced scale three stories model of a typical nuclear RC building composed of three walls and one column. Two walls have openings and the thickness of the walls and the slab is 10 cm. The specimen was designed according to the French nuclear standards. A PGA of 0.2 g was used. The experiment was done in order to study the torsion effect and the non-linear response of RC structures. Figure 2.14 shows the specimen shape and its dimensions.

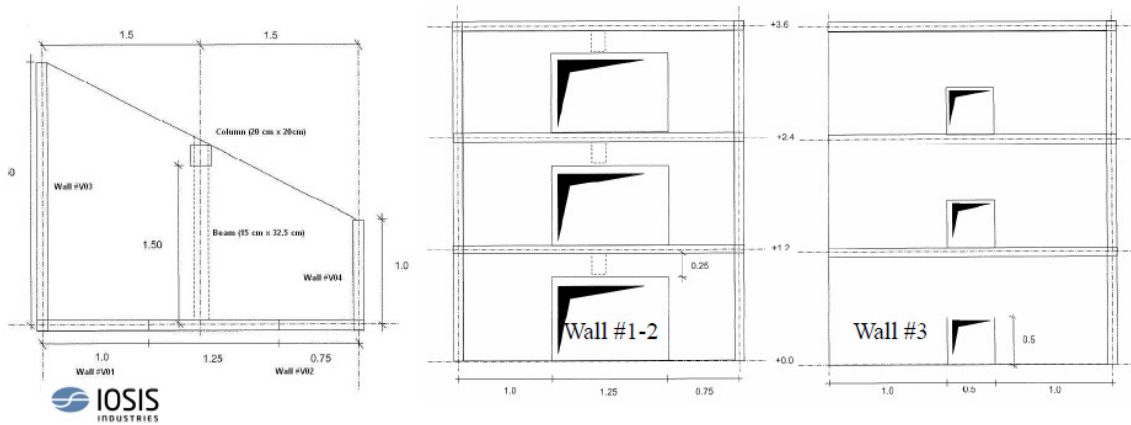


Figure 2. 14 Plan view and elevation of the SMART2008 specimen (Lermitte, Chaudat, and Payen, 2008)

The wall used as base for the model was the wall #1-2. This wall presents the larger openings. The vertical dimension was incremented by a factor of 2.58 while the horizontal dimension remains as in the original specimen. The reinforcement steel has the same distribution as in the original specimen too. Both the dimension and the reinforcement steel will be presented later.

2.2.2 RC Frame structure

Once the wall specimen design was obtained, the frame was designed and added to the model. The frame has three stories, with 3096 mm of height each one. The beam length is the same value of the wall width. The dimensions of the elements section were fixed as 508x508 mm for the columns, and 508x609.6 mm for the beams. Figure 2.15 shows the dimensions of the frame. In order to make the design more accurate live loads were added for the design. The design was performed following the directions of the ASCE 7-10 standard. For the seismic load, the requirements from ASCE 7-10 were also taken into consideration, through which the design spectrum was obtained. (Figure 2.16). The S_d and S_1 values for the spectrum design were 0.2243 and 0.12956 respectively.

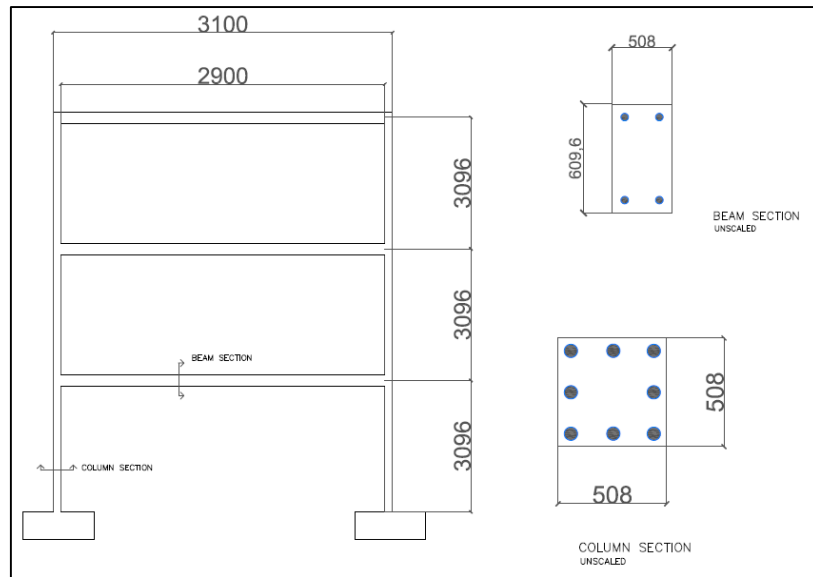


Figure 2. 15 Frame geometry (in mm)

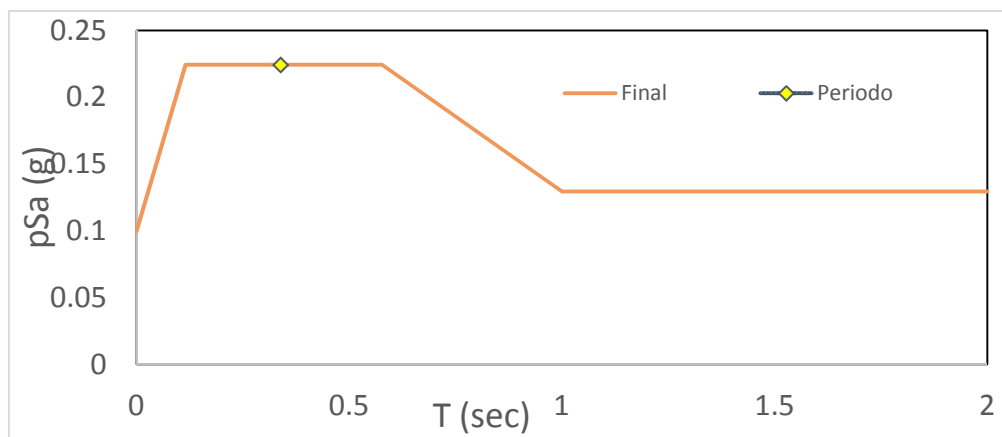


Figure 2. 16 Design Spectrum

2.2.3 RC frame -wall dual system

The final model is composed of a RC wall and a RC frame, both already described, linked by an equal degree of freedom constraint to transfer the forces between the systems uniformly. The constraint was located at each floor connecting the right side of the wall with the left column of the frame in order to simulate the effect of the slab. Figure 2.17 shows the geometry and the dimensions of the elements.

The wall has a thickness of 100 mm. Figure 2.18 shows the reinforcement details of the wall and frame sections (beams and columns).

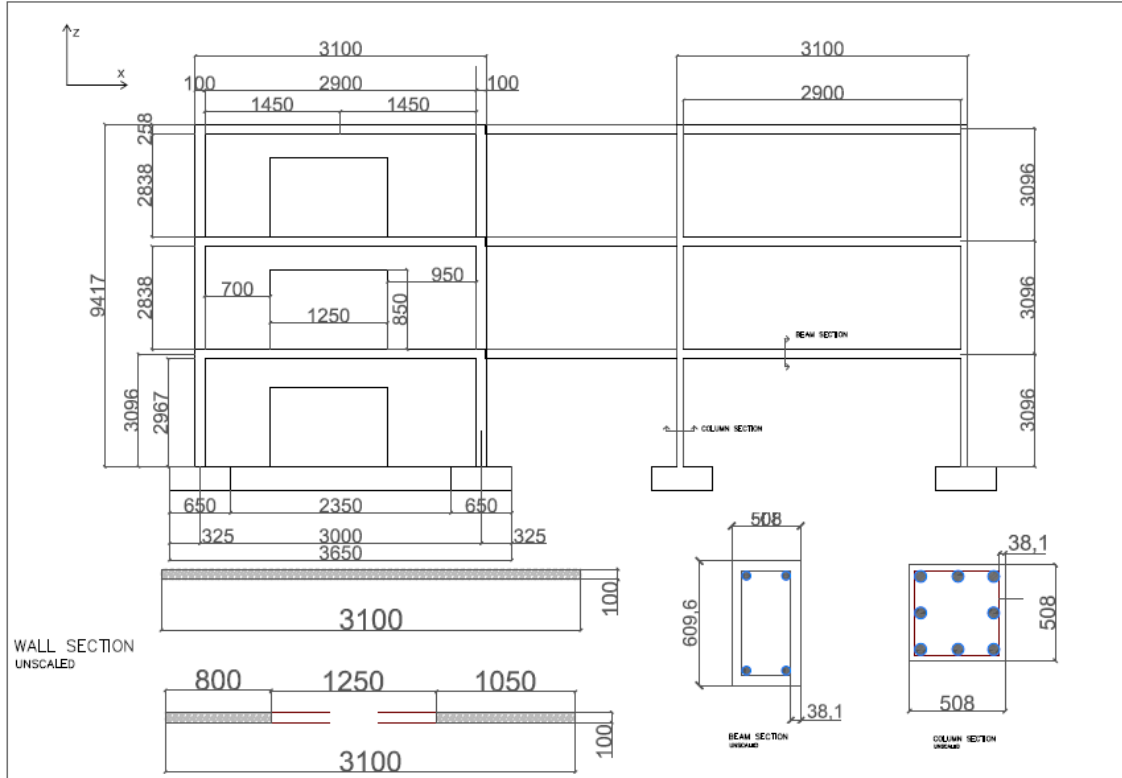
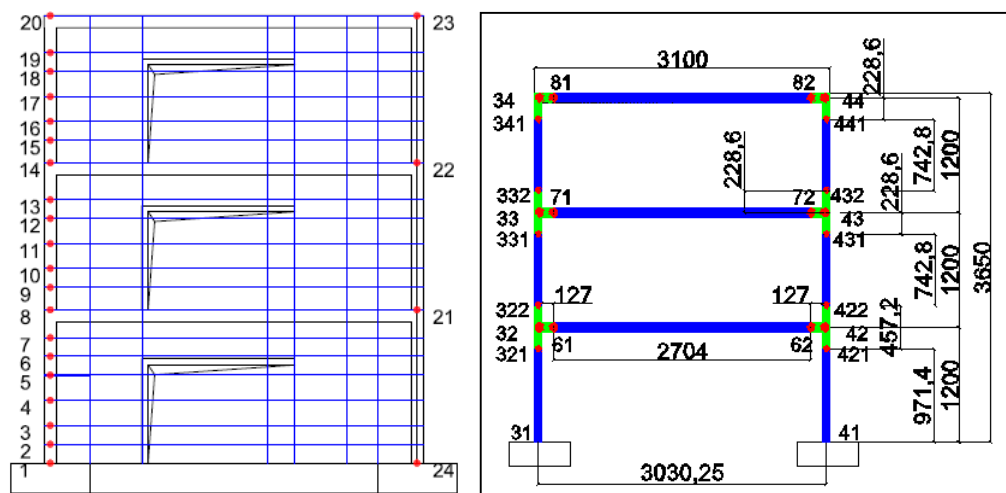


Figure 2. 17 Geometry and dimensions (in mm) of the RC wall and frame system



Deformed Shape (MODAL) - Mode 1; T = 0.37057; f = 2.69854

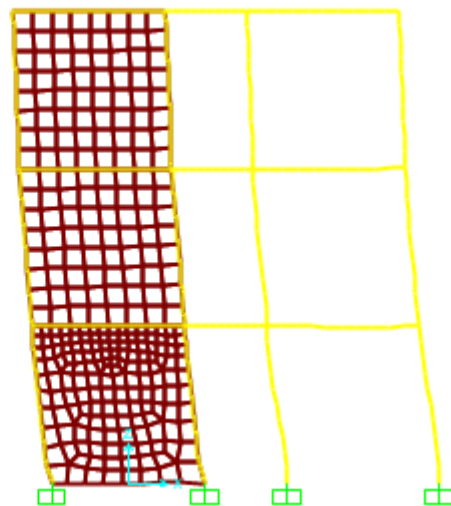


Figure 2. 19 Nodal distribution and SAP2000 modal analysis.

2.3 Materials

This section explains the different materials used in the modeling process in OpenSees. Both frame and wall are RC structures, but the material used to build each section of the model is different in both cases. The concrete of the frame sections has a compressive strength of 27.6 MPa, while the concrete of the wall has a compressive strength of 55.78 MPa. The steel yield strength used in the frame elements was 413 MPa and the steel yield strength used in the wall was

400 MPa and 475 MPa for the reinforcing steel in the body of the wall and in the boundary, respectively. The constitutive relationships used for the concrete and reinforcing steel in the frame and wall will be discussed in the next sections.

2.3.1 Frame sections

The concrete, whether confined or not confined, is modeled using the Kent-Scott and Park concrete model (Kent and Park 1971). The constitutive relationship used in OpenSees based on the Kent and Park (1971) model for the concrete model is named Concrete01. This presents unloading/reloading linear degradation of the stiffness according to the work of Karsan-Jirsa (1969) and no tensile strength is assumed. Figure 2.20 shows the constitutive model of the concrete, where f_{pc} is the concrete 28 day compressive strength, f_{pcu} is the concrete crushing strength, and ϵ_{psc0} and ϵ_{psU} are the concrete strain at maximum strength and concrete crushing, respectively. Beyond the crushing point the concrete strength remains constant. The initial slope for this model is given by $2*f_{pc}/\epsilon_{psc0}$.

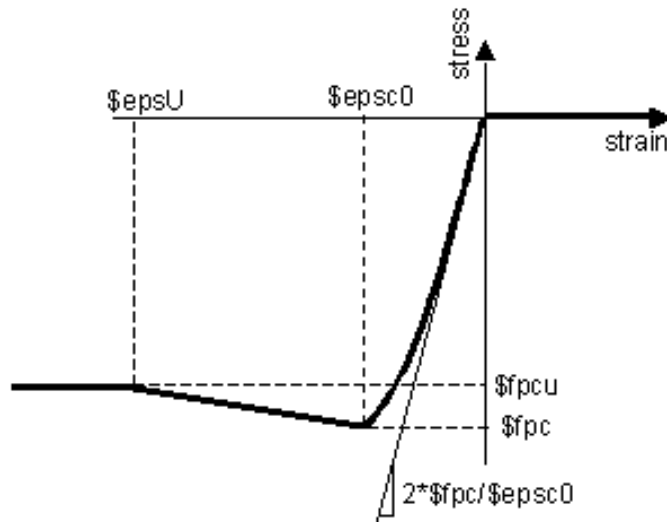


Figure 2. 20 Concrete 01 constitutive relationship (OpenSees, 2014)

The reinforcing steel was modeled using the model developed by Moehle and Kunnath (2006) which was specially intended to be used in a reinforced concrete fiber section as the steel reinforcing material. The Moehle and Kunnath (2006) steel constitutive model is based on the steel model proposed by Chang and Mander (1994). The model can be used to account for isotropic hardening, diminishing yield plateau and degrading strength and stiffness due to cyclic reversals. The parameters required for this model are the yield (F_y) and ultimate stress (F_u), the strain at ultimate stress (ϵ_u) and the strain at the on-set of hardening (ϵ_{sh}). The backbone curve is shown in Figure 2.21. Table 1 resumes the parameter values used for the frame model.

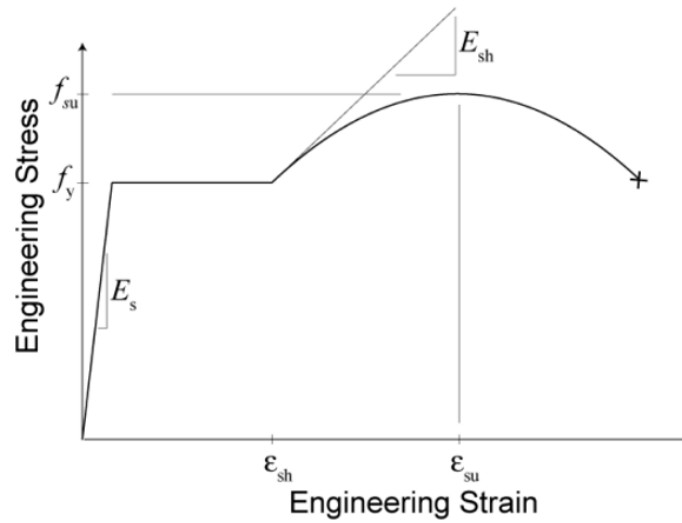


Figure 2. 21 Reinforcing steel constitutive relationship for frame elements (Chang and Mander, 1994)

Table 2. 1 Frame parameters for concrete and steel reinforcement

Concrete (MPa)		Steel (MPa)	
Parameter	Value	Parameter	Value
fpc	27.6	Fy	413
epsc0	0	Fu	720
epsU	0.01	ϵ_u	0.1
fpcu	0	ϵ_{sh}	0.008
Kfcb	1.21	Es	200000
Kfcc	1.6	R1	0.383
Kres	0.2	R2	16
		R3	8

2.3.2 Wall sections

The wall concrete was modeled using the uniaxial material ConcreteCM (Kolozvari et al. 2015). The material behaves according to a uniaxial hysteretic constitutive model for concrete based on the model developed by Chang and Mander (1994). The model is able to simulate the hysteretic behavior of confined and unconfined, for the compression and either the tension (Figure 2.22). Figure 2.22 shows the compressive and tensile envelope curves. The parameters required for this model are the initial tangent slope (E_c), the peak coordinates (ϵ'_c , f'_c), the tensile strength of concrete (f_t), the parameter r_c that is based in the Tsai (1988) equation parameter defining the shape of the envelope curve and ϵ_{-cr} to define normalized strain where the envelope curve starts following a straight line until ϵ_{sp} , the spalling strain, where the compressive stress become zero.

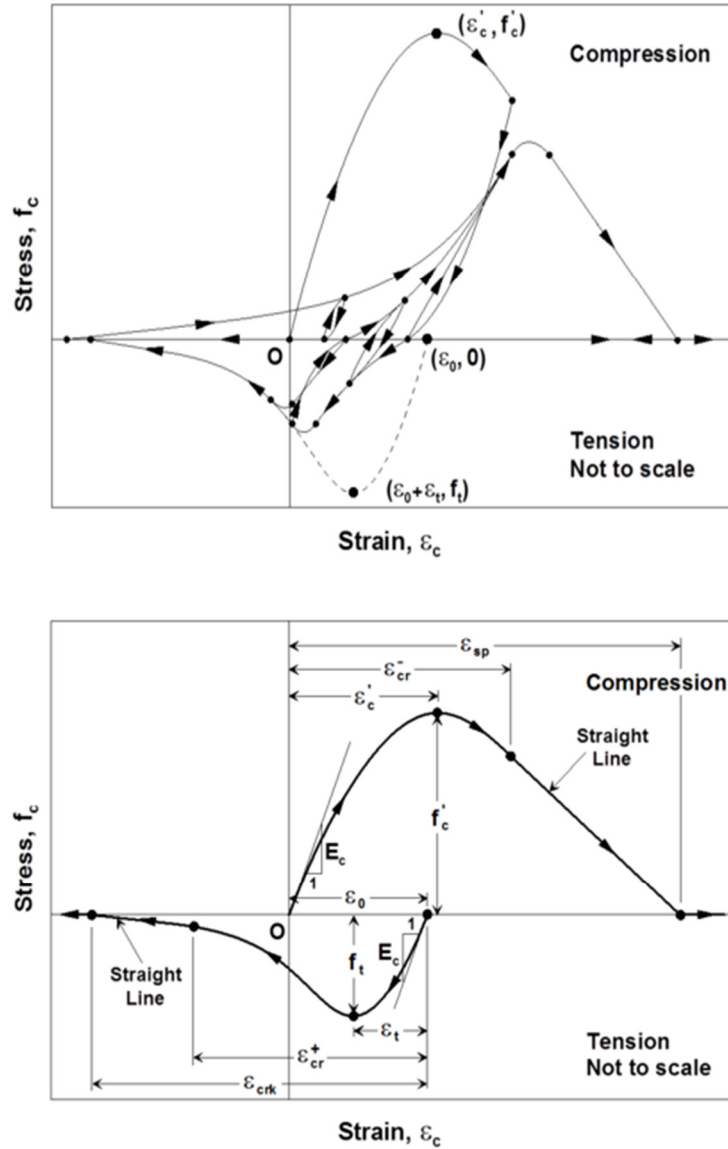


Figure 2.22 Hysteretic Constitutive Model for Concrete by Chang and Mander (1994) (top) and Compression and Tension Envelope Curves (bottom)

The reinforcement steel of the wall was modeled using the uniaxial material SteelMPF (Kolozvari et al., 2015). This command is based on the uniaxial constitutive nonlinear hysteretic material for steel proposed by Menegotto and Pinto (1973). Later, the model was extended by Filippou et al. (1983) in order to include isotropic strain hardening effects. Figure 2.23 shows the constitutive model proposed by Menegotto and Pinto (1973). The transition curve is described by two asymptotes, one represented by the slope E_0 (modulus of elasticity) and the asymptote E_1 , which is obtained multiplying the modulus of elasticity by the

parameter b , which represents the strain hardening ratio. The input data required are f_{yp} and f_{yn} representing the yield strength in tension and compression, respectively, the initial modulus (E_0), the strain hardening ratio in tension (b_p) and in compression (b_n), the initial value of the curvature parameter (R_0) and two isotropic hardening compression parameters, a_1 and a_2 . Table 2 shows a summary of the concrete and reinforcing steel parameters used for the wall.

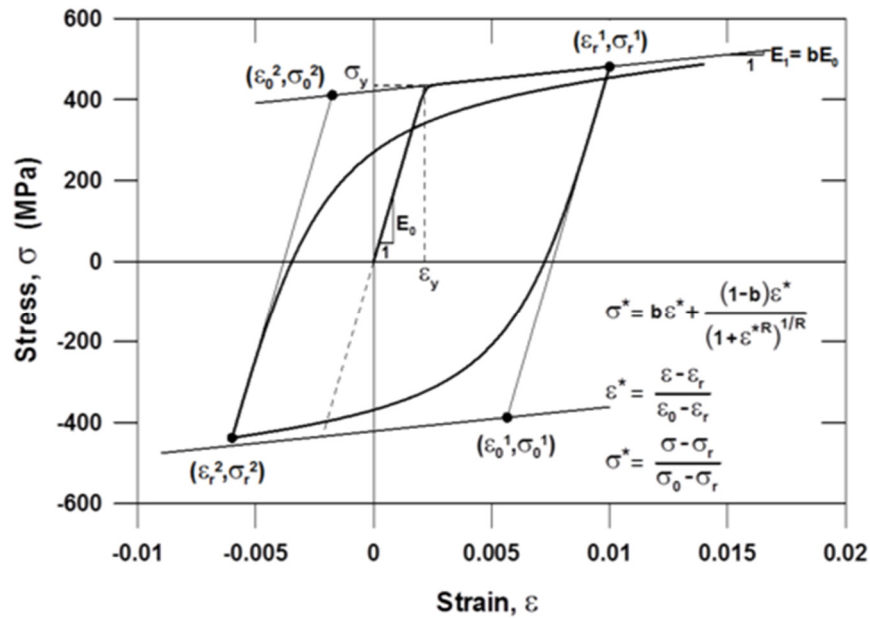


Figure 2. 23 Constitutive Model for Steel (Menegotto and Pinto, 1973)

Table 2. 2 Wall parameters for concrete and steel reinforcement

Concrete (MPa)		Steel (MPa)	
Parameter	Value	Parameter	Value
f_{cm}	55.7786	f_{ypw}	402.724841
E_c	37342.54	f_{ynw}	402.724841
ϵ'_{lc}	0.007558	f_{ypb}	475.738252
f'_{lc}	55.7786	f_{ynb}	475.738252
rc	12.07296	E_0	199947.961
ϵ_{-cr}	1.022	b_w	0.001
f_t	5.227955	b_b	0.002
		R_0	20
		a_1	0.925
		a_2	0.15

2.4 Element Modeling

This section explains the modeling process and elements used in detail. The elements of the frame are modeled using the OpenSees elements, `elasticBeamColumn` and `beamWithHinges`. Figure 2.24 presents the frame nodes distribution and the composition of the elements. The green elements represent those that are modeled using the `elasticBeamColumn` while the blue elements are built using the command `beamwithHinges`. The elastic elements are half the beam depth or half the column width as shown in Figure 2.24. These elements were described previously in Section 2.

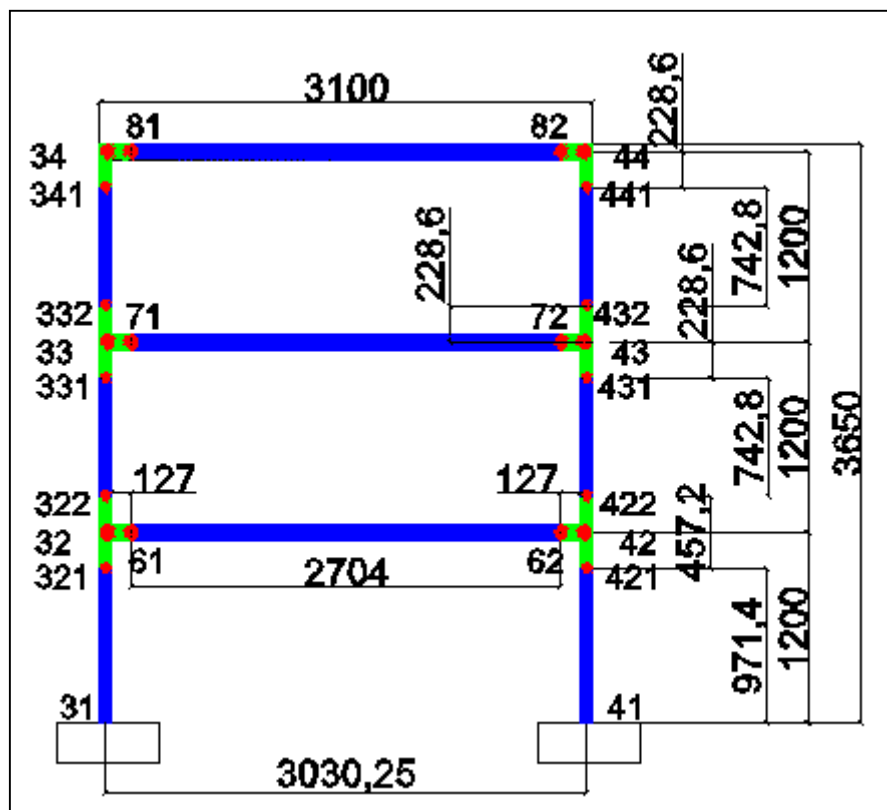


Figure 2. 24 Frame nodal distribution

2.5 Model analysis

The procedure of the analysis is composed by two parts: 1) dynamic analyses of the model under different earthquakes with several moment magnitudes and 2) push-over analysis applied after the dynamic analyses are performed (the model has suffered damage from the earthquakes).

Pushover and cyclic analyses were performed to determine if the model response was appropriate and later to determine several limit states. Pushover analyses were carried out for the two components of the dual-system model (RC frame and wall separated) and for the assembled RC frame-wall dual system model. Figure 2.23 shows the capacity curve (shear vs drift) for the different model components and the whole model. The pushover curves for the wall and the frame have the expected shape. Otherwise, the response of the dual frame model shows a good performance. The maximum capacity for the frame is 91 kips while the wall has 107 kips of maximum capacity. The combined model has a maximum capacity of 237.65 kips.

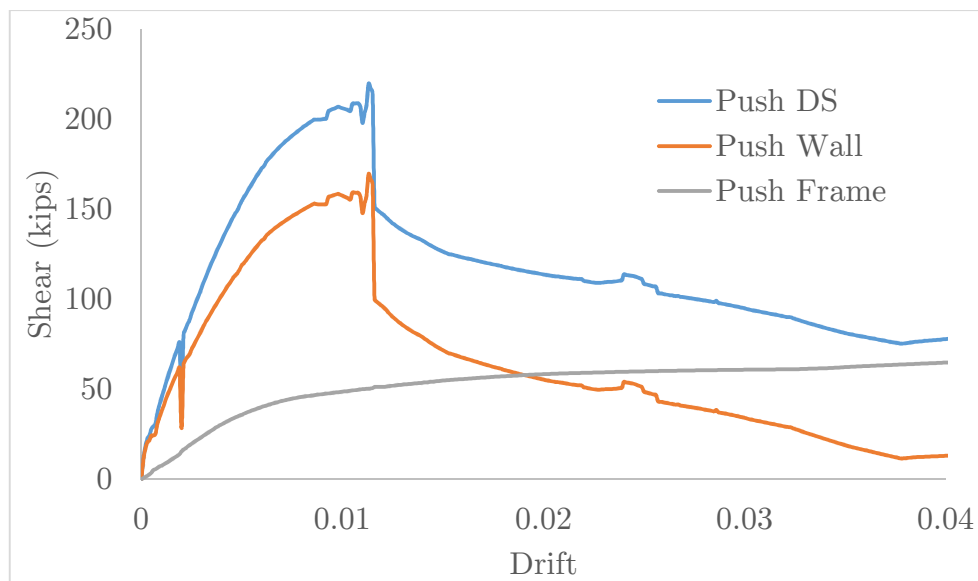


Figure 2. 25 Pushover analysis for each model: Frame, Wall and Dual System.

Additionally, the RC frame-wall model was subjected to cyclic loads. Figure 2.26 presents the results of this analysis compared the response obtained for the two different components and the whole system. Although, the convergence was not achieved completely for the RC frame-wall system model, the results show good correlation with the ones obtained under pushover.

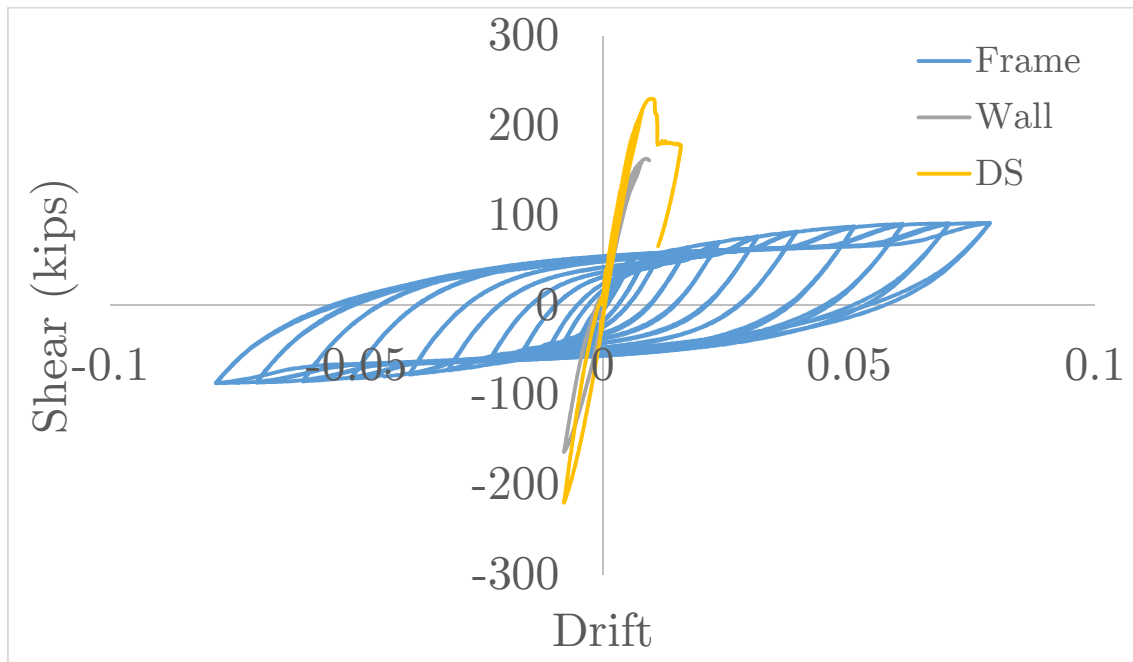


Figure 2. 26 Cyclic analysis for each model: Frame, Wall and Dual System

The next chapter will present the results obtained from the dynamic analyses and will discuss the selection of seed records for the analyses. In addition, the selection of the limit states for the model will be also presented.

Chapter 3. Evaluation of beyond design seismic accelerations

This chapter describes the analysis procedure and methodology used to achieve the objectives of this thesis. The analyses were performed in OpenSees. The objective is to examine the effect of beyond design accelerations in different response parameters of a RC frame-wall dual system model. The model was analyzed under seismic accelerations and a pushover was applied to the structure after applying the seismic accelerations. The model was already damaged before the pushover was applied to determine how the stiffness and strength degrades for different seismic magnitudes. The parameters to be analyzed are the stiffness of the structure, the shear strength and the displacement limit states.

Dynamic analyses

Due to the high variability in the response of structural systems due to ground motions, a total of 20 records compatible with different spectrum were used to perform the dynamic analyses. Twenty earthquake records whose spectra are consistent with the selected spectrum were obtained as seed records from the Pacific Earthquake Engineering Research Center (PEER) database. The initial level of matching of these records was estimated using the root mean square deviation (Drms) proposed by Beyer and Boomer (2007) and shown in Eq. (3.1-3.2). In these equations, $S_{\alpha T}$ is the target spectral acceleration and $S_{\alpha R}$ is the spectral acceleration of the record at period T_i .

$$D_{rms} = \sqrt{\frac{1}{N} \sum_{i=1}^N (aS_{\alpha R}(T_i) - S_{\alpha T}(T_i))^2} \quad (3.1)$$

$$a = \frac{\sum_{i=1}^N S_{\alpha T}(T_i)}{\sum_{i=1}^N S_{\alpha R}(T_i)} \quad (3.2)$$

The target spectrum used for the seed records is the geometric mean (Figure 3.1) from the deterministic spectra for earthquakes in a strike slip fault developed for magnitudes of 5, 5.5, 6, 6.5, 7, 7.5, 8 and 8.5. In this figure, it is also observed the design spectrum used to design the RC frame-wall model. The design spectrum for the specimen is close to the moment magnitude 6 target spectrum. Table 3.1 shows the earthquake name, station, D_{rms} and the parameter a of the selected seed records.

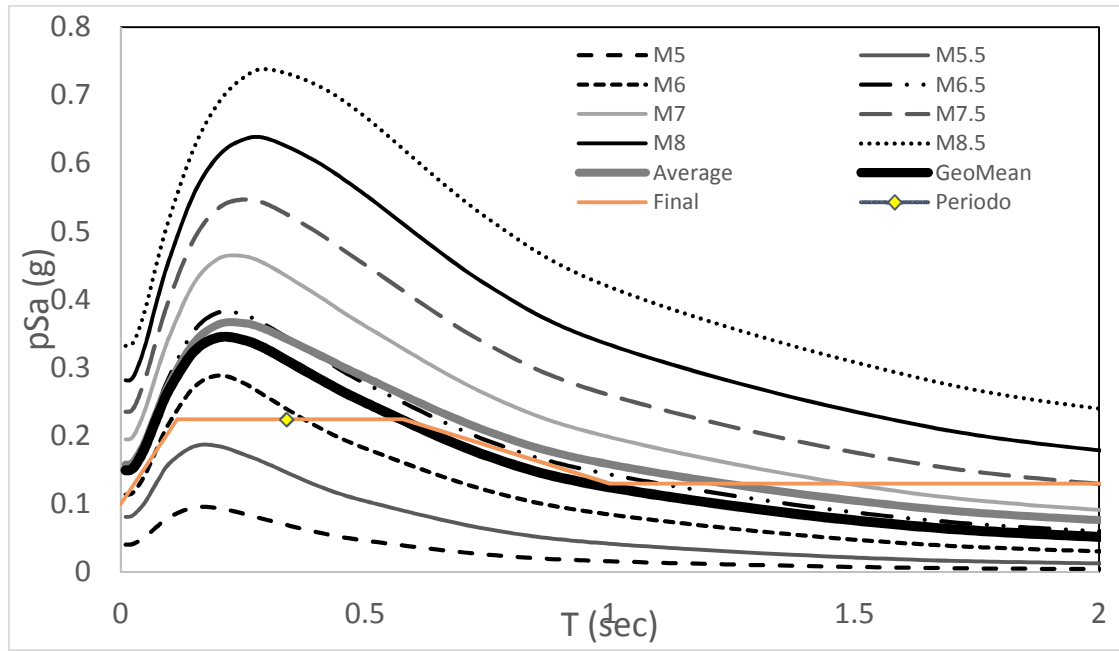


Figure 3. 1 Target and Design Spectra

The program “ArtifQuakeLetII” of Montejo and Suarez (2013) was used to generate compatible earthquake records with the selected spectra. This program uses an improved continuous wavelet transform (CWT) based algorithm for the generation of spectrum compatible records. For each magnitude, a total of 20 compatible records are used for the dynamic analyses (160 total). Figure 3.2 shows the seed earthquakes used for the analyses. Figures 3.3 and 3.4 show the maximum and residual displacements obtained from the dynamic analyses for each moment magnitude. The results show average values obtained from all the earthquakes

used in each magnitude case. As expected, maximum and residuals displacements increase as moment magnitude increases. However, the displacements are not that significant even for magnitudes as high as 8.5.

Table 3. 1 Seed earthquake records selected for the analysis.

RSN	Earthquake Name	Station Name	Earthquake Magnitude	a	Drms
284	Irpinia, Italy-01	Auletta	6.90	2.270567	0.022945
551	Chalfant Valley-02	Convict Creek	6.19	2.227131	0.022188
761	Loma Prieta	Fremont - Emerson Court	6.93	0.922637	0.02393
1549	Chi-Chi, Taiwan	TCU129	7.62	0.213532	0.023107
2093	Nenana Mountain, Alaska	TAPS Pump Station #09	6.70	7.966128	0.020071
2141	Big Bear City	San Bernardino - Fire Sta. #4	4.92	9.490095	0.02553
2162	Chi-Chi, Taiwan-02	CHY027	5.90	5.972799	0.02341
2165	Chi-Chi, Taiwan-02	CHY032	5.90	5.715803	0.025585
2951	Chi-Chi, Taiwan-05	CHY039	6.20	1.851114	0.022915
2982	Chi-Chi, Taiwan-05	CHY088	6.20	1.480533	0.024655
2988	Chi-Chi, Taiwan-05	CHY100	6.20	2.477284	0.025789
3302	Chi-Chi, Taiwan-06	CHY076	6.30	1.018403	0.024609
3320	Chi-Chi, Taiwan-06	CHY111	6.30	1.313881	0.026222
3859	Chi-Chi (aftershock 4), Taiwan	CHY006	6.20	1.521256	0.02498
4163	Niigata, Japan	FKSH03	6.63	1.809186	0.021162
6893	Darfield, New Zealand	DFHS	7.00	0.319518	0.025989
8163	El Mayor-Cuapah	SANTA ISABEL VIEJO	7.20	4.408169	0.02349
8233	Anza-02	Fountain Valley, I-5	4.92	61.91251	0.024176
8689	40204628	Black Mountain Los Altos	5.45	15.12428	0.022504
20712	21437727	Mountain View; Fire Station 3 Nor	4.18	186.9711	0.025885

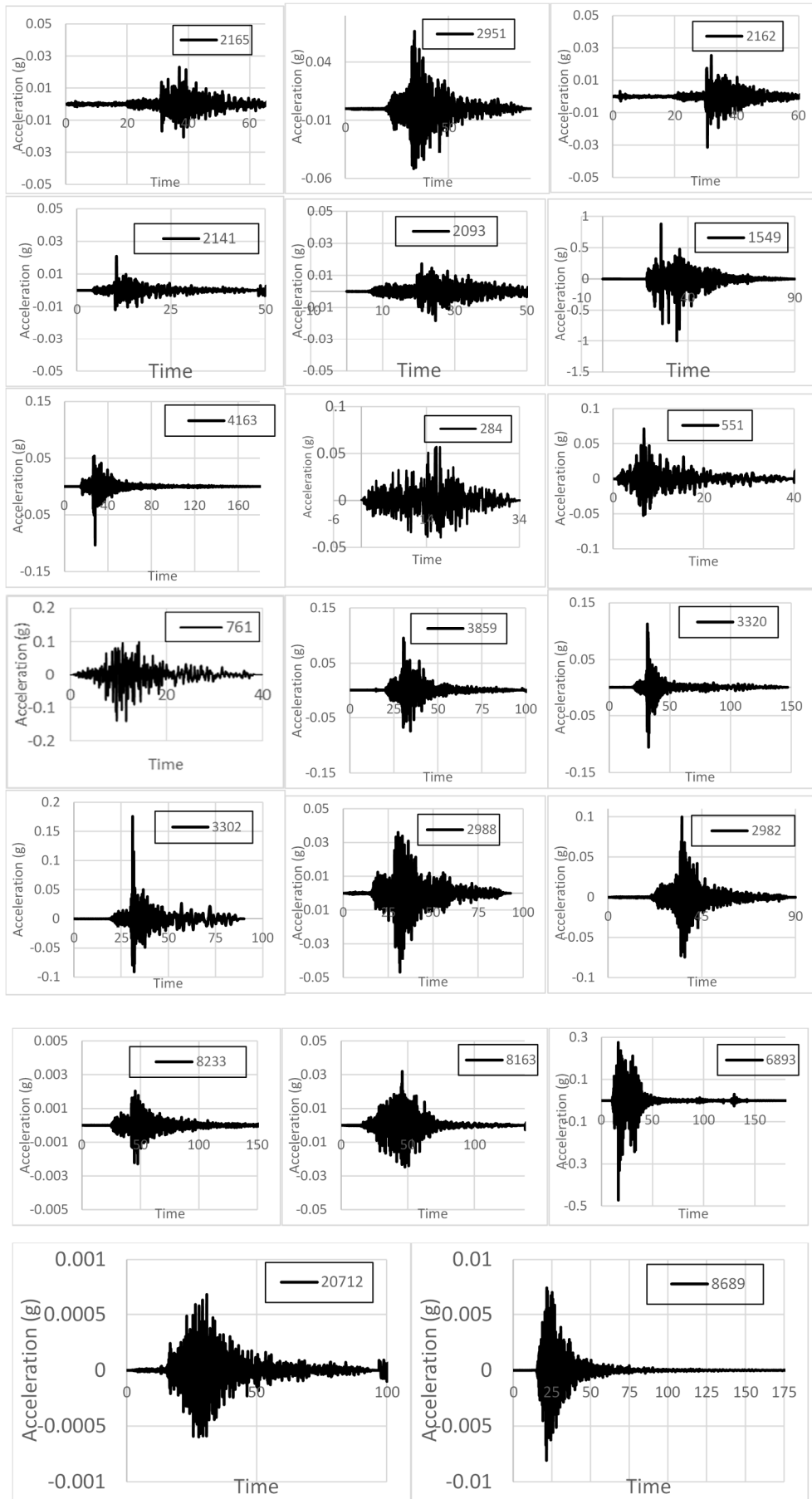


Figure 3. 2 Earthquake seeds for the analysis

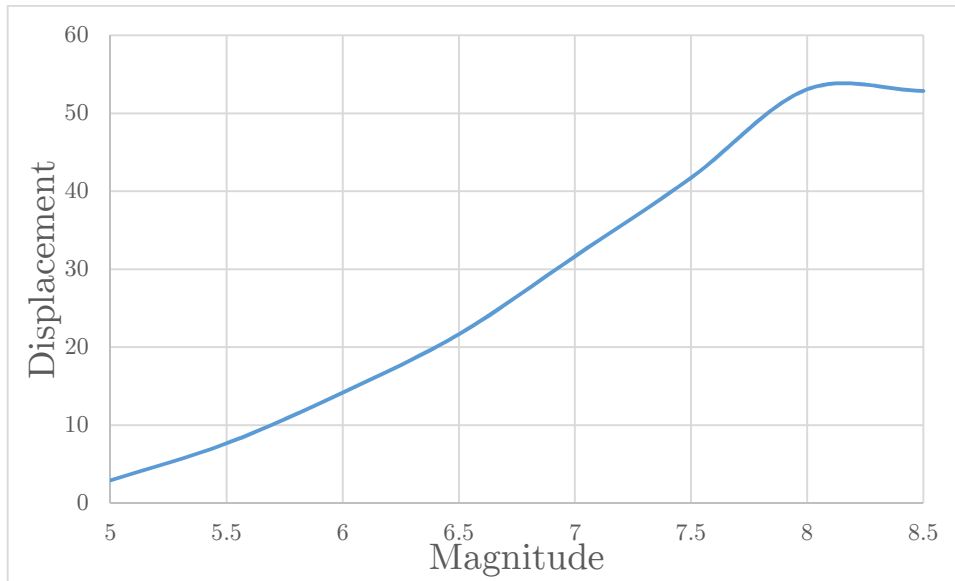


Figure 3. 3 Maximum displacement for dynamic analysis (in mm).

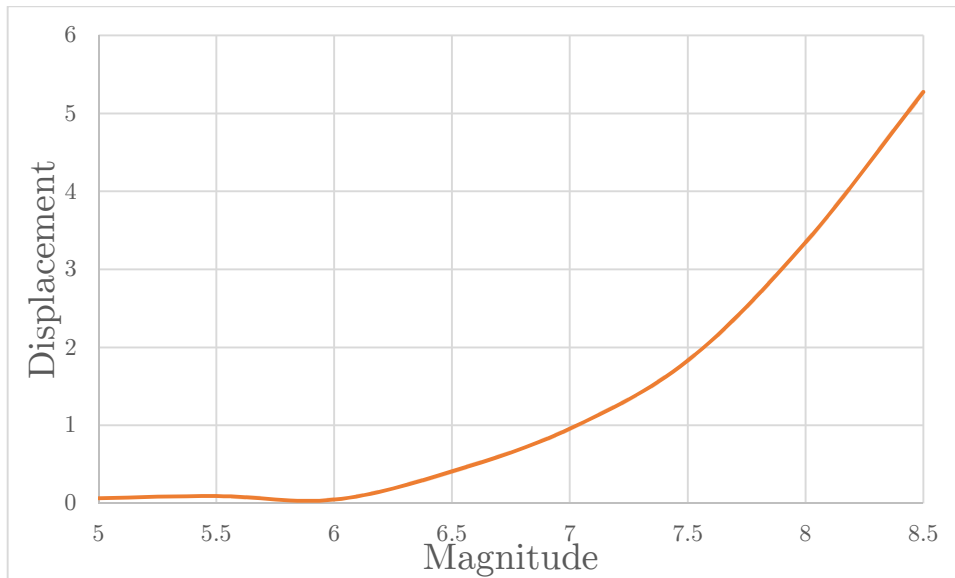


Figure 3. 4 Residual displacement from dynamic analysis (in mm).

The total length of each acceleration vector is twice the original length of the earthquake. The first half is the earthquake itself and the other half is a vector composed by zeros. The purpose of the zeros is to assure that the structure comes to rest before the pushover is applied. Then, the pushover was applied to the structure until a 0.1 % drift is achieved. Table 3.2 shows the drift results obtained from the dynamic analysis. A total of 130 of 160 cases were completed with the total earthquake duration and the pushover applied representing 81.25 % of the

total cases. There are several earthquake cases that failed to complete the dynamic analysis. The analysis tolerances were modified to reach convergence. Both analyses, pushover and dynamic, have different tolerances. There were several cases that although the dynamic and static tolerances were combined it was impossible to achieve analysis convergence. In order to collect the largest number of data it was determined that 15 earthquakes were sufficient. For equal or lower moment magnitudes than 6 (moment magnitude that coincides with the design spectrum for the natural period), the analysis is stable and most of the cases were completed. For higher moment magnitudes, the convergence became more difficult. For the highest magnitudes only 14 or 13 cases were run completely.

Table 3. 2 Cases completed after applying seismic load and pushover analysis (Maximum Drift).

Earthquake	M5 (Drift)	M5.5 (Drift)	M6 (Drift)	M6.5 (Drift)	M7 (Drift)	M7.5 (Drift)	M8 (Drift)	M8.5 (Drift)	Completed
284	0.1001	0.1001	0.0000	0.1002	0.0792	0.1001	0.0795	0.0695	7
551	0.1001	0.0153	0.1001	0.0000	0.1002	0.0000	0.0943	0.1001	6
761	0.0513	0.1001	0.1002	0.1001	0.1001	0.0516	0.0418	0.0528	8
1549	0.1002	0.1001	0.1001	0.1002	0.0218	0.0503	0.0000	0.0010	7
2093	0.1002	0.1002	0.1002	0.1002	0.1001	0.0000	0.0054	0.0882	7
2141	0.1001	0.0758	0.1001	0.1002	0.1002	0.0474	0.0001	0.1001	8
2162	0.1001	0.1001	0.0157	0.0697	0.1002	0.0359	0.1001	0.0762	8
2165	0.0210	0.0136	0.0136	0.1001	0.0860	0.0692	0.1001	0.0576	8
2951	0.0805	0.0145	0.1002	0.1002	0.0693	0.0943	0.0000	0.0000	6
2982	0.0576	0.1001	0.1001	0.0991	0.0000	0.0492	0.1001	0.0000	6
2988	0.1001	0.1001	0.1002	0.1002	0.0000	0.0000	0.0718	0.1002	6
3302	0.1001	0.1001	0.0611	0.1002	0.1001	0.1002	0.0744	0.1002	8
3320	0.1001	0.0000	0.0392	0.1001	0.0809	0.0000	0.1001	0.0193	6
3859	0.1001	0.1001	0.0345	0.1001	0.0780	0.0664	0.0000	0.1001	7
4163	0.1001	0.1002	0.1001	0.0000	0.0000	0.1002	0.0761	0.0799	6
6893	0.0727	0.1001	0.1002	0.0000	0.1002	0.0000	0.0000	0.0000	4
8163	0.0661	0.1001	0.1002	0.1001	0.0457	0.1001	0.0000	0.0787	7
8233	0.1001	0.1001	0.0697	0.1001	0.0000	0.1002	0.0485	0.0000	6
8689	0.0512	0.1001	0.1001	0.0838	0.0000	0.1002	0.0000	0.0707	6
20712	0.1001	0.1002	0.0000	0.1001	0.1001	0.0000	0.0000	0.0000	4
Total	20	19	18	17	15	14	13	14	130
% Occur	100	95	90	85	75	70	65	70	81.25

3.1 Analysis Parameters

The analysis is composed of three parts. First, the structure is analyzed under a pushover to assess its capacity. Second, the structure is excited with seismic load, producing damage in the system. Third, a pushover is applied when the seismic

load ends in order to determine how the stiffness and strength degrades for different seismic magnitudes. The dynamic analyses were performed using compatible records with target spectra for moment magnitudes from 5 to 8.5 as described in a previous section. For the purpose of this study, for each moment magnitude case, the average of the pushover curves obtained after each dynamic analysis was used. The resulting curve represents the average damage produced in the structure for each moment magnitude. To quantify the damage in the model, several parameters were studied in the average pushover curves, comparing these parameters with the respective ones in the pushover before the seismic accelerations were introduced.

The parameters that were analyzed are the following:

1. Stiffness of the structure
2. Shear strength
3. Displacement limit states.

3.2 Stiffness Degradation

The first parameter under study is the stiffness change in the structure. The degradation of the stiffness was calculated after the pushover was applied when the seismic load ends. The stiffness was analyzed in three points for each spectrum/earthquake case. The stiffness was determined at three points along the pushover curve: (1) at 15% V_u , (2) at 60% V_u and (3) when V_u (maximum shear) occurs. The case of 15 % of V_u , which represents the initial stiffness of the structure, was used by Luna (2015) to obtain the initial stiffness on RC wall specimens. The stiffness for each case was obtained as the slope of the curve (pushover response) in the points described using the shear and displacement at each point. Equation (3.3) presents the slope as the quotient between the shear force reached and the displacement achieved at the selected point.

$$K = \frac{F}{d} \quad (3.3)$$

Table 3.3 shows the average stiffness, drifts and shears from the different earthquakes in each spectrum case obtained from the analyses for the different points and magnitudes. In order to quantify the stiffness degradation, a ratio was used. The ratio of the stiffness calculated after the seismic load and pushover was applied with the stiffness before damage obtained from a pushover curve (Equation 3.4). Table 3.4 shows the ratio of stiffness calculated from all the analyses.

$$Ratio_{Stiffness-Wastage} = \frac{Stiffness\ after\ earthquake}{Stiffness\ before\ earthquake} \quad (3.4)$$

Table 3. 3 Stiffness for pushover analyses after dynamic analyses for different seismic magnitudes

<i>Dynamic analysis (Maximum average)</i>									
	Push Before	M5	M55	M6	M65	M7	M75	M8	M85
K15%Vu	21.80	29.03	24.51	20.00	16.12	14.72	14.17	12.37	12.62
Drift	0.001	0.001	0.001	0.001	0.001	0.001	0.001	0.001	0.001
Base Shear	158.6	140.8	141.2	141.5	141.1	140.8	130.9	138.2	137.7
K60%Vu	16.66	16.61	16.50	16.43	16.24	15.84	13.76	13.36	11.62
Drift	0.004	0.004	0.004	0.004	0.004	0.004	0.004	0.004	0.005
Base Shear	634.3	563.0	565.0	565.8	564.3	563.2	523.4	552.8	550.7
KVu	11.382	9.096	9.646	9.493	9.414	9.274	8.775	7.974	8.348
Drift	0.010	0.011	0.011	0.011	0.011	0.011	0.011	0.012	0.012
Base Shear	1057.1	938.4	941.6	943.0	940.4	938.6	872.3	921.3	917.8

Table 3. 4 Stiffness ratio for pushover analyses after dynamic analyses for different seismic magnitudes

Ratio (Kafter/Kbefore)								
	M5	M55	M6	M65	M7	M75	M8	M85
K15%Vu	1.332	1.125	0.917	0.739	0.675	0.650	0.567	0.579
K60%Vu	0.997	0.991	0.987	0.975	0.951	0.826	0.802	0.698

KVu	0.799	0.847	0.834	0.827	0.815	0.771	0.701	0.734
-----	-------	-------	-------	-------	-------	-------	-------	-------

Figure 3.3 shows the change of stiffness for the different moment magnitude cases. The initial stiffness presents a pronounced degradation in moment magnitudes from 5 to 6.5. This degradation is directly related with the damage experienced in the structure. For moment magnitudes higher than 6.5 the degradation of the initial stiffness becomes less marked. Moreover, the stiffness for both 60%Vu and at Vu presents a softer behavior than the initial stiffness. For moment magnitudes below design considerations the degradation is less pronounced, whereas when the moment magnitude 6 is exceeded the degradation becomes sharper. For moment magnitudes higher than 7, the degradation for 60%Vu and at Vu become more pronounced and, the degradation is more significant. The initial stiffness suffers a degradation more pronounced than at the others two points.

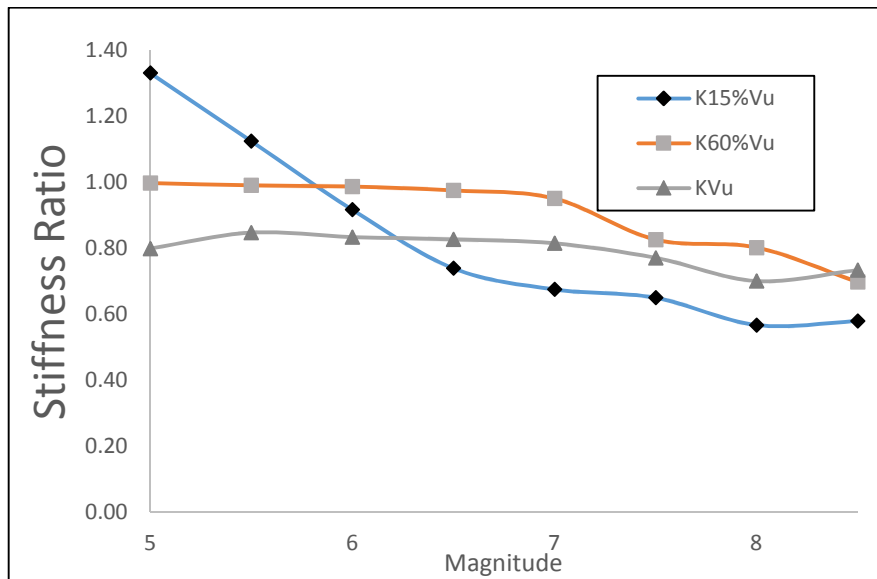


Figure 3. 5 Stiffness ratio as function of the seismic moment magnitude

3.3 Strength Degradation

The strength was analyzed using the peak shear strength obtained from the pushover curves before and after the earthquakes were applied. The peak shear value (Vu) was obtained in all the cases with the respective drift to achieve the

peak V_u . For the purpose of the study an average was performed from the earthquake cases for each moment magnitude. Table 3.5 presents the peak shear value and the drift reached for each moment magnitude and the pushover before the earthquake was applied. In order to quantify the strength degradation a ratio of the peak shear for the pushover after the earthquake to the peak shear before the earthquakes is used (Equation 3.5). Table 3.6 shows the values of the ratio for each moment magnitude.

$$Ratio_{Capacity} = \frac{Capacity\ after\ earthquake}{Capacity\ before\ earthquake} \quad (3.5)$$

The ratio presents a slightly decrease while the moment magnitude increases. It can be observed that for moment magnitudes lower to the design considerations the shear capacity suffers small changes when compared to smaller magnitudes cases. For moment magnitudes onwards of 6, the shear capacity in the average pushover curves decays. As it is expected, the shear capacity for each case is lower than the shear capacity before the earthquakes were applied. The drift at which the peak shear occurs is almost constant from all the cases studied, with an almost imperceptible increase for larger earthquakes. A reduction in the shear capacity from 11 to 13% is observed. Figure 3.4 presents the average pushover curves obtained from the analysis after the application of the seismic loads for the different moment magnitudes and the original pushover curve obtained before the seismic loads were applied. The peak shear tends to occur later as the moment magnitude increases. For the cases of M8 and M8.5, after the peak shear, the curve is flatter than the rest of the pushover curves. In general, the post peak response shows a stepper decrease in capacity for seismic magnitudes higher than 5 and the response tends to shift at the same time that the moment magnitude increases.

Table 3. 5 Strength for pushover analyses after dynamic analyses for different seismic magnitudes

Push analysis (Average)									
	Push Befor	M5	M55	M6	M65	M7	M75	M8	M85
Drift	0.010	0.011	0.011	0.011	0.011	0.011	0.011	0.012	0.012
Base Shear	1057.1	938.4	941.6	943.0	940.4	938.6	872.3	921.3	917.8

Table 3. 6 Strength ratio for pushover analyses after dynamic analyses for different seismic magnitudes

Ratio (Vafter/Vbefore)							
M5	M55	M6	M65	M7	M75	M8	M85
0.888	0.891	0.892	0.890	0.888	0.825	0.872	0.868

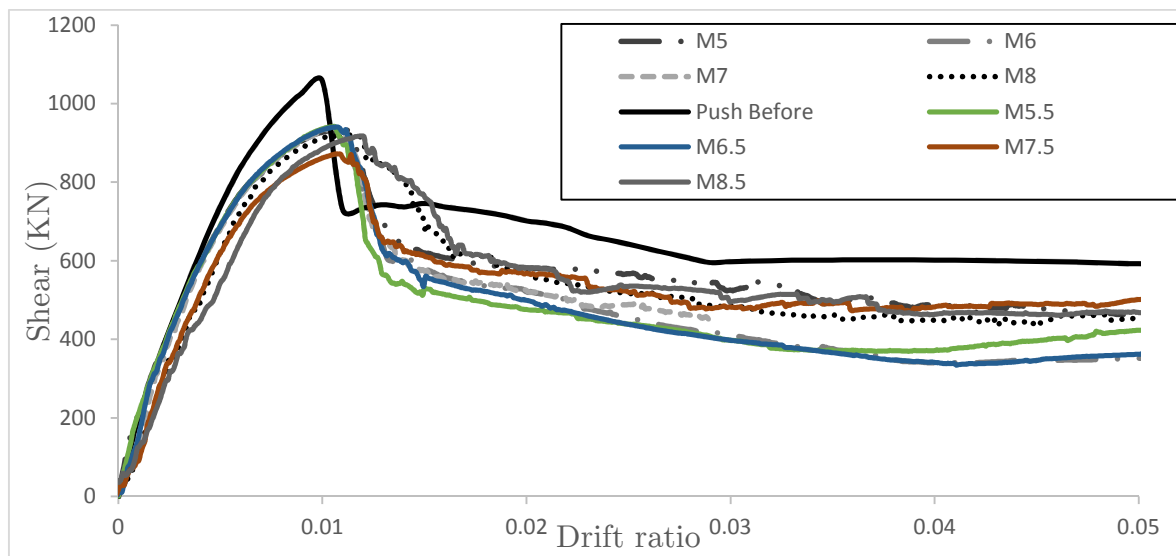


Figure 3. 6 Pushover curves before and after seismic load

3.4 Displacement/strain limit states

The strain limit states were evaluated in the pushover analyses post-earthquake average curves. From the pushover analyses before the seismic loads the strain limits were obtained. Both concrete and reinforcement steel strains were

considered to reach these limit states. The strain limits were studied in three points: (1) yielding, (2) serviceability and (3) damage control. The yielding point was defined when the strain of the steel achieves the value of 0.002 according to the reinforcing steel yield strength value. The serviceability limit state is defined at a concrete compression strain of 0.004 or steel tension strain of 0.015, whichever occurs first as suggested by Priestley et al. (1996) in the section. The damage control points for concrete and steel in compression, were defined as 0.018 or 0.06, respectively (Priestley et al., 1996), whichever occurs first in the section. For each element of each model the strain limit states were determined and at these points, the drifts and shears were obtained. Figures 3.5 and 3.6 present these parameters for the frame and the wall of the model. The strain limit states for the RC dual frame model are summarized in the Figure 3.7. Table 3.6 shows the drift and shear at which each of the limits attained in the beam and columns of the frame. The yielding point is dominated by the section of the columns with a drift of 0.004. The serviceability limit is controlled by the section in the beam 2 (second floor beam) and both columns with a drift of 0.008. Finally, the damage control was dominated by the section in the beam 2 with a drift of 0.022. The wall limit states do not control.

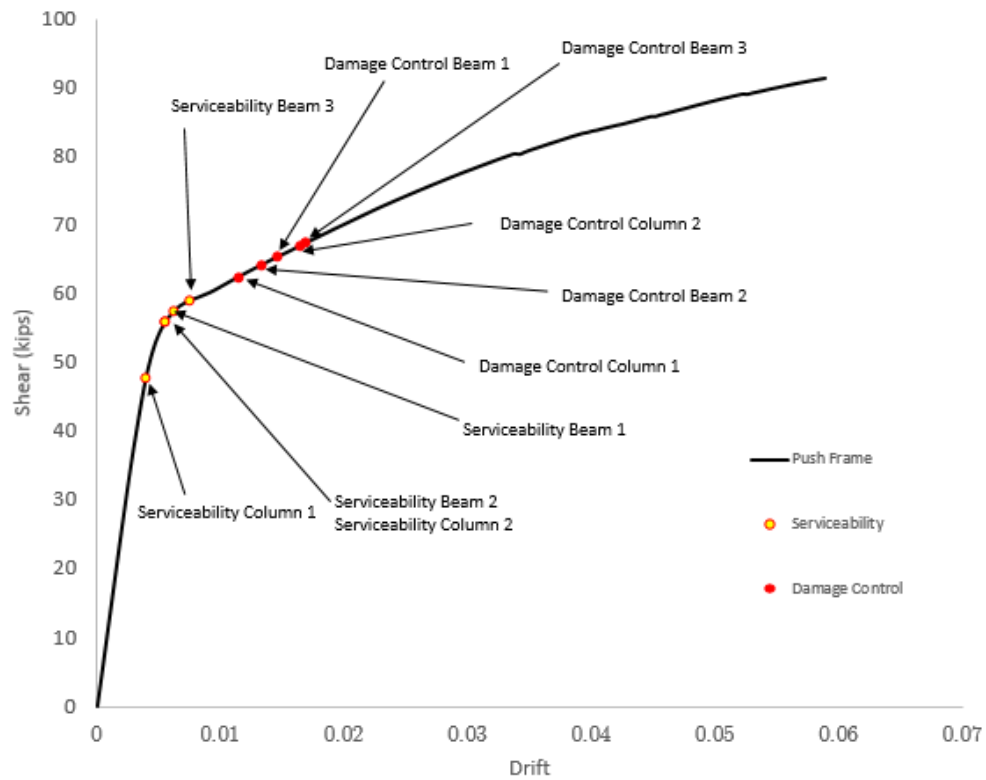


Figure 3. 7 Pushover state limits analysis for the frame specimen

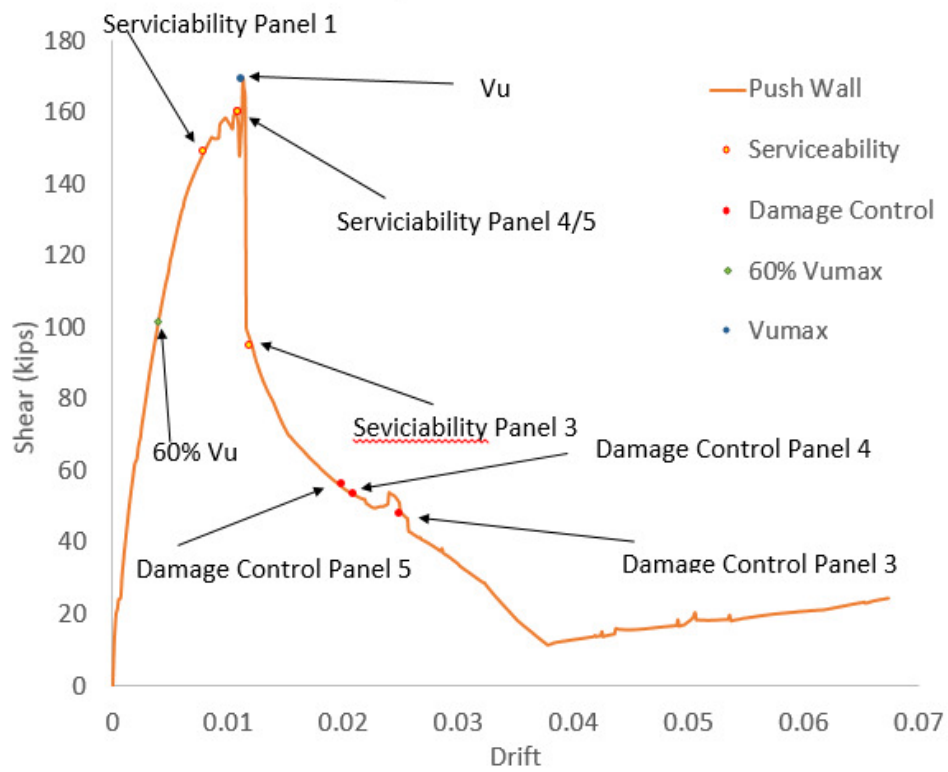


Figure 3. 8 Pushover state limits analysis for the wall specimen

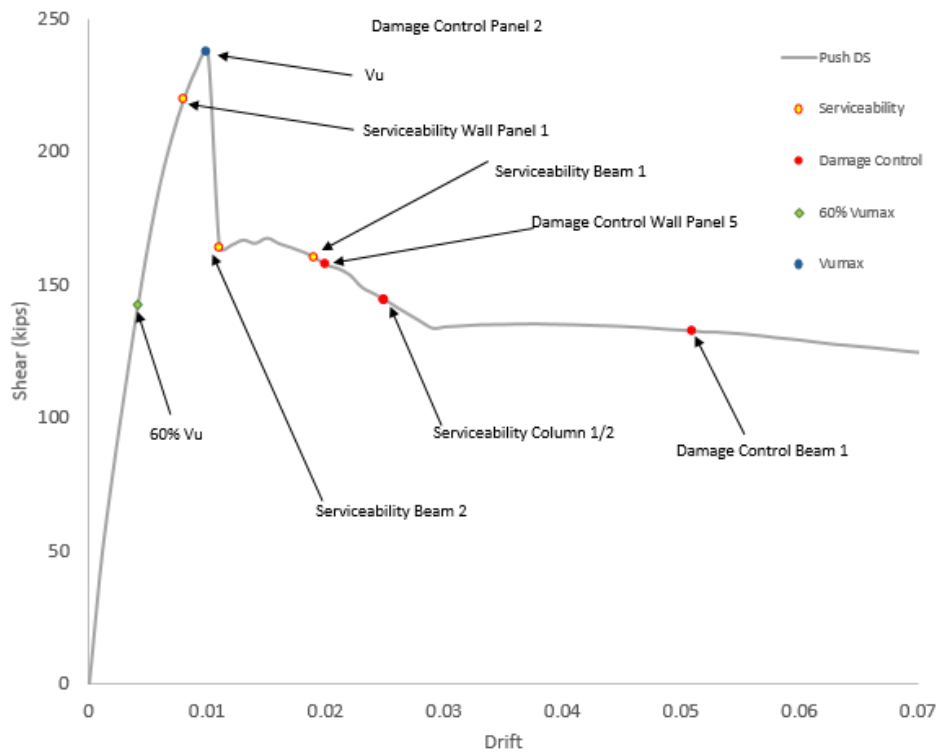


Figure 3. 9 Pushover state limits analysis for the DS specimen.

For most of the cases, the concrete strain dominated the steel strain for the strain limits. Furthermore, the deformation in the frame controls over the deformation in the wall due to its rigidity (the wall limit states do not control in the analysis), which implies that the elements taken for the damage analysis are those of the frame. With these strain limits, the drifts are identified for each state. Table 3.7 summarizes the drift and the shear for each strain state limit attained in the frame. The yielding point is dominated by the section in the columns with a drift of 0.004, whilst the serviceability limit is controlled by the section in the beam 2 (second floor beam) and both columns with a drift of 0.008. Finally, the damage control point is dominated by the section in the beam 2 with a drift of 0.0022. As expected, the columns are the first sections where the damage is significant, in both states yielding and serviceability, and for the damage control state the columns are the last reaching this state limit. The damage control limit state in the beam 3 was not reached, there was not enough displacement to achieve this state for that element. Table 3.8 shows the shears obtained for the different limit states and seismic magnitudes for the average pushover curves. A ratio between the shear at strain limit after and before earthquake were calculated (Equation 3.6). Table 3.9 presents the ratio obtained for each limit state and moment magnitude.

$$Ratio_{V_{after}/V_{before}} = \frac{\text{Shear at strain limit after earthquake}}{\text{Shear at strain limit before earthquake}} \quad (3.6)$$

Table 3. 7 Sequence of strain limits in the Pushover analysis before seismic loads.

Strain limit	Element	Drift	Shear (kips)	Shear (KN)
Yield	Column 1	0.004	139.51	620.57145
	Column 2	0.004	139.51	620.57145
	Beam 1	0.01	237.6488	1057.1146
	Beam 2	0.005	165.9552	738.20557
	Beam 3	0.008	220.0434	978.80188
Serviceability	Column 1	0.008	220.0434	978.80188
	Column 2	0.008	220.0434	978.80188
	Beam 1	0.015	167.6911	745.92723
	Beam 2	0.008	220.0434	978.80188
	Beam 3	0.035	135.25091	601.62607
Damage Control	Column 1	0.054	132.07204	587.48575
	Column 2	0.054	132.07204	587.48575
	Beam 1	0.046	134.28493	597.32917
	Beam 2	0.022	153.8296	684.2682
	Beam 3	0	0	0

Table 3. 8 Strain limits for pushover analyses after dynamic analyses for different seismic magnitudes

		Push analysis (Average)								
		Push Beto	M5	M55	M6	M65	M7	M75	M8	M85
Yield	Drift	0.004	0.004	0.004	0.004	0.004	0.004	0.004	0.004	0.004
Column 1	Base Shear	620.571	597.5	588.2	596.2	592.6	584.4	514.9	494.4	447.8
Serviceability	Drift	0.008	0.008	0.008	0.008	0.008	0.008	0.008	0.008	0.008
Column 1	Base Shear	978.802	872.9	873.2	869.8	875.4	871.3	807.1	853.1	810.7
Damage Control	Drift	0.022	0.022	0.022	0.022	0.022	0.022	0.022	0.022	0.022
Beam 2	Base Shear	684.268	577.8	466.9	501.3	472.4	498.4	558.2	542.4	547.7

Table 3. 9 Strain ratio for pushover analyses after dynamic analyses for different seismic magnitudes

		Ratio (Vafter/Vbefore)							
Strain limit		M5	M55	M6	M65	M7	M75	M8	M85
Yield		0.963	0.948	0.961	0.955	0.942	0.830	0.797	0.722
Serviceability		0.892	0.892	0.889	0.894	0.890	0.825	0.872	0.828
Damage Control		0.844	0.682	0.733	0.690	0.728	0.816	0.793	0.800

For the yielding and serviceability limit states, the shears obtained tend to slightly decrease as the seismic magnitude increases, but, the tendency is almost constant until magnitude 7. After moment magnitude 7, the decrease is more

significant. Although the serviceability points have a similar behavior, the decrease for moment magnitude largest than 7 is less pronounced. When compared with the undamaged situation (before dynamic excitation), the yielding and serviceability states occur at a higher shear than when the model already has some damage after the seismic loads. The reduction of shear at yielding is more significant than for the serviceability limit state. The damage control shears present a more erratic behavior. For moment magnitudes lower than 6, the shear tends to decrease while for moment magnitude higher or equal to 7, the shear reached to achieve the limit drift in the pushover curve increase, remaining almost constant for the largest moment magnitudes.

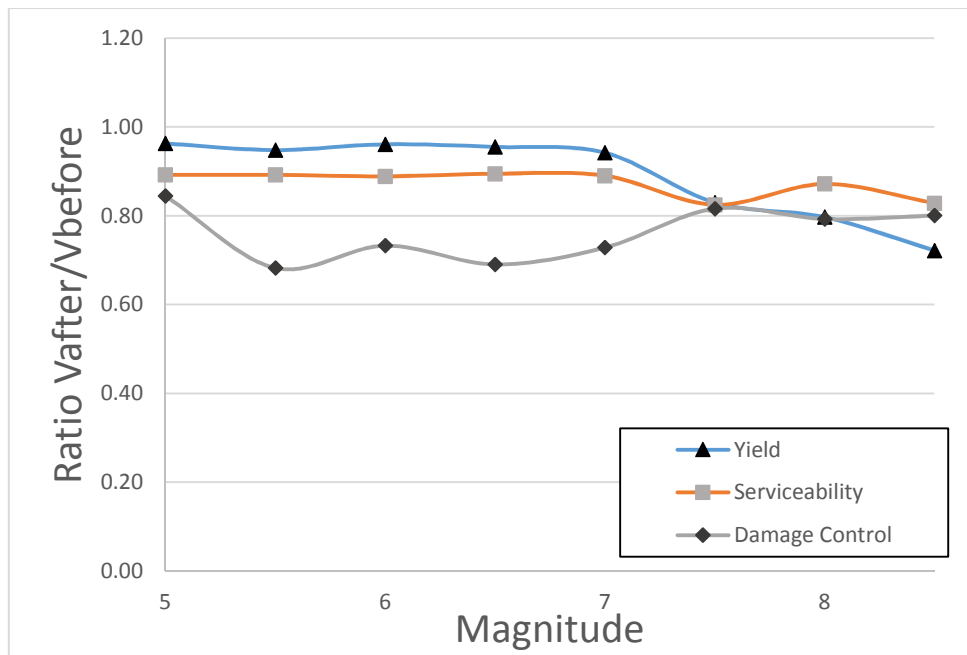


Figure 3. 10 Strain ratio as function of the seismic moment magnitude

3.5 Summary of Results

This chapter studied the effects of beyond design seismic accelerations in the response of a RC-wall-frame dual model, analyzing the degradation produced in the structure under seismic excitations exceeding design considerations. Earthquakes with target spectra for magnitudes larger than 6 exceed the design

spectrum considerations. The parameters to be analyzed are the stiffness of the structure, the shear strength and the displacement limit states. The initial stiffness decreases significantly as the moment magnitude increases. The stiffness degradation at 60% of peak shear and at the peak shear is less pronounced. However, as the moment magnitude increases the degradation becomes more significant, being more relevant when the design spectrum has been overcome. The initial stiffness suffers a degradation more pronounced than at the others two points. However, the decrease in the shear capacity after the seismic loads were applied are less pronounced than the stiffness changes. The shear capacity for each case is lower than the shear capacity before the earthquakes are applied. Moreover, the peak shear tends to occur at larger drifts as the moment magnitude increases. The post peak response shows a stepped decrease in capacity and the response tends to shift at the same time that the moment magnitude increases. Furthermore, the study of the limit states denotes a reduction of the shear needed, after moment magnitude 7, for the yielding and serviceability limit states to occur. The damage control shears presented more variability. Finally, Chapter 4 will include aging effect in the reinforced steel bar in the study of beyond design considerations.

Chapter 4. Evaluation of beyond design seismic accelerations considering aging effects

This chapter describes the analysis procedure and methodology used to achieve the objectives when the aging effect in the reinforcing steel bars is considered. The analyses were also performed in OpenSees. The objective is to examine the effect of beyond design accelerations in different response parameters of a RC frame-wall dual system model including the reinforcing steel aging mainly due to corrosion effects. The model considering the reduction in area in the reinforcing steel bars due to corrosion is analyzed under seismic accelerations and then a pushover is applied to the structure after applying the seismic accelerations. The model is already damaged before the pushover in order to determine how the stiffness and strength degrades for different seismic magnitudes. Similar as for the model without aging of reinforcing steel, the parameters to be analyzed are the stiffness of the structure, the shear strength and the displacement limit states.

4.1 Aging effects considerations

In Chapter 1 several methods to calculate the aging effect from different investigations were discussed and analyzed. For the purpose of this thesis, the methodology proposed by Ghosh et al. (2010) to introduce aging effects in the reinforcing steel in the analyses of reinforced concrete structures was selected. This research provides a framework for time-dependent fragility analysis of corroded bridges performance in seismic events, illustrating the impact of aging on component and system reliability and was described previously in Chapter 1. Basically, they proposed an equation (Eq. 1.1) to account for the loss of diameter in the reinforcing steel due to corrosion. This reduction is then incorporated in the model. The RC frame-wall dual system model has the same material and geometric properties as described in Chapter 2. The only difference is the

reduction in reinforcing steel area calculated according to the equation of Ghosh et al. (2010). The reduction selected was of 25 % of the total steel sectional area, for the longitudinal bars in both wall and frame. The transversal steel remains without any reduction in the cross section.

The model was analyzed under pushover loads to assess its capacity before the dynamic analyses. Figure 4.1 shows the shear vs. drift response of the structure when the pushover loads were applied comparing the capacity obtained before and after the aging effects were applied. The shear capacity suffers a significant reduction of the maximum peak. Also, the stiffness of the model is greatly reduced due to the decreasing in the slope of the curve until the peak strength. The pushover curve after applying the aging effects has a more jagged form due to the difficulties of convergence in OpenSees. The results with aging of the reinforcing steel were smoothed by applying a moving average, resulting in the curve presented.

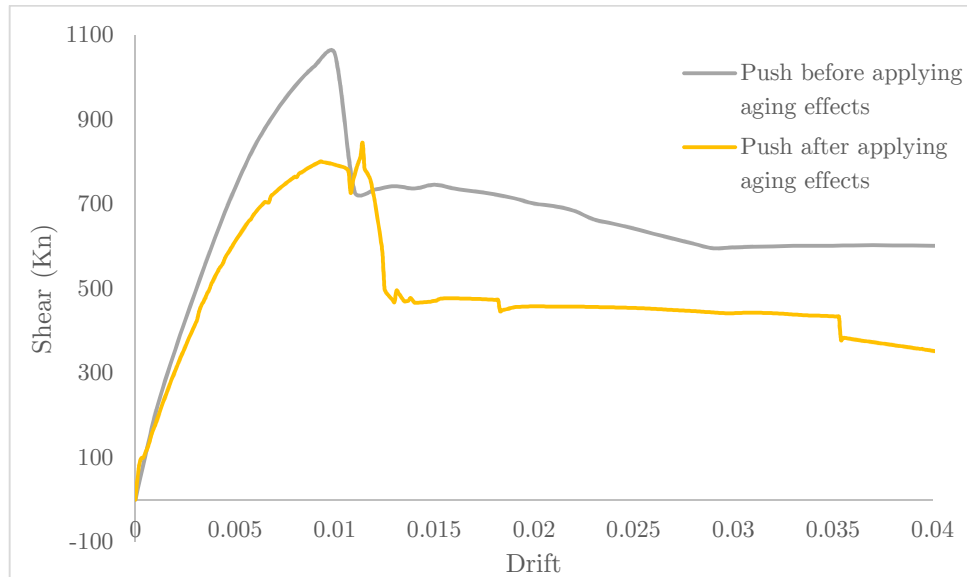


Figure 4. 1 Pushover before and after applying aging effects.

4.2 Analysis Parameters

The generalities of the analyses were presented in the Chapter 3. For the purpose of the study, to quantify the damage in the model, the same parameters were studied in the average pushover curves, comparing these parameters with the respective ones in the pushover before the seismic accelerations were introduced.

The parameters that were analyzed were the following (similar as in Chapter 3):

4. Stiffness of the structure
5. Shear strength
6. Displacement limit states.

A total of 141 of 160 cases were completed with the total earthquake duration and the pushover applied representing 88.125 % of the total cases. There are several earthquake cases that failed to complete the dynamic analyses. The analysis tolerances were modified to reach convergence. Both analyses, pushover and dynamic, have different tolerances. There were several cases that although the dynamic and static tolerances were combined it was impossible to achieve analysis convergence. In order to collect the largest number of data it was determined that 15 earthquakes were sufficient. For moment magnitudes equal or lower than 7, the analyses were stable and most of the cases were completed. For higher moment magnitudes, the convergence became more difficult. Table 4.1 shows the maximum drift obtained from all the cases. It also shows the number of cases that were run completely.

Table 4. 1 Cases completed after applying seismic load and pushover analysis (Maximum Drift).

Earthquake	M5 (Drift)	M5.5 (Drift)	M6 (Drift)	M6.5 (Drift)	M7 (Drift)	M7.5 (Drift)	M8 (Drift)	M8.5 (Drift)	Completed
284	0.1001	0.1001	0.0170	0.1002	0.1002	0.1002	0.1002	0.1001	8
551	0.1001	0.1001	0.1002	0.1001	0.1002	0.0538	0.0620	0.0123	8
761	0.1002	0.0208	0.1001	0.0986	0.0994	0.1001	0.0690	0.0524	8
1549	0.1002	0.1002	0.1001	0.1002	0.1002	0.0628	0.0161	0.0327	8
2093	0.1001	0.1001	0.1001	0.1001	0.1002	0.1001	0.0412	0.0138	8
2141	0.1001	0.1001	0.1002	0.1001	0.1002	0.1002	0.1001	0.0030	8
2162	0.1001	0.1001	0.1001	0.1001	0.1001	0.0253	0.0744	0.0315	8
2165	0.1001	0.0130	0.1002	0.1002	0.1001	0.0000	0.0000	0.0790	8
2951	0.1001	0.1001	0.1001	0.1002	0.1001	0.0991	0.0924	0.0712	6
2982	0.1001	0.1001	0.0000	0.0957	0.1002	0.0142	0.1002	0.1001	8
2988	0.0335	0.1001	0.1001	0.1002	0.0102	0.0805	0.0497	0.0863	7
3302	0.0903	0.1001	0.1001	0.1002	0.0488	0.0947	0.0557	0.0725	8
3320	0.1001	0.0461	0.1002	0.1001	0.0000	0.0665	0.0000	0.0804	8
3859	0.0653	0.0148	0.1002	0.1002	0.0000	0.0000	0.0000	0.0000	6
4163	0.0613	0.1001	0.1001	0.1002	0.0686	0.0000	0.0668	0.0000	4
6893	0.1001	0.1001	0.0423	0.1001	0.1002	0.0737	0.0723	0.0000	6
8163	0.1001	0.1001	0.0000	0.1002	0.0015	0.0000	0.0761	0.0071	7
8233	0.1001	0.1002	0.1001	0.0000	0.0000	0.0844	0.0000	0.0846	6
8689	0.1001	0.1002	0.0000	0.1002	0.1002	0.0551	0.1002	0.1002	5
20712	0.0547	0.0547	0.0465	0.0520	0.0438	0.0438	0.0438	0.0465	7
Total	20	20	17	19	16	16	16	17	141
% Occur	100	100	85	95	80	80	80	85	88.125

4.3 Stiffness Degradation

The first parameter under study is the stiffness change. Similar as in Chapter 3 for each spectrum/earthquake case, the stiffness was analyzed at three points. The stiffness was determined at three points along the pushover curve: (1) at 15% V_u , (2) at 60% V_u and (3) when V_u (maximum shear) occurs. The stiffness for each case was obtained as the slope of the curve (pushover response) in the points described using the shear and displacement at each point. Table 4.2 shows the average stiffness, drifts and shears from the different earthquakes in each spectrum case obtained from the analyses for the different points and magnitudes. In order to quantify the stiffness degradation, a ratio was used (Equation 3.4). Table 4.3 shows the ratio of the stiffness calculated after the seismic load and pushover was applied with the stiffness before damage obtained from a pushover curve.

Table 4. 2 Stiffness for pushover analyses after dynamic analyses for different seismic magnitudes

Dynamic analysis (Maximum average)									
	Push Before	M5	M55	M6	M65	M7	M75	M8	M85
K15%Vu	21.42	27.20	23.42	19.40	14.81	12.47	10.79	10.04	10.10
Drift	0.001	0.000	0.001	0.001	0.001	0.001	0.001	0.001	0.001
Base Shear	126.77	122.58	123.63	124.02	122.43	124.52	123.84	121.05	120.02
K60%Vu	14.4	15.0	14.8	14.7	14.1	14.0	12.8	11.7	10.1
Drift	0.004	0.004	0.004	0.004	0.004	0.004	0.004	0.004	0.005
Base Shear	507.1	490.3	494.5	496.1	489.7	498.1	495.4	484.2	480.1
KVu	8.0	7.9	8.4	8.2	8.2	8.2	8.1	8.1	7.6
Drift	0.011	0.011	0.011	0.011	0.011	0.011	0.011	0.011	0.011
Base Shear	845.2	817.2	824.2	826.8	816.2	830.1	825.6	807.0	800.2

Table 4. 3 Stiffness ratio for pushover analyses after dynamic analyses for different seismic magnitudes

Ratio (Kafter/Kbefore)									
	M5	M55	M6	M65	M7	M75	M8	M85	
K15%Vu	1.270	1.094	0.906	0.691	0.582	0.504	0.469	0.472	
K60%Vu	1.037	1.027	1.016	0.974	0.970	0.889	0.809	0.697	
KVu	0.992	1.048	1.032	1.023	1.027	1.018	1.020	0.953	

Figure 4.2 shows the change of stiffness for the different moment magnitude cases. The initial stiffness presents a pronounced degradation in moment magnitudes from 5 to 6.5. This degradation is directly related with the damage experienced in the structure. For moment magnitudes higher than 6.5 the degradation of the initial stiffness becomes less marked, until for moment magnitude 8 onwards that the degradation becomes almost flat. Furthermore, the stiffness for 60%Vu presents a softer behavior than the initial stiffness. For moment magnitudes below design considerations the degradation is less pronounced, almost flat, while for moment magnitudes higher than 6 the degradation starts to decay. Moreover, when the moment magnitude 7 is exceeded the degradation becomes more pronounced. Finally, the stiffness at Vu presents a flatter behavior. Initially, the ratio barely grows, but it quickly becomes flat and for moment magnitudes higher than 8 the degradation gently decreases. The initial stiffness suffers a degradation

more pronounced than at the others two points for moment magnitudes below to 7 when the degradation of the stiffness for 60% V_u is more significant.

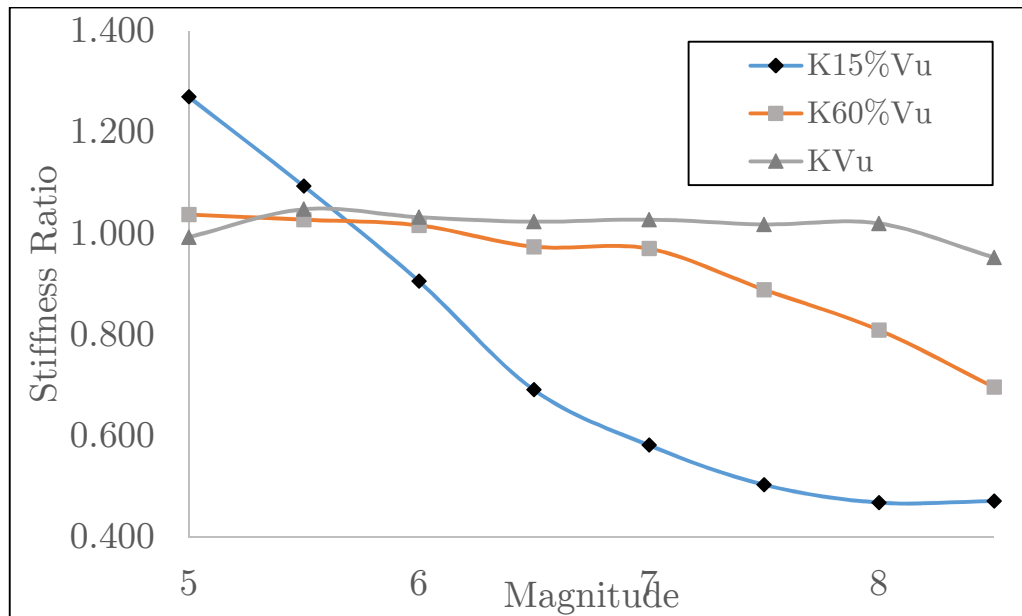


Figure 4. 2 Stiffness ratio as function of the seismic moment magnitude

4.4 Strength Degradation

The strength was analyzed using the peak shear strength in the pushover before and after the earthquakes were applied. Similar as in Chapter 3, the peak shear value (V_u) was obtained in all the cases with the respective drift to achieve the peak V_u . Table 4.4 presents the peak shear value and the drift reached for each moment magnitude and the pushover before the earthquake was applied. Table 3.6 shows the values of the ratio of the peak shear for the pushover after the earthquake to the peak shear before the earthquakes for each moment magnitude. The ratio presents a slightly increase until moment magnitudes 6. Then, for moment magnitude higher than 7 the ratio presents a slightly decrease while the moment magnitude increases. For moment magnitudes onwards of 6, the shear capacity in the average pushover curves increases. The shear capacity for each case is higher than the shear capacity before the earthquakes are applied. There is an increase of shear capacity between 3.4 to 5.2% in the studied cases. The drift

at which the peak shear occurs is almost constant from all the cases studied. Figure 4.3 presents the average pushover curves obtained from the analyses after application of the seismic loads for the different moment magnitudes and the original pushover curve obtained before the seismic load was applied. In general, the post peak response shows a stepper decrease in capacity for seismic magnitudes between 5 to 6.5 and the response tends to shift at the same time that the moment magnitude increases.

Table 4. 4 Strength for pushover analyses after dynamic analyses for different seismic magnitudes

Push analysis (Average)									
	Push Before	M5	M55	M6	M65	M7	M75	M8	M85
Drift	0.011	0.011	0.011	0.011	0.011	0.011	0.011	0.011	0.011
Base Shea	845.2	817.2	824.2	826.8	816.2	830.1	825.6	807.0	800.2

Table 4. 5 Strength ratio for pushover analyses after dynamic analyses for different seismic magnitudes

Ratio (Vafter/Vbefore)							
M5	M55	M6	M65	M7	M75	M8	M85
1.036	1.045	1.048	1.034	1.052	1.046	1.023	1.014

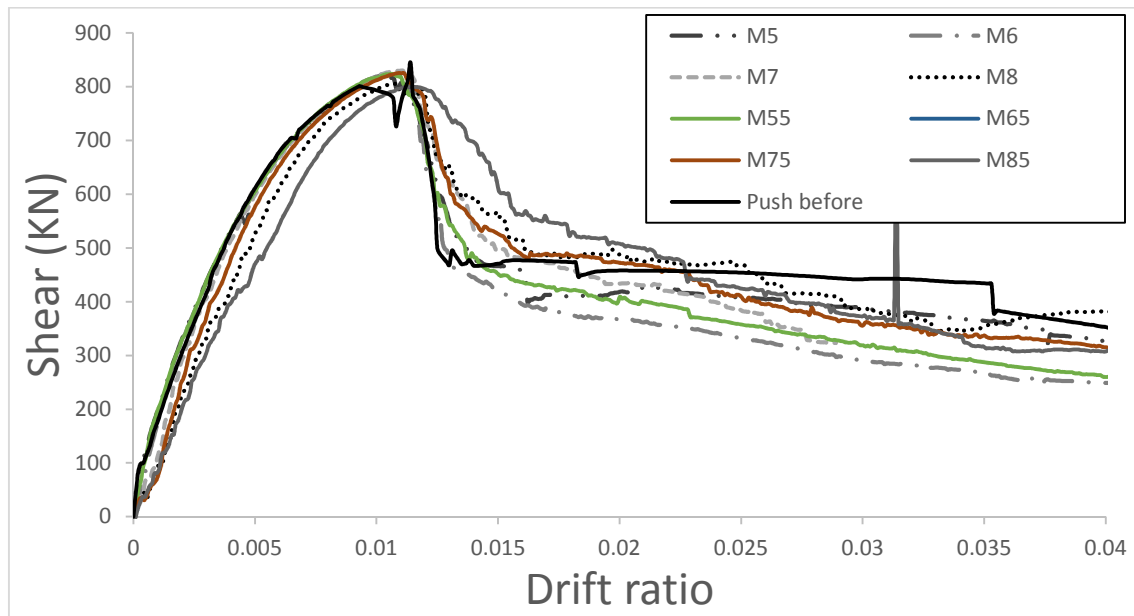


Figure 4. 3 Pushover curves before and after seismic load

4.5 Displacement/strain limit states

The strain limit states were evaluated in the pushover analyses post-earthquake average curves. The strain limits were studied in three points: (1) yielding, (2) serviceability and (3) damage control. Figures 4.4 and 4.5 present these parameters for the frame and the wall of the model. The strain limit states for the RC dual frame model are summarized in Figure 4.6. Table 4.6 shows the drift and shear at which each of the limits were attained in the beam and columns of the frame. The yielding point is dominated by the section of the column 1 with a drift of 0.004. The serviceability limit is controlled by the section in the column 1 with a drift of 0.008. Finally, the damage control was controlled by the section in the column 1 with a drift of 0.027. The wall limit states do not control. Table 4.7 shows the shears obtained for the different limit states and seismic magnitudes for the average pushover curves. Table 4.8 presents the ratio between the shear at strain limit after and before earthquake obtained for each limit state and moment magnitude.

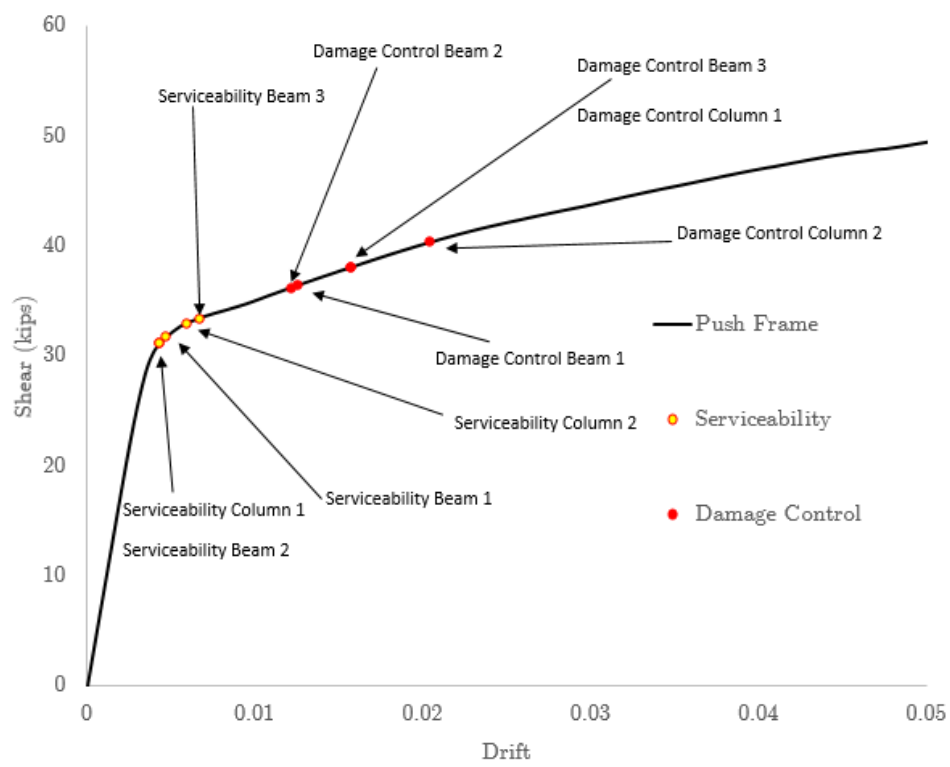


Figure 4. 4 Pushover state limits analysis for the frame

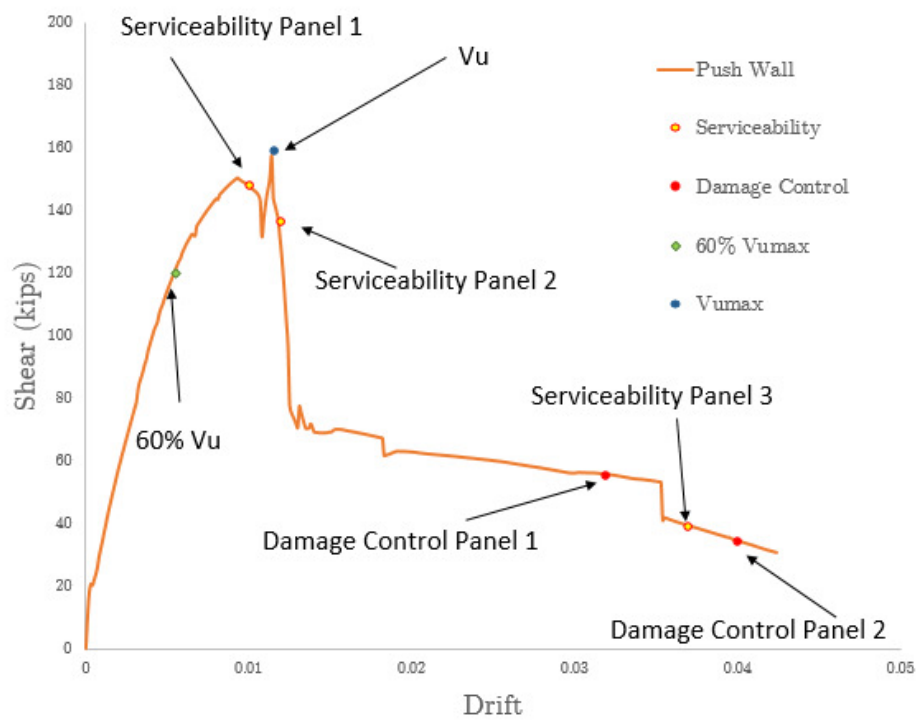


Figure 4. 5 Pushover state limits analysis for the wall specimen

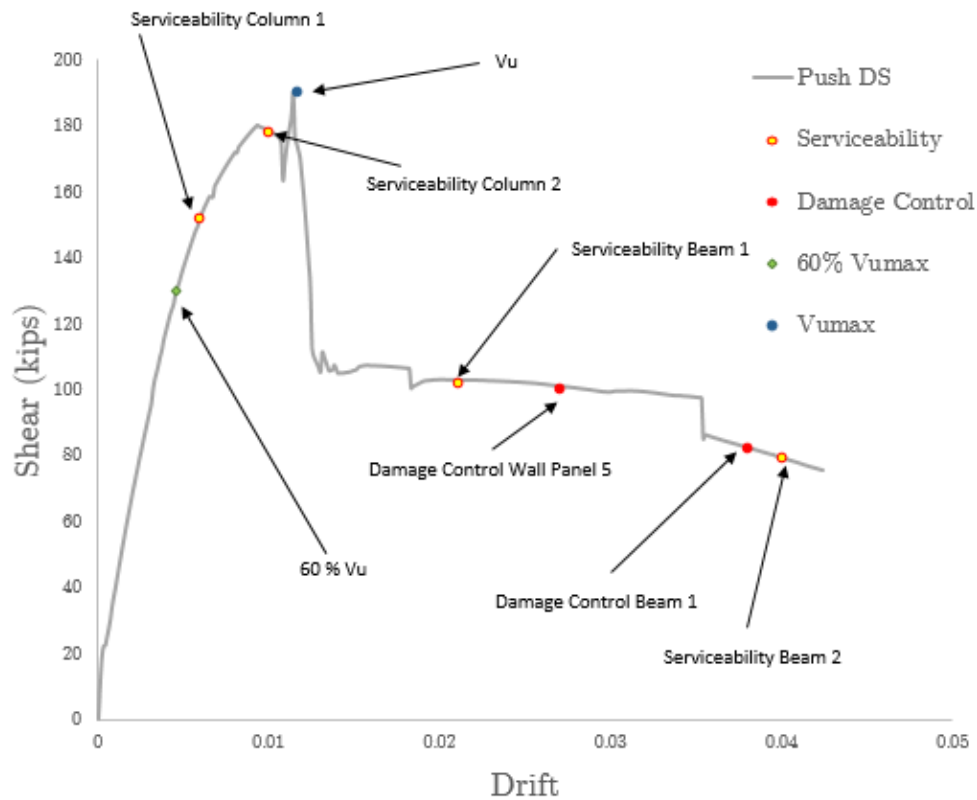


Figure 4. 6 Pushover state limits analysis for the Dual System.

Table 4. 6 Sequence of strain limits in the Pushover analysis before seismic loads.

Strain limit	Element	Drift	Shear (kips)	Shear (KN)
Yield	Column 1	0.004	93.33876	415.19152
	Column 2	0.006	128.30847	570.74455
	Beam 1	0.009	149.48734	664.95287
	Beam 2	0.007	139.43062	620.21835
	Beam 3	0.147	173.72447	772.765
Serviceability	Column 1	0.006	128.30847	570.74455
	Column 2	0.01	154.31961	686.44788
	Beam 1	0.021	127.69773	568.02785
	Beam 2	0.04	46.03501	204.77394
	Beam 3	0	0	0
Damage Control	Column 1	0.027	89.55587	398.36439
	Column 2	0.038	48.78103	216.98885
	Beam 1	0.112	56.87385	252.98751
	Beam 2	0	0	0
	Beam 3	0	0	0

Table 4. 7 Strain limits for pushover analyses after dynamic analyses for different seismic magnitudes

		Push analysis (Average)								
		Push Before	M5	M55	M6	M65	M7	M75	M8	M85
Yield	Drift	0.004	0.004	0.004	0.004	0.004	0.004	0.004	0.004	0.004
Column 1	Base Shear	528.458	531.9	530.3	526.6	513.7	513.7	478.7	425.2	396.9
Serviceability	Drift	0.008	0.008	0.008	0.008	0.008	0.008	0.008	0.008	0.008
Column 1	Base Shear	678.981	674.6	673.4	673.0	658.7	668.0	652.4	612.4	543.0
Damage Control	Drift	0.022	0.022	0.022	0.022	0.022	0.022	0.022	0.022	0.022
Column 1	Base Shear	449.078	402.3	341.5	316.7	353.1	353.1	383.8	416.5	400.4

Table 4. 8 Strain ratio for pushover analyses after dynamic analyses for different seismic magnitudes

		Ratio (Vafter/Vbefore)							
		M5	M55	M6	M65	M7	M75	M8	M85
Strain limit									
Yield		1.007	1.003	0.997	0.972	0.972	0.906	0.805	0.751
Serviceability		0.994	0.992	0.991	0.970	0.984	0.961	0.902	0.800
Damage Control		0.896	0.761	0.705	0.786	0.786	0.855	0.927	0.892

For the yielding limit state, the shears obtained tend to slightly decrease as the seismic magnitude increases, but, the tendency is almost constant until magnitude 7. When the magnitude 6 is overcome the shear required to achieve the yielding drift tends to decrease. After moment magnitude 7, the decrease is more significant. Moreover, for the serviceability limit state, the shears are almost constant for moment magnitudes below 7, although when the moment magnitude 7 is overcome the shear sharply decreases as the seismic magnitude increases. Even though, the serviceability points have a similar behavior, the decrease for moment magnitude largest than 7 is more pronounced. When compared with the undamaged situation, the yielding and serviceability states occur at a lower shear than when the model already has some damage after the seismic loads. Furthermore, the reduction of shear at yielding is more significant than for the serviceability limit state. The damage control shears present a more erratic behavior. For moment magnitudes lower or equal to 6, the shear tends to decrease, even though, for moment magnitude higher than 6, the shear reached to achieve the limit drift in the pushover curve increase, decreasing almost imperceptibly when the moment magnitude 8 have been overcome.

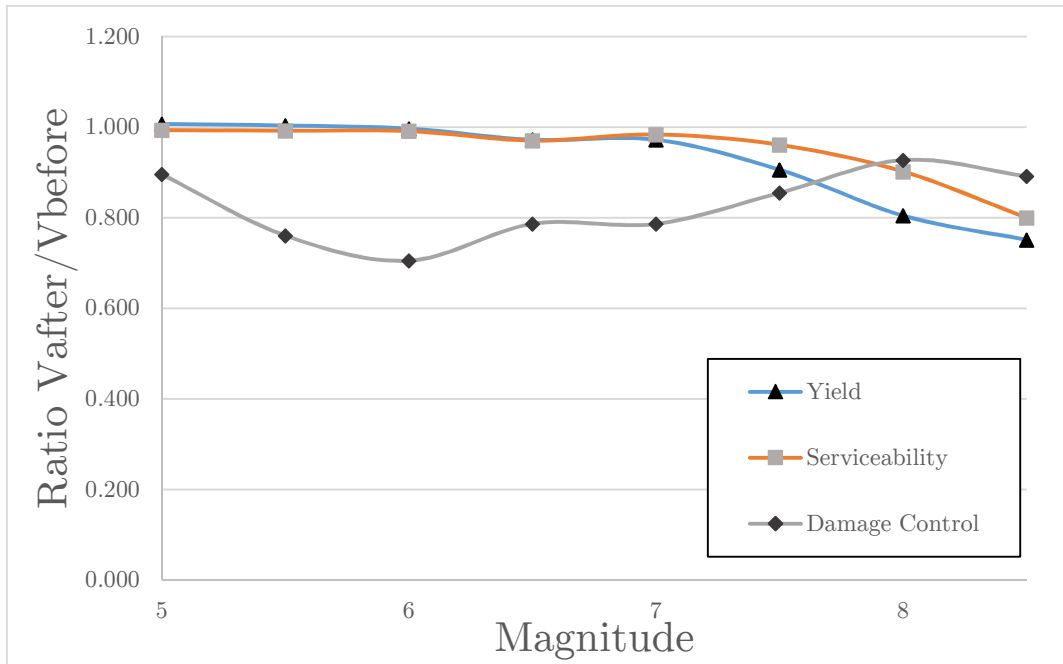


Figure 4. 7 Strain ratio as function of the seismic moment magnitude

4.6 Summary of Results

This chapter studied the effects of beyond seismic accelerations in the response of a RC-wall-frame dual model when the aging effects in the reinforcing steel are considered, analyzing the degradation produced in the structure under seismic excitations exceeding design considerations. The parameters analyzed were the stiffness of the structure, the shear strength and the displacement limit states. The initial stiffness decreases significantly as the moment magnitude increases. The stiffness degradation at 60% of peak shear is less pronounced for moment magnitudes below design considerations, while for moment magnitudes higher than 6 the degradation starts to decay. Moreover, the stiffness at V_u presents a flat behavior. The initial stiffness suffers a degradation more significant than at the others two points. Besides, the shear capacity for each case is higher than the shear capacity before the earthquakes are applied. As the moment magnitude increases, the shear peaks tend to occur almost at the same drift. Furthermore, the decrease in the shear capacity after the seismic load were applied are less pronounced than the stiffness changes. In general, the study of the limit states

denotes a reduction of the shear needed, for the yielding point the shear required highly decreases as the moment magnitude increases. For the serviceability point the decrease of shear is less pronounced. Additionally, the damage control shears presented more variability. However, the limit states are reached at a lower shear when the structure is undamaged. A comparison of the results obtaining with the model with and without the consideration of aging effects in the reinforcing bars is exposed next.

4.7 Comparison of Results

Chapter 3 and chapter 4 presented the results of the analysis with and without considering aging effects in the reinforcing steel bars, respectively. Figure 4.8 shows the pushover curves for both models. The maximum capacity of the RC frame-wall model, after the aging effects were considered, was reduced considerably. Moreover, the peak shear tends to occur at a higher drift. Figure 4.9 presents the design spectrum used for the original model. Also, a hypothetical design spectrum is presented, simulating a possible design obtained when the steel in the sections was reduced after applying the deterioration effect in the steel bars.

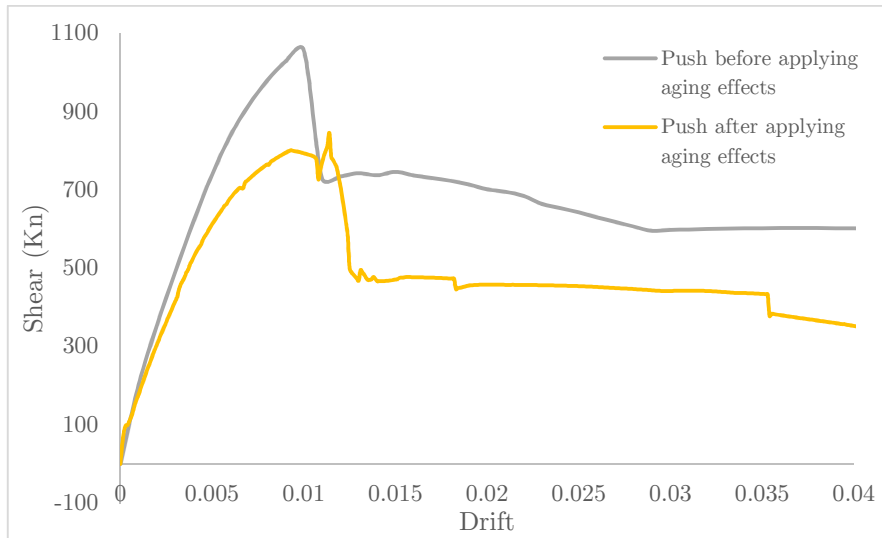


Figure 4. 8 Pushover before and after applying aging effects.

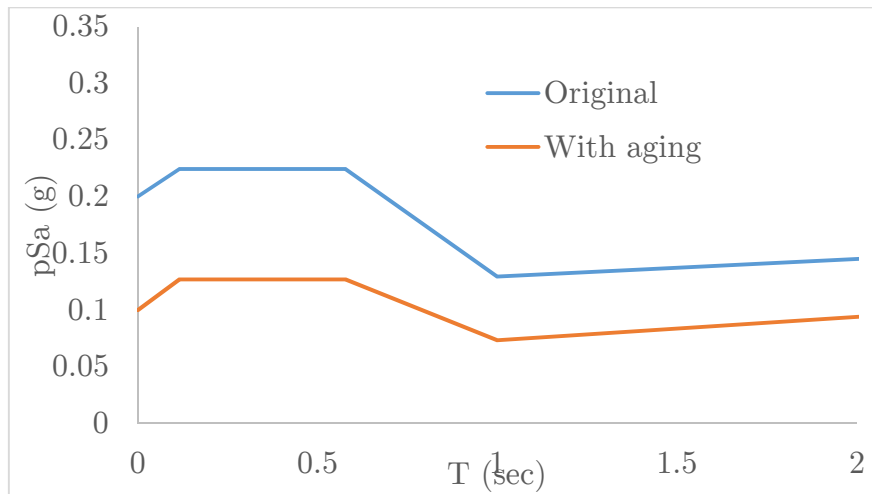


Figure 4. 9 Design Spectrum

The parameters that were compared are the stiffness of the structure at different points (15% V_u , 60% V_u , and at V_u), the shear strength and the displacement limit states. Figures 4.10 to 4.12 show the comparison of the ratios of stiffness in the structure obtained for the original model and when the aging effects were applied. This ratio was obtained dividing the stiffness when the seismic and pushover loads are applied with the stiffness of the original (undamaged) model without aging of the reinforcing steel to facilitate the comparison.

For the initial stiffness, the degradation pattern is similar in both cases, even almost parallel. The degradation is more significant in the case with aging effects due to the “previous damage” induced in the structure due to the corrosion of the

steel bars. The stiffness at 60% V_u has a similar situation. For the condition without aging effects, for moment magnitudes below 7, the degradation is minimal. Then, the degradation becomes more pronounced. The condition with aging effect in the reinforcing steel has a similar behavior, although the curves start to decay earlier for a moment magnitude of 6. For the condition without aging effects the stiffness at V_u decreases as the moment magnitude increases. For the condition with aging effect, the degradation is less pronounced and is almost constant. In the three cases, the curve including aging is below the curve before applying deterioration in the steel. It means that the structure without aging effects has a greater capacity to absorb damage, whereas when there is the effect of deterioration in steel, the structure loses capacity to be damaged. Figure 4.13 shows the changes in stiffness (inverse of previous ratio) at different points as the moment magnitude increases, together with the lines showing the design condition and a hypothetical design condition when the reinforcing steel is reduced. It can be noticed, that besides from the first point of the initial stiffness (at 15% V_u), the stiffness changes from the original (undamaged) model for 15% V_u and 60% V_u increase significantly after the design consideration is exceeded. These changes are not that marked at peak shear (V_u).

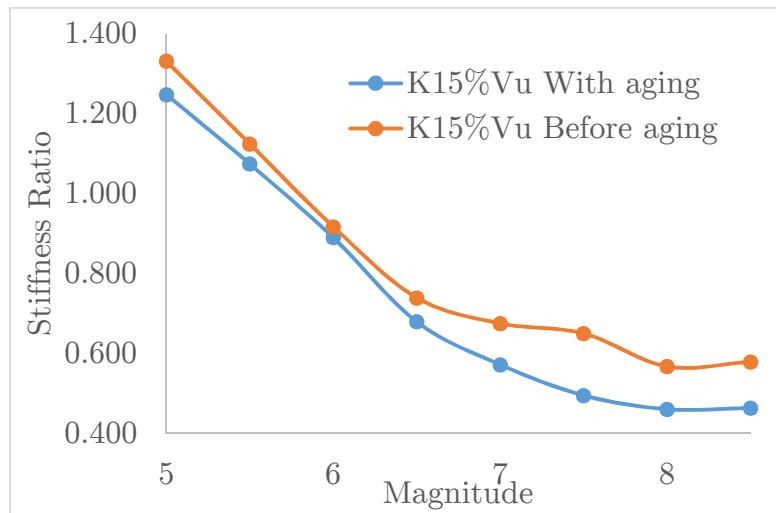


Figure 4. 10 Comparison of the initial stiffness degradation

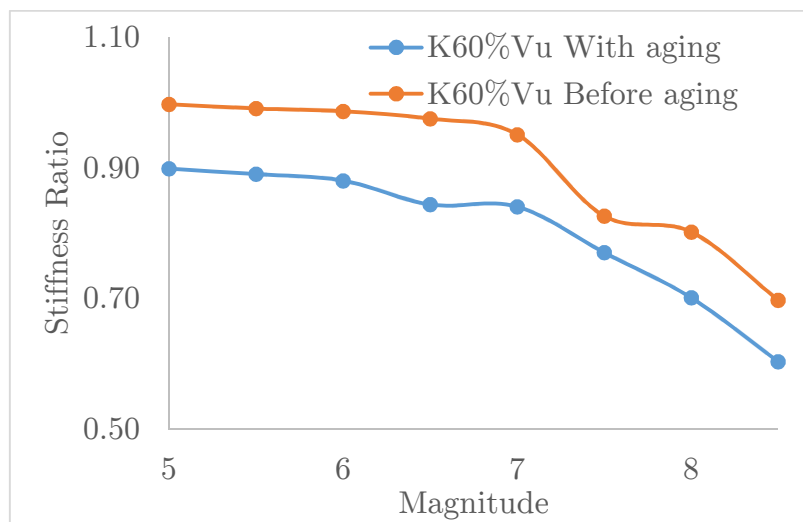


Figure 4. 11 Comparison of the stiffness degradation at 60%Vu maximum

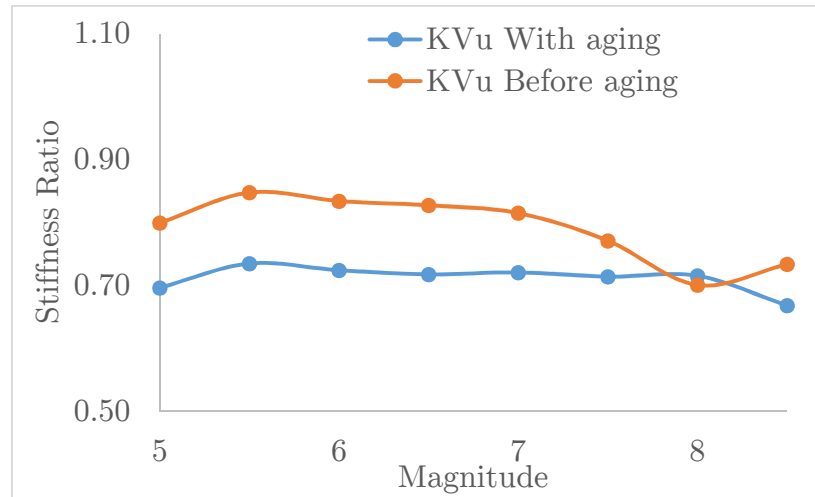


Figure 4.12 Comparison of the stiffness degradation at V_u maximum

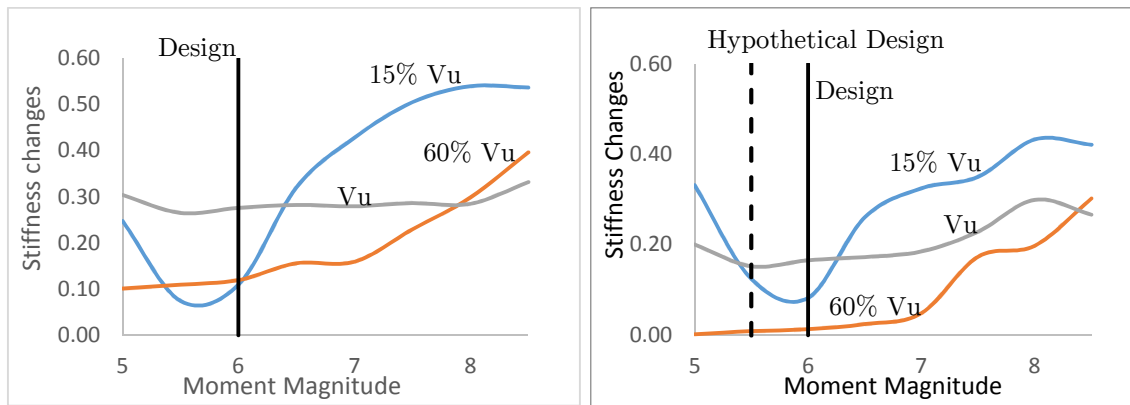


Figure 4.13 Comparison of the changes in stiffness degradation with (left) and without (right) aging effects

The strength degradation was also studied using the peak shear strength in the pushover before and after the earthquakes were applied with aging effects of the rebar included. Figure 4.14 shows the ratio of shear capacity in the structure for both situations. The shear capacity ratio was obtained by dividing the peak shear after the dynamic and pushover loads were applied with the peak shear of the original (undamaged-without aging) structure. The curve obtained for the original structure is over the case considering the aging effect. This means that for the condition with aging effect that the structure has lost capacity due to the degradation of the reinforcement steel bars. In both cases, the degradation in

peak shear capacity after the dynamic and pushover loads are applied is minimal and follows a constant pattern.

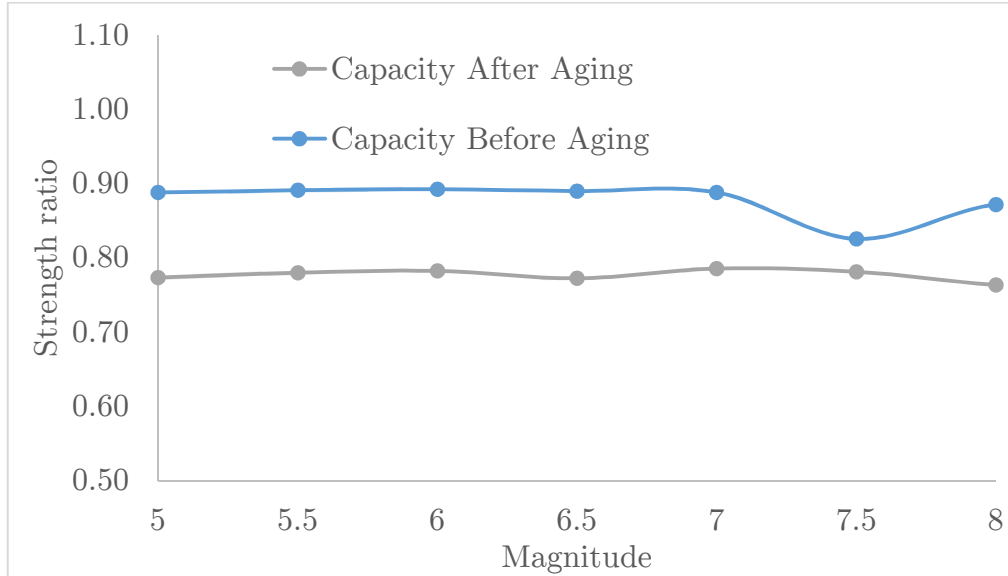


Figure 4. 14 Change of capacity

The last parameters that are compared are the strain limit states. The strain limit states were evaluated in the pushover analyses post-earthquake average curves at three different points: (1) yielding, (2) serviceability and (3) damage control. For the strains that controlled each limit as explained in previous chapters, the drift and shear at these points were obtained. Figures 4.15 to 4.17 show the ratio of the shear obtained at the strain limits for the original model and when the aging effects were considered. This ratio was calculated by dividing the shear at the limits obtained after the dynamic and pushover were applied with the shear at the limits for the original model without aging effects. For the three limit states, the curve before applying the aging effect is over the curve considering the aging effects, which means that the strain limit state has been achieved later in the pushover curve. For the yielding point, the response for both cases is similar, for moment magnitudes below to 7, the shear needed to achieve the limit state remains almost constant. Then, the shear needed to reach the yield limit state

tends to decay as the moment magnitude increases for moment magnitudes higher than 7. For the serviceability state, for both model conditions, the shear needed to achieve the limit remains almost constant. For the model with the consideration of aging effects of the rebar, for moment magnitudes higher than 7, the shear needed to reach the limit state tends to decay more as moment magnitude increases when compared to the undamaged original model. Finally, the ratios for the damage control point has in both cases an erratic behavior. At the damage control limit state, the behavior of the model is controlled by the decay in the capacity of the wall in the system that has a more brittle behavior when compared to the frame. This situation made the convergence of the model more difficult and could have influence in the results. Some researchers (Vidot and Kowalsky 2011, Goodnight et. al 2013) had found that the strain vs. drift relationship is unique and independent of the load history. The unique relationship could also have influence in the shears obtained at a particular drift/strain before the damage control limit state, meaning that the shears also have a minimal change from the undamaged original model for the yielding (from 3.7 to 5.2%) and serviceability (from 10% to 11%) limit states before the design conditions are exceeded. After the design condition is exceeded or the structure has more damage, the shear attained at yielding and serviceability limit states changes more significantly. The percentage changes in shear after magnitude 6 (exceedance of the design condition) varied from 5.8 to 28% and from 11 to 17.5% at yielding and serviceability limit states, respectively for cases without aging effects. At damage control limit state, the shears do not follow a definable pattern varying between 15.6 % to 32% from moment magnitudes 5 to 8.5 and with and without considering aging effects in the reinforcing steel. When the reduction in the reinforcing steel is introduced to account for aging, the behavior is similar for the limit states with higher variation in the shear needed to attain the limit when compared with the original undamaged-unaged model. For yielding, a little before

the original design considerations are exceeded as the moment magnitude increases the shears varied from 15.5 to 36% when compared to the original model. For the damage control, shears needed to attain the limit varied as much as 50% when aging of the reinforcing steel is considered.

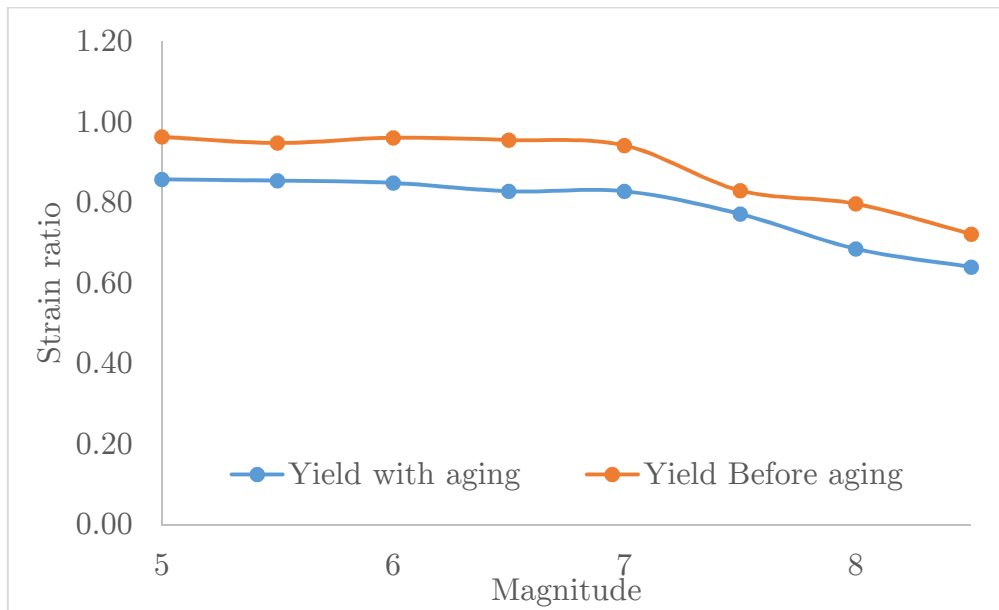


Figure 4. 15 Comparison of the yielding strain ratio as function of the seismic moment magnitude

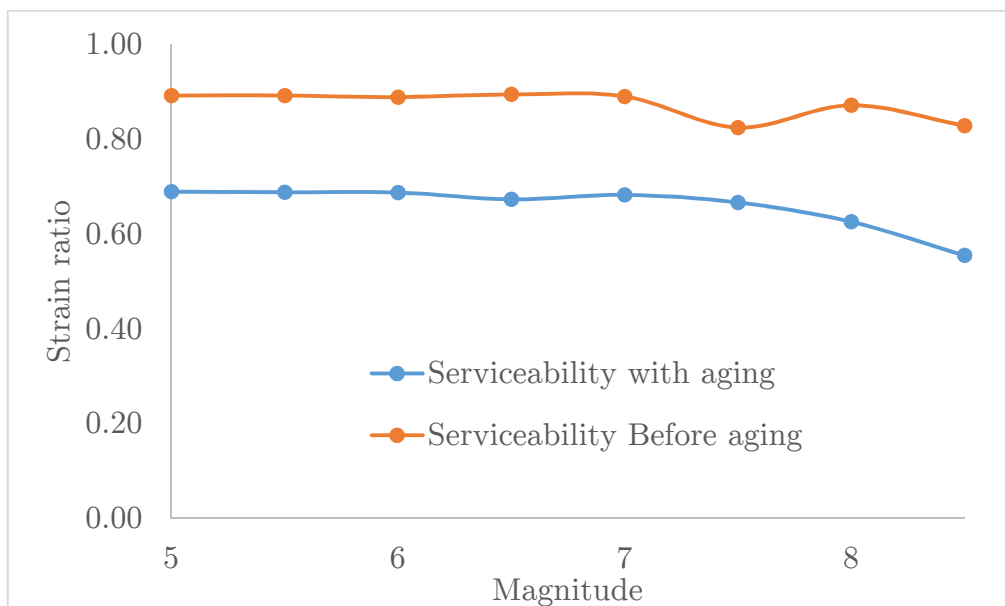


Figure 4. 16 Comparison of the serviceability strain ratio as function of the seismic moment magnitude

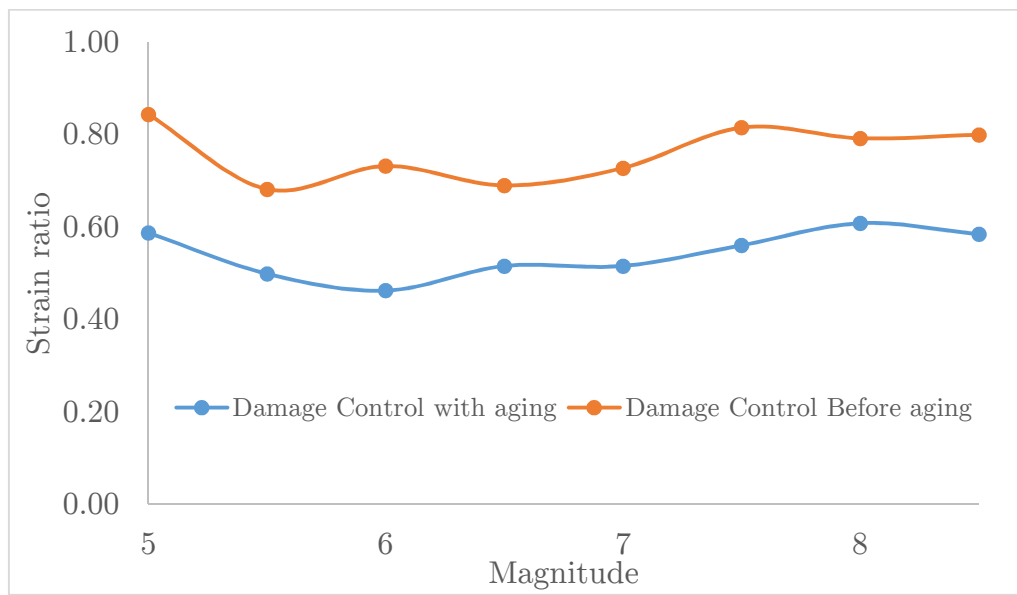


Figure 4. 17 Comparison of the damage control strain ratio as function of the seismic moment magnitude

Chapter 5. Conclusions

This chapter summarizes the analysis procedure and methodology used to achieve the objectives of this thesis. The results obtained in chapter 3 and chapter 4 are compared in order to study the change of behavior in the model due to the aging effect and beyond design accelerations. Finally, several conclusions are formulated, and recommendation for future works are proposed.

5.1 Summary

Nuclear power plants (NPPs) and other civil structures in the US and Japan have recently experienced strong ground motions exceeding the original design values. It is of vital importance to evaluate the capacity of structural components in the buildings that composed a nuclear power plant to have a reliable idea of the level of seismic damage after linear range that they can safely manage. In this thesis, the impact of beyond design earthquake accelerations in the response of a reinforced concrete (RC) frame-wall system was evaluated with and without the considerations of aging effects in the reinforcing steel. The analyses were performed in OpenSees. The model was analyzed under dynamic accelerations and after that a pushover load was applied to assess changes in stiffness, strength and limit states of the damage structure. The dynamic analyses were performed using compatible records (20 seeds) with target spectra for moment magnitudes from 5 to 8.5. A total of 160 compatible scaled earthquakes were used in the analyses.

5.2 Conclusions

The following conclusions can be drawn from the comparison of the results obtained with the analyses for the RC frame-wall model with and without the inclusion of aging effects in the reinforcing steel. These conclusions are based on the results obtained from the dynamic and pushover analysis of the RC frame-

wall system model used for this thesis and depend on the particular constitutive material relationships and properties used in the model. Future analyses and tests of RC frame-wall systems will enable the conclusions presented above to be refined.

- **From the stiffness analyses it was determined the following:**
 - The initial stiffness (at 15% V_u) has a more pronounced change as the moment magnitude increases with and without the inclusion of aging effects of the reinforcing bars that the stiffness at the other two points.
 - As the design moment magnitude is exceeded the reduction in stiffness is more noticeable at 15% and 60% V_u .
 - At V_u , the stiffness changes are more constant and there is not a definite moment magnitude point in which significant changes can be noticed.
- **From the shear strength analyses it was noticed the following:**
 - From the models with and without aging effects, the degradation in peak shear capacity after the dynamic and pushover loads were applied was minimal and follows a constant pattern. The exceedance of design moment magnitude has not a noticeable effect in the peak shear capacity, besides from the expected reduction in capacity as moment magnitude increases.
- **From the strain/drift limit states it was determined the following:**
 - In general, the shear needed to attain the yielding and serviceability limit states before the design conditions are exceeded have minimal changes when the reduction in steel due to aging is not considered. After the design condition is exceeded or the structure has more damage, the shear attained at yielding and serviceability limit states changes more significantly. When the reduction in steel due to aging

is incorporated, the model presents higher deformations, less stiffness and more nonlinearity, affecting more the shears at limits states.

- At the damage control limit state, the shears do not follow a definable pattern no matters if the design condition (moment magnitude) was exceeded. However, the changes in the shear needed to attain damage control are more significant when the aging effects in the reinforcing steel are considered.

5.3 Recommendations for future works

- For future studies, it would be important to evaluate more RC frame-wall specimens and spectrum cases to study in more detail the effects of beyond design considerations in these systems.
- Additional aging effects are important to be incorporated in the model. For example, include concrete aging in addition of the reinforcing steel aging due to corrosion.
- Compare results obtained from the analytical models with experimental testing of dual systems to revise conclusions about the different parameters.

6. References

1. Agency, Nuclear Energy, Committee On, T H E Safety, O F Nuclear, Finite Element, Analysis Of, Ageing Reinforced, et al. 2002. "NEA / CSNI / R (2002) 13 Unclassified."
2. Bechtoula, Hakim, Masanobu Sakashita, Susumu Kono, Fumio Watanabe, and Marc O. Eberhard. 2006. "Cyclic Performance of Lower Stories of Mid-Rise Reinforced Concrete Frame Buildings." *ACI Structural Journal* 103 (4): 513–21.
3. Bessason, Bjarni, and Jón Örvar Bjarnason. 2016. "Seismic Vulnerability of Low-Rise Residential Buildings Based on Damage Data from Three Earthquakes (Mw6.5, 6.5 and 6.3)." *Engineering Structures* 111 (May 2008). Elsevier Ltd: 64–79. doi:10.1016/j.engstruct.2015.12.008.
4. Beyer, K., and Bommer, J.J. (2007). Selection and Scaling of Real Accelerograms for Bi-Directional Loading: A Review of Current Practice and Code Provisions, *Journal of Earthquake Engineering* 11 (sup1), 13-45
5. BLN (2009). "Identification and Assessment of Material Models for Age-Related Degradation of Structures and Passive Components in Nuclear Pwer Plants". BNL Report-82249-2009 KAERI/TR-3757/2009.
6. Bourahla, N., Attar, A., Taфраout, S., Djidjeli, F., Kenai, S. (2008)"Effect of ageing degradation on the performance of reinforcement concrete bridge piers under seismic excitations". ICCBT 2008.
7. Braverman, J.I., et al., (2000). "Assessment of Age-Related Degradation of Structures and Passive Components for U.S. Nuclear Power Plants." NUREG/CR-6679. Brookhaven National Laboratory, Upton, N.Y.
8. Carrillo WJ, Alcocer SM. (2008). Shaking Table Tests of Low-Rise Concrete Walls For Housing. 14th World Conf Earthq Eng.
9. Chang, G.A. and Mander, J.B. (1994), "Seismic Energy Based Fatigue

- Damage Analysis of Bridge Columns: Part I – Evaluation of Seismic Capacity”, NCEER Technical Report No. NCEER-94-0006, State University of New York, Buffalo.
10. Coronelli, D. (2002). “Corrosion Cracking and Bond Strength Modeling for Corroded Bars in Reinforced Concrete”, *ACI Structural Journal*, V. 99, No. 3, July-Aug. 2002, pp. 267-276.
 11. Filippou F.C., Popov, E.P., and Bertero, V.V. (1983). "Effects of Bond Deterioration on Hysteretic Behavior of Reinforced Concrete Joints". Report EERC 83-19, Earthquake Engineering Research Center, University of California, Berkeley.
 12. Ghosh, Jayadipita, S M Asce, Jamie E Padgett, and A M Asce. 2010. “Aging Considerations in the Development of Time-Dependent Seismic Fragility Curves,” no. December: 1497–1511.
 13. Goodnight, J., Kowalsky, M., and Nau, J. (2013). The Effect of Load History on Performance Limit States of Circular Bridge Columns. Accepted Manuscript of ASCE Journal of Bridge Engineering.
 14. Hanjari, K.Z., Kettil, P. and Lundgren,K. (2011). “Analysis of Mechanical Behavior of Corroded Reinforced Concrete Structures”, *ACI Structural Journal*, V. 108, No. 5, July-Aug. 2002, pp. 267-276.
 15. Higgins, C. and Farrow III, W.C (2006), “Tests of Reinforced Concrete Beams with Corrosion Damaged Stirrups,” *ACI Structural Journal*, V. 103, No. 1, pp. 133-141.
 16. Jünemann, R., J. C. de la Llera, M. A. Hube, L. A. Cifuentes, and E. Kausel. 2015. “A Statistical Analysis of Reinforced Concrete Wall Buildings Damaged during the 2010, Chile Earthquake.” *Engineering Structures* 82: 168–85. doi:10.1016/j.engstruct.2014.10.014.
 17. Karsan, I. and Jirsa, J. (1969) “Behavior of concrete under compressive loadings”, *ASCE Journal of Structural Division*, V. 95, No. 12, pp. 2543–

- 2563.
18. Katona, Tamás János. 2012. "Seismic Safety Analysis and Upgrading of Operating Nuclear Power Plants."
 19. Kent, D. C. and Park, R. (1971), "Flexural members with confined concrete." *Journal of Structural Engineering*, V. 97, No.7, pp.1969–1990.
 20. Kolozvari, K, T Tran, J Wallace, and K Orakcal. 2012. "Modeling of Cyclic Shear-Flexure Interaction in Reinforced Concrete Structural Walls." doi:10.1061/(ASCE)ST.1943-541X.0001083.
 21. Kolozvari, K., Tran, T., Orakcal, K. and Wallace, J.W 2014. "Modeling of Cyclic Shear-Flexure Interaction in Reinforced Concrete Structural Walls. II: Experimental Validation." *Journal of Structural Engineering* 141(5): 4014136. [http://ascelibrary.org/doi/10.1061/\(ASCE\)ST.1943-541X.0001083](http://ascelibrary.org/doi/10.1061/(ASCE)ST.1943-541X.0001083).
 22. Kolozvari K., Orakcal K., and Wallace J. W. (2015). "Shear-Flexure Interaction Modeling of reinforced Concrete Structural Walls and Columns under Reversed Cyclic Loading", *Pacific Earthquake Engineering Research Center, University of California, Berkeley*, [PEER Report No. 2015/12](#)
 23. Kolozvari, Kristijan, Kutay Orakcal, and John Wallace. 2015. "PACIFIC EARTHQUAKE ENGINEERING Shear-Flexure Interaction Modeling for Reinforced Concrete Structural Walls and Columns under Shear-Flexure Interaction Modeling for Reinforced."
 24. Lay, S. and Schiebl, P. 2003. *Life cycle Management of concrete Infrastructures for improved Sustainability*. European Community Fifth Framework Program: GROWTH.
 25. Lermite, Sandrine, Thierry Chaudat, and Thierry Payen. 2008. "Smart 2008: Seismic Design and Best-Estimate Methods Assessment for Rc Buildings Subjected To Torsion," 1–8.
 26. Li, Yong. 2012. "GI 199 and 2011 Mineral, VA Earthquake Impact to

- North Anna Nuclear Power Plant.” *15th World Conference on Earthquake Engineering (15WCEE)*.
27. Luna, B. N. (2015). "Seismic response of low aspect ratio reinforced concrete shear walls for buildings and safety-related nuclear structures." PhD dissertation, University at Buffalo, Buffalo, NY.
 28. McKenna, F., Fenves, G.L., Scott, M.H., and Jeremic, B. (2000) "Open System for Earthquake Engineering Simulation-OpenSees", <http://opensees.berkeley.edu>.
 29. Menegotto, M., and Pinto, P.E. (1973). Method of analysis of cyclically loaded RC plane frames including changes in geometry and non-elastic behavior of elements under normal force and bending. Preliminary Report IABSE, vol 13.
 30. Mohle, J. and Kunnath, S. (2006) "Reinforcing Steel: OpenSees User's Manual", <http://opensees.berkeley.edu>.
 31. Mohammed, A.M.; Almansour, H.; Martin- Pérez, (2011), “Combined effect of reinforcement corrosion and seismic loads on RC bridge columns: Modeling,” 2nd International Engineering Mechanics and Materials Specialty Conference Ottawa, Ontario, June 14-17, 2011, pp. 1-10.
 32. Montejo, L., and Suarez, L. (2013). An improved CWT-based algorithm for the generation of spectrum compatible records, *International Journal of Advanced Structural Engineering* 5(1), 26.
 33. Mullard, J. A., and Stewart, M. G., (2011), “Corrosion-Induced Cover Cracking: New Test Data and Predictive Models”, *ACI Structural Journal*, V. 108, No. 1, pp. 71-79.
 34. Naus, D. J. (2006), “The Effect of Elevated Temperature on Concrete Materials and Structures – A Literature Review,” NUREG/CR-6900, U.S. Nuclear Regulatory Commission, Washington, D.C.2006.

35. Naus, D.J. (2007). "Primer on durability of nuclear power plant reinforced concrete structures – a review of pertinent factors." NUREG/CR-6927, Oak Ridge National Laboratory.
36. OpenSEES (Open System for Earthquake Engineering Simulation), <http://opensees.berkeley.edu>, 2014.
37. Orakcal K. (2004), "Nonlinear Modeling and Analysis of Slender Reinforced Concrete Walls", PhD Dissertation, Department of Civil and Environmental Engineering, University of California, Los Angeles.
38. Park, Y.J. (1998). "Effects of Aging Degradation on Seismic Performance of RC structures." Brookhaven National Laboratory.
39. Park, J.K., Kim, S.K., Lee, S.K. (1998). "Probabilistic corrosion rate estimation model for longitudinal strength members of bulk carriers." *Ocean Engineering*, 25(10), 837-860.
40. Priestley, M. J. N., Seible, F. and Calvi, G.M. (1996) "Seismic Design and Retrofit of Bridges". John Wiley Sons Inc. New York. 686 pp.
41. Takada, T. (2012). "On Seismic Design Qualification of NPPs After Fukushima Event in Japan." *15th World Conference on Earthquake Engineering (15WCEE)*, no. 7.
42. Ting, S.C. and Nowak, A.S (1991). "Effect of Steel Area Loss on Flexural Behavior of RC beams", *ACI Structural Journal*, V. 88, No. 3, pp. 309-314.
43. Tran, T., Wallace, J., (2012). Experimental Study of Nonlinear Flexural and Shear Deformations of Reinforced Concrete Structural Walls. 15th World Conference on Earthquake Engineering, Lisbon, Portugal.
44. Tsai W.T. (1988), "Uniaxial Compressional Stress-Strain Relation of Concrete", *ASCE Journal of Structural Engineering*, V. 114, No. 9, pp. 2133-2136.
45. Richard, Benjamin, Paolo Martinelli, François Voldoire, Mathieu Corus, Thierry Chaudat, Salim Abouri, and Nicolas Bonfils. 2015. "SMART 2008:

- Shaking Table Tests on an Asymmetrical Reinforced Concrete Structure and Seismic Margins Assessment.” *Engineering Structures* 105. Elsevier Ltd: 48–61. doi:10.1016/j.engstruct.2015.09.036.
46. Scott M. and Fenves, G. (2006) "Plastic Hinge Integration Methods for Force-Based Beam-Column Elements". *ASCE Journal of Structural Engineering*, V. 132, No. 2, pp. 244-252.
 47. Ulugtekin D. (2010), “Analytical Modeling of Reinforced Concrete Panel Elements Under Reversed Cyclic Loadings,” M.S. Thesis, Department of Civil Engineering, Bogazici University.
 48. US-NRC (1995). “Assessment of in service condition of safety-related nuclear plants structures.” H. Ashar and G. Bagchi, NUREG-1522,U.S. Nuclear Regulatory Commission, Washington, D.C.,June.
 49. US-NRC (2007), "Evaluation of Seismic Design Criteria ASCE/SEI Standard 43-05 for Application to Nuclear Plants." NUREG/CR-6926 BNL/ NUREG/CR-77569/2007.
 50. US-NRC (2012), “A Summary of Aging Effects and Their Management in Reactor Spent Fuel Pools, Refueling Cavities, Tori, and Safety-Related Concrete Structures." NUREG/CR-7111 ORNL/TM-2011/410.
 51. Verderame, Gerardo M., Paolo Ricci, Flavia De Luca, Carlo Del Gaudio, and Maria Teresa De Risi. 2014. “Damage Scenarios for RC Buildings during the 2012 Emilia (Italy) Earthquake.” *Soil Dynamics and Earthquake Engineering*. doi:10.1016/j.soildyn.2014.06.034.
 52. Vidot-Vega, A.L. and Kowalsky, M.J., (2011). Impact of Seismic Input on Strain/Displacement Response of RC Members and Frames, *ACI Structural Journal*, Vol. 108, No. 2, pp. 178-187.
 53. Vulcano, A.; Bertero, V. V.; and Colotti, V. (1988). “Analytical Modeling of RC Structural Walls,” *Proceedings, 9th World Conference on*

Earthquake Engineering, V. 6, Tokyo Kyoto, Japan, pp. 41-46.

54. Yamakawa, T., (1995), "An Experimental Study on Deterioration of Aseismic Behavior of R/C Structural Walls Damaged by Electrolytic Corrosion Testing Method." Concrete under Severe Conditions: Environment and Loading, Volume 2.

Appendix 1

```

# -----
#
# Created by: Adrian Argente del Castillo Garrido
# Date: 7/2017
# -----
# Program in OP to simulate the dualsystem model composed by a frame
and a wall.
# This case presents wall's fc 4 ksi //////////
# -----
# Start of model generation (Units: in, kips)
# -----
wipe; # removes all constructed objects
puts "Defining model"
# Set Up Directories
set modelName "DS_Finalanalysis"; # Model Name fc4
set dataDir SFI_MVLEM_${modelName}; # Name of output folder
file mkdir $dataDir;
source BuildRCrectSection.tcl; # procedure for definining rectangular
RC fiber section
# Create ModelBuilder for 2D element (with two-dimensions and 2
DOF/node)
model BasicBuilder -ndm 2 -ndf 3
puts "Start"
# ===== WALL PROPERTIES
=====
set H 365.6694888; # Wall height
set t 3.93701; # Wall thickness
set L 157.4804; # Frame translation
set tO 0.0001; # 0.0001 $t
set reduframesteel 0.8;
set agingredufactor 0.75;
# ===== Frame PROPERTIES
=====
# ===== COLUMN PROPERTIES
=====
set pi 3.14159265;
set g 9.810; # gravity [m/s2]
set fc -4; # concrete comp. strength [Ksi]
set fcm -27.6; # concrete comp. strength [Ksi]
set Ec [expr 5000*sqrt(-$fcm)]; # concrete modulus of elasticity [MPa]
set Ec [expr $Ec*0.145]; # concrete modulus of elasticity [MPa]
set eps0 -0.002; # UNCONFINED concrete strain
# set Ec [expr 5000*sqrt(-$fc)]; # concrete modulus of elasticity
[MPa]
# set Denh 2400; # concrete density [kg/m3]
# set Denhn [expr $g*2400]; # concrete density [N/mm3]
# set Denhg [expr $Denhn/(1000*1000*1000)]; # concrete density [N/mm3]
# set GammaConcrete 2.354e-5; # Reinforced-Concrete floor
slabs;N/mm^3
# ===== COLUMN Aux
=====
set LCol1 121.8898296; # column length [in]
set HCol1 20; # column dimension [in]
set bCol1 $HCol1;
set ACol1 [expr $HCol1*$bCol1]; # cross-sectional area [mm2]
set I1 [expr 1./12*$bCol1*pow($HCol1,3)]; # section moment of inertia [mm4]
set IzCol1 [expr $I1*0.9]; # section moment of inertia eff [mm4]
set ECol $Ec; # section modulus of elasticity [MPa]
# ===== COLUMN =====
set LCol $LCol1; # column length [in]
set HCol 20.; # column dimension [in]
set bCol $HCol;
set numBars 8; # number of longitudinal bars
set cover 1.5; # cover for longitudinal bars [in]

```

```

set Dbar [expr 1*$reduframesteel*$agingredufactor]; # longitudinal bar
diameter [in]
set dbar 0.5; # transversal bar diameter [in]
set numBarsTopCol 3;
set numBarsBotCol 3;
set numBarsIntCol 2;
set barArea [expr ($pi/4)*pow($Dbar,2)]; # area of longitudinal bars [in2]
set rsec [expr $HCol/2]; # section radius [in] (8.860)
set rcore [expr $rsec-$cover+($dbar/2)]; # core section [in] (7.993)
set rbars [expr $rsec-$cover-($Dbar/2)]; # bar distribution radius [in]
set ACol [expr $HCol*$bCol]; # cross-sectional area [in2]
set I [expr 1./12*$bCol*pow($HCol,3)]; # section moment of inertia [in4]
set IzCol [expr $I*0.9]; # effective section moment of inertia [in4]
set IzelastC 4281.272126; # effective section moment of inertia
elastic[in4]
set E $Ec; # section modulus of elasticity [MPa]
set LpC 17.91552541; # equivalent plastic hinge length [in] 11.46593626
# ===== BEAM PROPERTIES =====
# ===== BEAM 1 =====
set LBeam 118.11; # Beam length [in]
set HBeam 24; # Beam dimension [in]
set bBeam $HCol;
set coverH 1.5;
set coverB 1.5;
# ===== Top =====
set numBarst 6; # number of longitudinal bars
set covert 1.5; # cover for longitudinal bars [in]
set Dbart [expr 0.875*$reduframesteel*$agingredufactor]; # longitudinal
bar
diameter [in] #7
set dbarbeam 0.375; # transversal bar diameter [in]
set barAreat [expr $pi/4*pow($Dbart,2)]; # area of longitudinal bars [in2]
# ===== Bottom =====
set numBarsbl 6; # number of longitudinal bars
set coverb 1.5; # cover for longitudinal bars [in]
set Dbarb [expr 0.875*$reduframesteel*$agingredufactor]; # longitudinal
bar
diameter [in]
set numBarsTopBeam1 6;
set numBarsBotBeam1 6;
set numBarsIntBeam1 0;
set barAreatopBeam1 [expr $pi/4*pow($Dbart,2)];
set barAreatbotBeam1 [expr $pi/4*pow($Dbarb,2)];
set barAreaIntBeam1 [expr $pi/4*pow($Dbarb,2)];
set barAreat [expr $pi/4*pow($Dbarb,2)]; # area of longitudinal bars [in2]
set rsecbeam [expr $HCol/2]; # section radius [in] (8.860)
set rcorebeam [expr $rsecbeam-$coverb+($dbarbeam/2)]; # core section [in]
(7.993)
set rbarsbeam [expr $rsecbeam-$rcorebeam-($Dbarb/2)]; # bar distribution
radius [in]
set ABeam [expr $HBeam*$bBeam]; # cross-sectional area [in2]
set IBeam [expr 1./12*$bBeam*pow($HBeam,3)]; # section moment of inertia
[in4]
set IzBeam [expr $IBeam*0.5]; # effective section moment of inertia [in4]
set IzelastB 8713.902356; # effective section moment of inertia
elastic[in4]
set EBeam $Ec; # section modulus of elasticity [ksi]
set LpBeam 15.76566236; # equivalent plastic hinge length [in]--
puts "1"
# ===== BEAM 2 =====
set LBeam 118.11; # Beam length [in]

```

```

set HBeam 24; # Beam dimension [in]
set bBeam $HCol;
set coverH 1.5;
set coverB 1.5;
# ===== Top =====
set numBarst 5; # number of longitudinal bars
set covert 1.5; # cover for longitudinal bars [in]
set Dbart [expr 0.875*$reduframesteel*$agingredufactor]; # longitudinal
bar
diameter [in]
set dbarbeam 0.375; # transversal bar diameter [in]
set barAreat [expr $pi/4*pow($Dbart,2)]; # area of longitudinal bars [in2]
# ===== Bottom=====
set numBarsb 5; # number of longitudinal bars
set coverb 1.5; # cover for longitudinal bars [in]
set Dbarb [expr 0.875*$reduframesteel*$agingredufactor]; # longitudinal
bar
diameter [in]
set numBarsTopBeam2 5;
set numBarsBotBeam2 5;
set numBarsIntBeam2 0;
set barAreatopBeam2 [expr $pi/4*pow($Dbart,2)];
set barAreabotBeam2 [expr $pi/4*pow($Dbarb,2)];
set barAreaIntBeam2 [expr $pi/4*pow($Dbarb,2)];
set barAreat [expr $pi/4*pow($Dbarb,2)]; # area of longitudinal bars [in2]
set rsecbeam [expr $HCol/2]; # section radius [in] (8.860)
set rcorebeam [expr $rsecbeam-$covert+($dbarbeam/2)]; # core section [in]
(7.993)
set rbarsbeam [expr $rsecbeam-$rcorebeam-($Dbarb/2)]; # bar distribution
radius [in]
set ABeam [expr $HBeam*$bBeam];; # cross-sectional area [in2]
set IBeam [expr 1./12*$bBeam *pow($HBeam,3)];; # section moment of inertia
[in4]
set IzBeam [expr $IBeam*0.5]; # effective section moment of inertia [in4]
set IzelastB 8713.902356; # effective section moment of inertia
elastic[in4]
set EBeam $Ec; # section modulus of elasticity [ksi]
set LpBeam 15.76566236; # equivalent plastic hinge length [in]--
puts "2"
# ===== BEAM 3 =====
set LBeam 118.11; # Beam length [in]
set HBeam 24; # Beam dimension [in]
set bBeam $HCol;
set coverH 1.5;
set coverB 1.5;
# ===== Top =====
set numBarst 3; # number of longitudinal bars
set covert 1.5; # cover for longitudinal bars [in]
set Dbart [expr 0.875*$reduframesteel*$agingredufactor]; # longitudinal
bar
diameter [in]
set dbarbeam 0.375; # transversal bar diameter [in]
set barAreat [expr $pi/4*pow($Dbart,2)]; # area of longitudinal bars [in2]
# ===== Bottom=====
set numBarsb 3; # number of longitudinal bars
set coverb 1.5; # cover for longitudinal bars [in]
set Dbarb [expr 0.875*$reduframesteel*$agingredufactor]; # longitudinal
bar
diameter [in]
set numBarsTopBeam3 3;
set numBarsBotBeam3 3;
set numBarsIntBeam3 0;
set barAreatopBeam3 [expr $pi/4*pow($Dbart,2)];

```

```

set barAreabotBeam3 [expr $pi/4*pow($Dbarb,2)];
set barAreaintBeam3 [expr $pi/4*pow($Dbarb,2)];
set barAreat [expr $pi/4*pow($Dbarb,2)]; # area of longitudinal bars [in2]
set rsecbeam [expr $HCol/2]; # section radius [in] (8.860)
set rcorebeam [expr $rsecbeam-$covert+($dbarbeam/2)]; # core section [in]
(7.993)
set rbarsbeam [expr $rsecbeam-$rcorebeam-($Dbarb/2)]; # bar distribution
radius [in]
set ABeam [expr $HBeam*$bBeam];; # cross-sectional area [in2]
set IBeam [expr 1./12*$bBeam *pow($HBeam,3)];; # section moment of inertia
[in4]
set IzBeam [expr $IBeam*0.5]; # effective section moment of inertia [in4]
set IzelastB 8713.902356; # effective section moment of inertia
elastic[in4]
8567.34927
set EBeam $Ec; # section modulus of elasticity [ksi]
set LpBeam 15.76566236; # equivalent plastic hinge length [in]--
puts "3"
#=====Masees=====
=
# Calculate Floor masses - nodal mass
set g 32.2; # Acceleration due to gravity, 386.4 in/(sec^2)
set pi 3.141593; # pi
set Negligible 1.0e-9; # A very small number to avoid problems with
zero
set GammaConcrete 0.15; # Reinforced-Concrete density Kips/ft3
set tf [expr $t/12];
# Calculate Frame masses - nodal mass
set AColft [expr $ACol/144];
set ABeamft [expr $ABeam/144];
set LColft [expr $LCol/12];
set LBeamft [expr $LBeam/12];
set columnweight [expr $AColft*$LColft*$GammaConcrete];
set beamweight [expr $ABeamft*$LBeamft*$GammaConcrete];
set weightnode [expr 0.5*$beamweight+$columnweight];
set weighttopnode [expr 0.5*$beamweight+$columnweight*0.5];
set additionalmass 365; # Additional mass 430-60% 365-50%
set additionalmassfloor [expr 0.5*$additionalmass];
set weightnodeframe [expr $additionalmassfloor+$weightnode];
set weighttopnodeframe [expr 0.5*$additionalmassfloor+$weighttopnode];
set FrameNodalMass [expr $weightnodeframe/$g/12]; # Floor nodal mass
set FrameTopNodalMass [expr $weighttopnodeframe/$g/12]; # Floor nodal mass
# Calculate Wall masses - nodal mass
set di 8;
set width [expr
11.81103+17.7165+7.87402+33.4646+7.87402+17.7165+9.84252+11.81103];
set widthft [expr $width/12];
set widthhole [expr 7.87402+33.4646+7.87402];
set widthholeft [expr $widthhole/12];
set Hft [expr $H/12/3];
set Hhole [expr 86.4020/12];
set wallarea [expr $Hft*$widthft];
set wallhole [expr $Hhole*$widthholeft];
set usefullarea [expr $wallarea-$wallhole];
set Vwall [expr $usefullarea*$tf];
set wallweight [expr $Vwall*$GammaConcrete];
set wallweighttopr [expr $wallweight*0.5];
set wallweighttoperfloor [expr $wallweighttopr+$additionalmass/1];
set wallmassperfloor1 [expr $wallweighttoperfloor/$g/12];
set wallmassperfloor [expr $wallmassperfloor1/$di];
set wallmasstopperfloor1 [expr $wallweighttoperfloor/$g/12];

```



```

set wallmassstopperfloor [expr $wallmassstopperfloor1/$di];
puts "error 1"
puts "Ec_$Ec"
puts "AColft_$AColft"
puts "ABeamft_$ABeamft"
puts "columnweight_$columnweight"
puts "beamweight_$beamweight"
puts "weightnode_$weightnode"
puts "weighttopnode_$weighttopnode"
puts "widthft_$widthft"
puts "Hft_$Hft"
puts "Hhole_$Hhole"
puts "wallarea_$wallarea"
puts "wallhole_$wallhole"
puts "Vwall_$Vwall"
puts "wallweight_$wallweight"
puts "usefullarea_$usefullarea"
puts "wallweightperfloor_$wallweightperfloor"
puts "FrameNodalMass_$FrameNodalMass "
puts "FrameTopNodalMass_$FrameTopNodalMass"
puts "wallmassperfloor_$wallmassperfloor"
puts "wallmasstopperfloor_$wallmasstopperfloor"
puts "weightnodeframe_$weightnodeframe"
puts "error 2"
#=====Coordinates=====
===== axial load ratio
# Create nodes
# node nodeId xCrd yCrd
#Wall elements position
#=====Pared 1
node 1 0 0;
puts "error 3"
node 2 0 15.2362;
puts "error 4"
node 3 0 30.4724;
node 4 0 50.78;
node 5 0 71.1024;
node 6 0 86.4020;
node 7 0 101.5748;
node 8 0 121.8898296 -mass $wallmassperfloor $wallmassperfloor
$Negligible;
puts "error 5"
# =====Pared 2
node 9 0 142.2048;
node 10 0 157.4410299;
node 11 0 177.7560015;
node 12 0 198.0709731;
node 13 0 213.3072018;
node 14 0 243.7796592 -mass $wallmassperfloor $wallmassperfloor
$Negligible;
#=====Pared 3
node 15 0 264.0946308;
node 16 0 279.3308595;
node 17 0 299.6458311;
node 18 0 319.9608027;
node 19 0 335.1970314;
node 20 0 365.6694888 -mass $wallmasstopperfloor $wallmasstopperfloor
$Negligible;
node 24 118.11 0;
node 21 118.11 121.8898296;
node 22 118.11 243.7796592;
node 23 118.11 365.6694888;
#Frame position and hinges positions
set XC1 $L;
set XC2 [expr $L+118.1103];

```

```

set XB1 [expr $L+$HCol*0.5];
set XB2 [expr $L+118.1103-$HCol*0.5];
#=====Column 1
node 31 $XC1 0;
node 321 $XC1 [expr 121.8898296-$HCol*0.5];
node 32 $XC1 121.8898296 -mass $FrameNodalMass $FrameNodalMass
$Negligible;
node 322 $XC1 [expr 121.8898296+$HCol*0.5];
node 331 $XC1 [expr 243.7796592-$HCol*0.5];
node 33 $XC1 243.7796592 -mass $FrameNodalMass $FrameNodalMass
$Negligible;
node 332 $XC1 [expr 243.7796592+$HCol*0.5];
node 341 $XC1 [expr 365.6694888-$HCol*0.5];
node 34 $XC1 365.6694888 -mass $FrameTopNodalMass $FrameTopNodalMass
$Negligible;
#=====Column 2
node 41 $XC2 0;
# node 411 $XC2 [expr 0+$HCol]; #Node created to read the acceleration
node 421 $XC2 [expr 121.8898296-$HCol*0.5];
node 42 $XC2 121.8898296 -mass $FrameNodalMass $FrameNodalMass
$Negligible;
node 422 $XC2 [expr 121.8898296+$HCol*0.5];
node 431 $XC2 [expr 243.7796592-$HCol*0.5];
node 43 $XC2 243.7796592 -mass $FrameNodalMass $FrameNodalMass
$Negligible;
node 432 $XC2 [expr 243.7796592+$HCol*0.5];
node 441 $XC2 [expr 365.6694888-$HCol*0.5];
node 44 $XC2 365.6694888 -mass $FrameTopNodalMass $FrameTopNodalMass
$Negligible;
#=====Beam 1
node 61 $XB1 121.8898296;
node 62 $XB2 121.8898296;
#=====Beam 2
node 71 $XB1 243.7796592;
node 72 $XB2 243.7796592;
#=====Beam 3
node 81 $XB1 365.6694888;
node 82 $XB2 365.6694888;
print node;
# Boundary conditions
fix 1 1 1 1; # Fixed condition at node 1
fix 24 1 1 1; # Fixed condition at node 24
fix 31 1 1 1; # Fixed condition at node 31
fix 41 1 1 1; # Fixed condition at node 41
# Set Control Node and DOF for the frame
set IDctrlNodef 34;
set IDctrlDOF 1;
set IDReactNode1 31;
set IDReactNode2 41;
# Set Control Node and DOF for the wall
set IDctrlNodew 20;
set IDctrlDOF 1;
set IDctrlNode $IDctrlNodew;
# # ===== CONCRETE PROPERTIES (Concrete 01) For Column
=====
# ===== CONCRETE PROPERTIES (Concrete 01)
=====
# confined concrete at beams and columns
set Kfcb 1.21; # ratio of confined to unconfined concrete
strength [Beam]
set Kresb 0.2; # ratio of residual/ultimate to maximum
stress [Beam]
set Kfcc 1.6; # ratio of confined to unconfined
concrete strength [Col]
set Kresc 0.2; # ratio of residual/ultimate to maximum
stress [Col]

```

```

set f1C [expr $Kfcb*$fc]; # CONFINED concrete (mander model), maximum
stress [MPa] [Beam]
set f1Cc [expr $Kfcc*$fc]; # CONFINED concrete (mander model), maximum
stress [MPa] [Col]
set eps0 -0.002; # UNCONFINED concrete strain
set fac [expr $f1C/-$Ec];
set facc [expr $f1Cc/-$Ec];
set eps1C [expr $eps0*(1+5*($fac-1))]; # strain at confined concrete
strength
[Beam]
set eps1Cc [expr $eps0*(1+5*($facc-1))]; # strain at confined concrete
strength
[Col]
set f2C [expr $Kresb*$f1C]; # crushing strength [MPa] [Beam]
set f2Cc [expr $Kresc*$f1Cc]; # crushing strength [MPa] [Col]
set eps2C -0.03;
# unconfined concrete at beams and columns
set f1U $fc; # UNCONFINED concrete, maximum stress [MPa]
set eps1U $eps0; # strain at maximum strength of unconfined
concrete
set f2U 0.001; # crushing strength [MPa]
set eps2U -0.0064; # strain at ultimate stress
set IDconcCore 20; #ID number for core concrete
at beams
set IDconcCover 21; #ID number for cover concrete
(unconfined)
set IDconcCorec 22; #ID number for core concrete
at columns
uniaxialMaterial Concrete01 $IDconcCore $f1C $eps1C $f2C $eps2C; #
Core concrete
(confined) [Beam]
uniaxialMaterial Concrete01 $IDconcCorec $f1Cc $eps1Cc $f2Cc $eps2C; #
Core concrete
(confined) [Col]
uniaxialMaterial Concrete01 $IDconcCover $f1U $eps1U $f2U $eps2U; #
Cover concrete
(unconfined) $fc1U $eps1U $fc2U $eps2U
#===== REINFORCING STEEL PROPERTIES (fictional)
=====
set Fy 60.000; # STEEL yield stress [ksi]
set Fu 104.500; # STEEL max stress [ksi]
set Es 29000.000; # STEEL modulus [ksi]
set Esh 726.000; # Tangent at initial strain hargening [ksi]
set eish 0.008; # Strain corresponding to initial strain hardening
set eult 0.100; # Strain at peak stress
set alpha 0.506; # usually constant for a material type
set Cf 0.250; # adjust the number of cycles to failure
set Cd 0.500; # Strength reduction constant
set R1 0.383;
set R2 16.000;
set R3 8.000;
set IDSteelc 23;
uniaxialMaterial ReinforcingSteel $IDSteelc $Fy $Fu $Es $Esh $eish
$eult -MPCurveParams $R1
$R2 $R3; # -CMFatigue $Cf $alpha $Cd
#===== SECTION GENERATION
=====
# Define section tags
set ColSecTag 1
set BeamSecTag 2
puts "2"
#===== Divisiones?????
set nfCoreY 20; # number of radial divisions in the core (number of
"rings")

```

```

set nfCoreZ 20; # number of theta divisions in the core (number of
"wedges")
set nfCoverY 20; # number of radial divisions in the cover
set nfCoverZ 20; # number of theta divisions in the cover
# ===== COLUMN 1 =====
# BuildRCrectSection $ColSecTag $HCol $bCol $cover $cover $IDconcCore
$IDconcCover $IDSteelc
$numBarsTopCol $barArea $numBarsBotCol $barArea $numBarsIntCol
$barArea $nfCoreY $nfCoreZ
$nfCoverY $nfCoverZ
puts "3"
# -----
----
# Define uniaxial materials for 2D RC Panel Constitutive Model (FSAM)
# -----
----
# STEEL .....
# uniaxialMaterial SteelMPF $mattag $fyp $fyn $EO $bp $bn $RO $a1 $a2
# steel X
set fyX 58.4103; # fy[Mpa]
set bx 0.01; # strain hardening
# steel Y web
set fyYw 58.4103; # fy[Mpa]
set byw 0.01; # strain hardening
# steel Y boundary
set fyYb 69.0; # fy[MPA]
set byb 0.002; # strain hardening
# steel misc
set Esy 29000.0; # Young's modulus[MPa]
set Esx $Esy; # Young's modulus
set RO 20.0; # initial value of curvature parameter
set A1 0.925; # curvature degradation parameter
set A2 0.15; # curvature degradation parameter
# Build steel materials
uniaxialMaterial SteelMPF 1 $fyX $fyX $Esx $bx $bx $RO $A1 $A2; #
steel X
uniaxialMaterial SteelMPF 2 $fyYw $fyYw $Esy $byw $byw $RO $A1 $A2; #
steel Y web
uniaxialMaterial SteelMPF 3 $fyYb $fyYb $Esy $byb $byb $RO $A1 $A2; #
steel Y boundary
# CONCRETE .....
# uniaxialMaterial ConcreteCM $mattag $fpcc $sepcc $Ec $rc $xcrn $ft
$set $rt $xcrp
<-GapClose $gap>
set fcm -55.7786;
# CONCRETE ..... case 1
.....
# unconfined
set fpc1 8.09; # peak compressive stress[Ksi] 8.09 4.0
set ec01 -0.002; # strain at peak compressive stress
set ftin [expr 0.7*sqrt(-$fcm)]; # peak tensile stress[MPa]
set ft1 [expr $ftin*0.145]; # peak tensile stress [ksi] 0.335798
set Ec1 [expr 5000*sqrt(-$fcm)]; # concrete modulus of elasticity [MPa]
set Ec [expr $Ec1*0.145]; # concrete modulus of elasticity [ksi]
set Ec1 $Ec; # Young's modulus[Ksi] 5403.2172
set et1 [expr $ft1/$Ec1]; # strain at peak tensile stress cambiar 0.00008
set xcrnul 1.022; # cracking strain - compression
set xcrp1 10000; # cracking strain - tension
set rul 15; # shape parameter - compression
set rtl 1.2; # shape parameter - tension
set kw 1.4637;
set Ecc [expr 5000*sqrt(-$fcm*$kw)]; # concrete modulus of elasticity [MPa]
set Ecc [expr $Ecc*0.145]; # concrete modulus of elasticity [ksi]
# puts "Wall Ecc_$Ecc"
# confined

```

```

set fpcc1 [expr $fpc1*$kw]; # peak compressive stress[ksi] 10.479723
set ec0c1 -0.007558160187084; # strain at peak compressive stress
0.005873
set Ecc1 $Ecc; # Young's modulus[ksi] 5953.9187
set xcrnc1 1.023; # cracking strain - compression
set rc1 12.072964; # shape parameter - compression
# CONCRETE ..... case 2
.....
# unconfined
set fpc2 8.09; # peak compressive stress[Ksi] 8.09
set ec02 -0.002; # strain at peak compressive stress
set ftin [expr 0.7*sqrt(-$fcm)]; # peak tensile stress[MPa]
set ft2 [expr $ftin*0.145]; # peak tensile stress [ksi] 0.335798
set et2 [expr $ft2/$Ec1]; # strain at peak tensile stress cambiar
set Ec1 [expr 5000*sqrt(-$fcm)]; # concrete modulus of elasticity [MPa]
set Ec [expr $Ec1*0.145]; # concrete modulus of elasticity [ksi]
set Ec2 $Ec; # Young's modulus[Ksi] 5403.2172
set xcrnu2 1.022; # cracking strain - compression
set xcrp2 10000; # cracking strain - tension
set ru2 15; # shape parameter - compression
set rt2 1.2; # shape parameter - tension
set kw 1.4637;
set Ecc [expr 5000*sqrt(-$fcm*$kw)]; # concrete modulus of elasticity [MPa]
set Ecc [expr $Ecc*0.145]; # concrete modulus of elasticity [ksi]
# puts "Wall Ecc_$Ecc"
# confined
set fpcc2 [expr $fpc2*$kw]; # peak compressive stress[ksi] 10.479723
set ec0c2 -0.007498212031673; # strain at peak compressive stress
0.005873
set Ecc2 $Ecc; # Young's modulus[ksi] 5953.9187
set xcrnc2 1.023; # cracking strain - compression
set rc2 12.072964; # shape parameter - compression
# CONCRETE ..... case 3
.....
# unconfined
set fpc3 8.09; # peak compressive stress[Ksi] 8.09
set ec03 -0.002; # strain at peak compressive stress
set ftin [expr 0.7*sqrt(-$fcm)]; # peak tensile stress[MPa]
set ft3 [expr $ftin*0.145]; # peak tensile stress [ksi] 0.335798
set et3 [expr $ft3/$Ec1]; # strain at peak tensile stress cambiar
set Ec1 [expr 5000*sqrt(-$fcm)]; # concrete modulus of elasticity [MPa]
set Ec [expr $Ec1*0.145]; # concrete modulus of elasticity [ksi]
set Ec3 $Ec; # Young's modulus[Ksi] 5403.2172
set xcrnu3 1.022; # cracking strain - compression
set xcrp3 10000; # cracking strain - tension
set ru3 15; # shape parameter - compression
set rt3 1.2; # shape parameter - tension
set kw 1.4637;
set Ecc [expr 5000*sqrt(-$fcm*$kw)]; # concrete modulus of elasticity [MPa]
set Ecc [expr $Ecc*0.145]; # concrete modulus of elasticity [ksi]
# puts "Wall Ecc_$Ecc"
# confined
set fpcc3 [expr $fpc3*$kw]; # peak compressive stress[ksi] 10.479723

set ec0c3 -0.007274155121133; # strain at peak compressive stress
0.005873
set Ecc3 $Ecc; # Young's modulus[ksi] 5953.9187
set xcrnc3 1.023; # cracking strain - compression
set rc3 12.072964; # shape parameter - compression
# Build concrete materials
# uniaxialMaterial ConcreteCM $mathtag $fpcc $epcc $Ec $rc $xcrn $ft
$et $rt $xcrp
<-GapClose $gap>

```

```

uniaxialMaterial ConcreteCM 41 -$fpc1 $ec01 $Ec1 $ru1 $xcrnu1 $ft1
$set1 $rt1
$xcrp1 -GapClose 0; # unconfined concrete Case 1
uniaxialMaterial ConcreteCM 51 -$fpcc1 $ec0c1 $Ecc1 $rc1 $xcrnc1 $ft1
$set1 $rt1
$xcrp1 -GapClose 0; # confined concrete
uniaxialMaterial ConcreteCM 42 -$fpc2 $ec02 $Ec2 $ru2 $xcrnu2 $ft2
$set2 $rt2
$xcrp2 -GapClose 0; # unconfined concrete Case 2
uniaxialMaterial ConcreteCM 52 -$fpcc2 $ec0c2 $Ecc2 $rc2 $xcrnc2 $ft2
$set2 $rt2
$xcrp2 -GapClose 0; # confined concrete
uniaxialMaterial ConcreteCM 43 -$fpc3 $ec03 $Ec3 $ru3 $xcrnu3 $ft3
$set3 $rt3
$xcrp3 -GapClose 0; # unconfined concrete Case 3
uniaxialMaterial ConcreteCM 53 -$fpcc3 $ec0c3 $Ecc3 $rc3 $xcrnc3 $ft3
$set3 $rt3
$xcrp3 -GapClose 0; # confined concrete
# -----
# Define 2D RC Panel Material (FSAM)
# -----
set reduratio 0.3;
set agingredufactorwall 0.75;
# Reinforcing ratios
#Boundary
# Pared 1
set rouXb1b [expr 0.002513274*$reduratio*$agingredufactorwall]; # X
boundary
set rouYb1b [expr 0.007539822*$reduratio*$agingredufactorwall]; # Y
boundary
set rouXb1a [expr 0.008168141*$reduratio*$agingredufactorwall]; # X
boundary
set rouYb1a [expr 0.007539822*$reduratio*$agingredufactorwall]; # Y
boundary
# Pared 2
set rouXb2b [expr 0.002513274*$reduratio*$agingredufactorwall]; # X
boundary
set rouYb2b [expr 0.006283185*$reduratio*$agingredufactorwall]; # Y
boundary
set rouXb2a [expr 0.013823008*$reduratio*$agingredufactorwall]; # X
boundary
set rouYb2a [expr 0.006283185*$reduratio*$agingredufactorwall]; # Y
boundary
# Pared 3
set rouXb3b [expr 0.002513274*$reduratio*$agingredufactorwall]; # X
boundary
set rouYb3b [expr 0.006283185*$reduratio*$agingredufactorwall]; # Y
boundary
set rouXb3a [expr 0.010681415*$reduratio*$agingredufactorwall]; # X
boundary
set rouYb3a [expr 0.006283185*$reduratio*$agingredufactorwall]; # Y
boundary
# Zona del hueco
set rouXwN 0.0; # X web
set rouYwN 0.0; # Y web
# Pared 1
set rouXw12b [expr 0.002513274*$reduratio*$agingredufactorwall]; # X web
set rouYw12b [expr 0.008517207*$reduratio*$agingredufactorwall]; # Y web
set rouXw12a [expr 0.008168141*$reduratio*$agingredufactorwall]; # X web
set rouYw12a [expr 0.008517207*$reduratio*$agingredufactorwall]; # Y web
set rouXw13a [expr 0.008168141*$reduratio*$agingredufactorwall]; # X web
set rouYw13a [expr 0.005864306*$reduratio*$agingredufactorwall]; # Y web
set rouXw14a [expr 0.008168141*$reduratio*$agingredufactorwall]; # X web
set rouYw14a [expr 0.005519347*$reduratio*$agingredufactorwall]; # Y web
set rouXw15a [expr 0.008168141*$reduratio*$agingredufactorwall]; # X web
set rouYw15a [expr 0.005864306*$reduratio*$agingredufactorwall]; # Y web

```

```

set rouXw16b [expr 0.002513274*$reduratio*$agingredufactorwall]; # X web
set rouYw16b [expr 0.008517207*$reduratio*$agingredufactorwall]; # Y web
set rouXw16a [expr 0.008168141*$reduratio*$agingredufactorwall]; # X web
set rouYw16a [expr 0.008517207*$reduratio*$agingredufactorwall]; # Y web
set rouXw17b [expr 0.002513274*$reduratio*$agingredufactorwall]; # X web
set rouYw17b [expr 0.00678584*$reduratio*$agingredufactorwall]; # Y web
set rouXw17a [expr 0.008168141*$reduratio*$agingredufactorwall]; # X web
set rouYw17a [expr 0.00678584*$reduratio*$agingredufactorwall]; # Y web
# Pared 2
set rouXw22b [expr 0.002513274*$reduratio*$agingredufactorwall]; # X web

set rouYw22b [expr 0.005166175*$reduratio*$agingredufactorwall]; # Y web
set rouXw22a [expr 0.013823008*$reduratio*$agingredufactorwall]; # X web
set rouYw22a [expr 0.005166175*$reduratio*$agingredufactorwall]; # Y web
set rouXw23a [expr 0.013823008*$reduratio*$agingredufactorwall]; # X web
set rouYw23a [expr 0.005864306*$reduratio*$agingredufactorwall]; # Y web
set rouXw24a [expr 0.013823008*$reduratio*$agingredufactorwall]; # X web
set rouYw24a [expr 0.005519347*$reduratio*$agingredufactorwall]; # Y web
set rouXw25a [expr 0.013823008*$reduratio*$agingredufactorwall]; # X web
set rouYw25a [expr 0.005864306*$reduratio*$agingredufactorwall]; # Y web
set rouXw26b [expr 0.002513274*$reduratio*$agingredufactorwall]; # X web
set rouYw26b [expr 0.00572468*$reduratio*$agingredufactorwall]; # Y web
set rouXw26a [expr 0.013823008*$reduratio*$agingredufactorwall]; # X web
set rouYw26a [expr 0.00572468*$reduratio*$agingredufactorwall]; # Y web
set rouXw27b [expr 0.002513274*$reduratio*$agingredufactorwall]; # X web
set rouYw27b [expr 0.002010619*$reduratio*$agingredufactorwall]; # Y web
set rouXw27a [expr 0.013823008*$reduratio*$agingredufactorwall]; # X web
set rouYw27a [expr 0.002010619*$reduratio*$agingredufactorwall]; # Y web
# Pared 3
set rouXw32b [expr 0.002513274*$reduratio*$agingredufactorwall]; # X web
set rouYw32b [expr 0.005166175*$reduratio*$agingredufactorwall]; # Y web
set rouXw32a [expr 0.010681415*$reduratio*$agingredufactorwall]; # X web
set rouYw32a [expr 0.005166175*$reduratio*$agingredufactorwall]; # Y web
set rouXw33a [expr 0.010681415*$reduratio*$agingredufactorwall]; # X web
set rouYw33a [expr 0.005864306*$reduratio*$agingredufactorwall]; # Y web
set rouXw34a [expr 0.010681415*$reduratio*$agingredufactorwall]; # X web
set rouYw34a [expr 0.005519347*$reduratio*$agingredufactorwall]; # Y web
set rouXw35a [expr 0.010681415*$reduratio*$agingredufactorwall]; # X web
set rouYw35a [expr 0.005864306*$reduratio*$agingredufactorwall]; # Y web
set rouXw36b [expr 0.002513274*$reduratio*$agingredufactorwall]; # X web
set rouYw36b [expr 0.00572468*$reduratio*$agingredufactorwall]; # Y web
set rouXw36a [expr 0.010681415*$reduratio*$agingredufactorwall]; # X web
set rouYw36a [expr 0.008517207*$reduratio*$agingredufactorwall]; # Y web
set rouXw37b [expr 0.002513274*$reduratio*$agingredufactorwall]; # X web
set rouYw37b [expr 0.002010619*$reduratio*$agingredufactorwall]; # Y web
set rouXw37a [expr 0.010681415*$reduratio*$agingredufactorwall]; # X web
set rouYw37a [expr 0.002010619*$reduratio*$agingredufactorwall]; # Y web
# Shear resisting mechanism parameters
set nu 0.2; # friction coefficient
set alfadow 0.012; # dowel action stiffness parameter
set c 0.42;
# nDMaterial FSAM $mattag $rho $sX $sY $conc $rouX $rouY $nu $alfadow
# Pared 1
nDMaterial FSAM 100 0.0 1 2 41 $rouXwN $rouYwN $nu $alfadow; # Web2
(unconfined concrete) hueco
nDMaterial FSAM 101 0.0 1 2 41 $rouXw12b $rouYw12b $nu $alfadow; #
Web2 (unconfined concrete) Down
nDMaterial FSAM 102 0.0 1 2 43 $rouXw12a $rouYw12a $nu $alfadow; #
Web3 (unconfined concrete) Top
nDMaterial FSAM 103 0.0 1 2 43 $rouXw13a $rouYw13a $nu $alfadow; #
Web4 (unconfined concrete) Top
nDMaterial FSAM 104 0.0 1 2 43 $rouXw14a $rouYw14a $nu $alfadow; #
Web5 (unconfined concrete) Top

```



```

nDMaterial FSAM 105 0.0 1 2 43 $rouXw15a $rouYw15a $nu $alfadow; #
Web6 (unconfined concrete) Top
nDMaterial FSAM 106 0.0 1 2 42 $rouXw16b $rouYw16b $nu $alfadow; #
Web7 (unconfined concrete) Down
nDMaterial FSAM 107 0.0 1 2 43 $rouXw16a $rouYw16a $nu $alfadow; #
Web2 (unconfined concrete) Top
nDMaterial FSAM 108 0.0 1 2 42 $rouXw17b $rouYw17b $nu $alfadow; #
Web3 (unconfined concrete) Down
nDMaterial FSAM 109 0.0 1 2 43 $rouXw17a $rouYw17a $nu $alfadow; #
Web4 (unconfined concrete) Top
# Pared 2
nDMaterial FSAM 201 0.0 1 2 41 $rouXw22b $rouYw22b $nu $alfadow; #
Web2 (unconfined concrete) Down
nDMaterial FSAM 202 0.0 1 2 43 $rouXw22a $rouYw22a $nu $alfadow; #

Web3 (unconfined concrete) Top
nDMaterial FSAM 203 0.0 1 2 43 $rouXw23a $rouYw23a $nu $alfadow; #
Web4 (unconfined concrete) Top
nDMaterial FSAM 204 0.0 1 2 43 $rouXw24a $rouYw24a $nu $alfadow; #
Web5 (unconfined concrete) Top
nDMaterial FSAM 205 0.0 1 2 43 $rouXw25a $rouYw25a $nu $alfadow; #
Web6 (unconfined concrete) Top
nDMaterial FSAM 206 0.0 1 2 42 $rouXw26b $rouYw26b $nu $alfadow; #
Web7 (unconfined concrete) Down
nDMaterial FSAM 207 0.0 1 2 43 $rouXw26a $rouYw26a $nu $alfadow; #
Web2 (unconfined concrete) Top
nDMaterial FSAM 208 0.0 1 2 42 $rouXw27b $rouYw27b $nu $alfadow; #
Web3 (unconfined concrete) Down
nDMaterial FSAM 209 0.0 1 2 43 $rouXw27a $rouYw27a $nu $alfadow; #
Web4 (unconfined concrete) Top
# Pared 3
nDMaterial FSAM 301 0.0 1 2 41 $rouXw32b $rouYw32b $nu $alfadow; #
Web2 (unconfined concrete) Down
nDMaterial FSAM 302 0.0 1 2 43 $rouXw32a $rouYw32a $nu $alfadow; #
Web3 (unconfined concrete) Top
nDMaterial FSAM 303 0.0 1 2 43 $rouXw33a $rouYw33a $nu $alfadow; #
Web4 (unconfined concrete) Top
nDMaterial FSAM 304 0.0 1 2 43 $rouXw34a $rouYw34a $nu $alfadow; #
Web5 (unconfined concrete) Top
nDMaterial FSAM 305 0.0 1 2 43 $rouXw35a $rouYw35a $nu $alfadow; #
Web6 (unconfined concrete) Top
nDMaterial FSAM 306 0.0 1 2 42 $rouXw36b $rouYw36b $nu $alfadow; #
Web7 (unconfined concrete) Down
nDMaterial FSAM 307 0.0 1 2 43 $rouXw36a $rouYw36a $nu $alfadow; #
Web2 (unconfined concrete) Top
nDMaterial FSAM 308 0.0 1 2 42 $rouXw37b $rouYw37b $nu $alfadow; #
Web3 (unconfined concrete) Down
nDMaterial FSAM 309 0.0 1 2 43 $rouXw37a $rouYw37a $nu $alfadow; #
Web4 (unconfined concrete) Top
#Boundary
nDMaterial FSAM 6 0.0 1 3 51 $rouXb1b $rouYb1b $nu $alfadow; #
Boundary (confined concrete only) Down left
nDMaterial FSAM 61 0.0 1 3 52 $rouXb1b $rouYb1b $nu $alfadow; #
Boundary (confined concrete only) Down right
nDMaterial FSAM 7 0.0 1 3 53 $rouXb1a $rouYb1a $nu $alfadow; #
Boundary (confined concrete only) Top
nDMaterial FSAM 8 0.0 1 3 51 $rouXb2b $rouYb2b $nu $alfadow; #
Boundary (confined concrete only) Down left
nDMaterial FSAM 81 0.0 1 3 52 $rouXb2b $rouYb2b $nu $alfadow; #
Boundary (confined concrete only) Down right
nDMaterial FSAM 9 0.0 1 3 53 $rouXb2a $rouYb2a $nu $alfadow; #
Boundary (confined concrete only) Top
nDMaterial FSAM 10 0.0 1 3 51 $rouXb3b $rouYb3b $nu $alfadow; #
Boundary (confined concrete only) Down left
nDMaterial FSAM 1011 0.0 1 3 52 $rouXb3b $rouYb3b $nu $alfadow; #
Boundary (confined concrete only) Down right
nDMaterial FSAM 11 0.0 1 3 53 $rouXb3a $rouYb3a $nu $alfadow; #
Boundary (confined concrete only) Top
#===== SECTION GENERATION
=====

```



```

# Define section tags
set ColSecTag 1
set BeamSecTag1 2
set BeamSecTag2 3
set BeamSecTag3 4
puts "2"
#===== Divisiones?????
set nfCoreY 20; # number of radial divisions in the core (number of
"rings")
set nfCoreZ 20; # number of theta divisions in the core (number of
"wedges")
set nfCoverY 20; # number of radial divisions in the cover
set nfCoverZ 20; # number of theta divisions in the cover
# ===== COLUMN =====

BuildRCrectSection $ColSecTag $HCol $bCol $cover $cover $IDconcCorec
$IDconcCover $IDSteelc
$numBarsTopCol $barArea $numBarsBotCol $barArea $numBarsIntCol
$barArea $nfCoreY $nfCoreZ
$nfCoverY $nfCoverZ
# ===== Beam 1 =====
BuildRCrectSection $BeamSecTag1 $HBeam $bBeam $coverH $coverB
$IDconcCore $IDconcCover
$IDSteelc $numBarsTopBeam1 $barAreatopBeam1 $numBarsBotBeam1
$barAreabotBeam1
$numBarsIntBeam1 $barAreaaintBeam1 $nfCoreY $nfCoreZ $nfCoverY
$nfCoverZ
# ===== Beam 2 =====
BuildRCrectSection $BeamSecTag2 $HBeam $bBeam $coverH $coverB
$IDconcCore $IDconcCover
$IDSteelc $numBarsTopBeam2 $barAreatopBeam2 $numBarsBotBeam2
$barAreabotBeam2
$numBarsIntBeam2 $barAreaaintBeam2 $nfCoreY $nfCoreZ $nfCoverY
$nfCoverZ
# ===== Beam 3 =====
BuildRCrectSection $BeamSecTag3 $HBeam $bBeam $coverH $coverB
$IDconcCore $IDconcCover
$IDSteelc $numBarsTopBeam3 $barAreatopBeam3 $numBarsBotBeam3
$barAreabotBeam3
$numBarsIntBeam3 $barAreaaintBeam3 $nfCoreY $nfCoreZ $nfCoverY
$nfCoverZ
puts "3"
# Define section tags
# set ColSecTag 1
# set BeamSecTag 2
# -----
# Define SFI_MVLEM elements
# -----
set IDColTransf 1; # all columns
set IDBeamtranf 2;
set ColTransftype Linear;
geomTransf $ColTransftype $IDColTransf;
# Command: geomTransf Linear $transfTag <-jntOffset $dXi $dYi $dXj
$dYj>
geomTransf Linear $IDBeamtranf;
# ----- Wall elements
# -----
# element SFI_MVLEM eleTag iNode jNode m c -thick fiberThick -width
fiberWidth -mat matTags
#=====Pared 1
element SFI_MVLEM 1 1 2 8 $c -thick $t $t $tO $tO $tO $t $t $t -width
11.81103 17.7165
7.87402 33.4646 7.87402 17.7165 9.84252 11.81103 -mat 6 101 100 100
100 106 108 6
element SFI_MVLEM 2 2 3 8 $c -thick $t $t $tO $tO $tO $t $t $t -width
11.81103 17.7165
7.87402 33.4646 7.87402 17.7165 9.84252 11.81103 -mat 6 101 100 100
100 106 108 6

```

```

element SFI_MVLEM 3 3 4 8 $c -thick $t $t $tO $tO $tO $t $t $t -width
11.81103 17.7165
7.87402 33.4646 7.87402 17.7165 9.84252 11.81103 -mat 6 101 100 100
100 106 108 6
element SFI_MVLEM 4 4 5 8 $c -thick $t $t $tO $tO $tO $t $t $t -width
11.81103 17.7165
7.87402 33.4646 7.87402 17.7165 9.84252 11.81103 -mat 6 101 100 100
100 106 108 6
element SFI_MVLEM 5 5 6 8 $c -thick $t $t $tO $tO $tO $t $t $t -width
11.81103 17.7165
7.87402 33.4646 7.87402 17.7165 9.84252 11.81103 -mat 6 101 100 100
100 108 11 6
element SFI_MVLEM 6 6 7 8 $c -thick $t $t $t $t $t $t $t $t -width
11.81103 17.7165
7.87402 33.4646 7.87402 17.7165 9.84252 11.81103 -mat 7 102 103 104
105 107 109 7
element SFI_MVLEM 7 7 8 8 $c -thick $t $t $t $t $t $t $t $t -width
11.81103 17.7165
7.87402 33.4646 7.87402 17.7165 9.84252 11.81103 -mat 7 102 103 104
105 107 109 7
#=====Pared 2
element SFI_MVLEM 8 8 9 8 $c -thick $t $t $tO $tO $tO $t $t $t -width
11.81103 17.7165
7.87402 33.4646 7.87402 17.7165 9.84252 11.81103 -mat 8 201 100 100
100 206 208 8
element SFI_MVLEM 9 9 10 8 $c -thick $t $t $tO $tO $tO $t $t $t -width
11.81103 17.7165
7.87402 33.4646 7.87402 17.7165 9.84252 11.81103 -mat 8 201 100 100
100 206 208 8
element SFI_MVLEM 10 10 11 8 $c -thick $t $t $tO $tO $tO $t $t $t -
width 11.81103
17.7165 7.87402 33.4646 7.87402 17.7165 9.84252 11.81103 -mat 8 201
100 100 100 206 208 8
element SFI_MVLEM 11 11 12 8 $c -thick $t $t $tO $tO $tO $t $t $t -
width 11.81103
17.7165 7.87402 33.4646 7.87402 17.7165 9.84252 11.81103 -mat 8 201
100 100 100 206 208 8
element SFI_MVLEM 12 12 13 8 $c -thick $t $t $t $t $t $t $t $t -width
11.81103 17.7165
7.87402 33.4646 7.87402 17.7165 9.84252 11.81103 -mat 8 201 100 100
100 206 208 8
element SFI_MVLEM 13 13 14 8 $c -thick $t $t $t $t $t $t $t $t -width
11.81103 17.7165
7.87402 33.4646 7.87402 17.7165 9.84252 11.81103 -mat 9 202 203 204
205 207 209 9
#=====Pared 3
element SFI_MVLEM 14 14 15 8 $c -thick $t $t $tO $tO $tO $t $t $t -
width 11.81103
17.7165 7.87402 33.4646 7.87402 17.7165 9.84252 11.81103 -mat 10 301
100 100 100 306 308 10
element SFI_MVLEM 15 15 16 8 $c -thick $t $t $tO $tO $tO $t $t $t -
width 11.81103
17.7165 7.87402 33.4646 7.87402 17.7165 9.84252 11.81103 -mat 10 301
100 100 100 306 308 10
element SFI_MVLEM 16 16 17 8 $c -thick $t $t $tO $tO $tO $t $t $t -
width 11.81103
17.7165 7.87402 33.4646 7.87402 17.7165 9.84252 11.81103 -mat 10 301
100 100 100 306 308 10

element SFI_MVLEM 17 17 18 8 $c -thick $t $t $tO $tO $tO $t $t $t -
width 11.81103
17.7165 7.87402 33.4646 7.87402 17.7165 9.84252 11.81103 -mat 10 301
100 100 100 306 308 10
element SFI_MVLEM 18 18 19 8 $c -thick $t $t $t $t $t $t $t $t -width
11.81103 17.7165
7.87402 33.4646 7.87402 17.7165 9.84252 11.81103 -mat 10 301 100 100
100 306 308 10
element SFI_MVLEM 19 19 20 8 $c -thick $t $t $t $t $t $t $t $t -width
11.81103 17.7165

```

```

7.87402 33.4646 7.87402 17.7165 9.84252 11.81103 -mat 11 302 303 304
305 307 309 11
# ----- Aux Column element Section
-----
element elasticBeamColumn 2000 1 8 $ACol1 $ECol $IzCol1 $IDColTransf
element elasticBeamColumn 2100 8 14 $ACol1 $ECol $IzCol1 $IDColTransf
element elasticBeamColumn 2200 14 20 $ACol1 $ECol $IzCol1 $IDColTransf
element elasticBeamColumn 2300 24 21 $ACol1 $ECol $IzCol1 $IDColTransf
element elasticBeamColumn 2400 21 22 $ACol1 $ECol $IzCol1 $IDColTransf
element elasticBeamColumn 2500 22 23 $ACol1 $ECol $IzCol1 $IDColTransf
# ----- Beam Rigid Links Section
-----
# # rigidLink $type $masterNodeTag $slaveNodeTag
# #=====Pared 1
# rigidLink beam 8 21
# #=====Pared 2
# rigidLink beam 14 22
# #=====Pared 3
# rigidLink beam 20 23
#Right
#=====Pared 1
equalDOF 8 21 1 2
#=====Pared 2
equalDOF 14 22 1 2
#=====Pared 3
equalDOF 20 23 1 2
# ----- Frame elements
-----
# ----- Column element Section
-----
#===== Define elastic elements
element elasticBeamColumn 21 321 32 $ACol $ECol $IzCol1 $IDColTransf
element elasticBeamColumn 22 32 322 $ACol $ECol $IzCol1 $IDColTransf
element elasticBeamColumn 23 331 33 $ACol $ECol $IzCol1 $IDColTransf
element elasticBeamColumn 24 33 332 $ACol $ECol $IzCol1 $IDColTransf
element elasticBeamColumn 25 341 34 $ACol $ECol $IzCol1 $IDColTransf
element elasticBeamColumn 26 421 42 $ACol $ECol $IzCol1 $IDColTransf
element elasticBeamColumn 27 42 422 $ACol $ECol $IzCol1 $IDColTransf
element elasticBeamColumn 28 431 43 $ACol $ECol $IzCol1 $IDColTransf
element elasticBeamColumn 29 43 432 $ACol $ECol $IzCol1 $IDColTransf
element elasticBeamColumn 30 441 44 $ACol $ECol $IzCol1 $IDColTransf
#===== Define inelastic elements
#element beamWithHinges $eleTag $iNode $jNode $secTagI $Lpi $secTagJ
$Lpj $E $A $IzBeam
$transfTag
element beamWithHinges 100 31 321 $ColSecTag $LpC $ColSecTag $LpC $E
$ACol $IzCol $IDColTransf
element beamWithHinges 101 322 331 $ColSecTag $LpC $ColSecTag $LpC $E
$ACol $IzCol
$IDColTransf
element beamWithHinges 102 332 341 $ColSecTag $LpC $ColSecTag $LpC $E
$ACol $IzCol
$IDColTransf
element beamWithHinges 200 41 421 $ColSecTag $LpC $ColSecTag $LpC $E
$ACol $IzCol $IDColTransf
# element beamWithHinges 210 411 421 $ColSecTag $LpC $ColSecTag $LpC
$E $ACol $IzCol
$IDColTransf
element beamWithHinges 201 422 431 $ColSecTag $LpC $ColSecTag $LpC $E
$ACol $IzCol

$IDColTransf
element beamWithHinges 202 432 441 $ColSecTag $LpC $ColSecTag $LpC $E
$ACol $IzCol
$IDColTransf
# ----- Beam element Section
-----
#===== Define elastic elements
element elasticBeamColumn 37 32 61 $ABeam $EBeam $IzCol1 $IDColTransf

```

```

element elasticBeamColumn 32 33 71 $ABeam $EBeam $IzelastB
$IDColTransf
element elasticBeamColumn 33 34 81 $ABeam $EBeam $IzelastB
$IDColTransf
element elasticBeamColumn 34 62 42 $ABeam $EBeam $IzelastB
$IDColTransf
element elasticBeamColumn 35 72 43 $ABeam $EBeam $IzelastB
$IDColTransf
element elasticBeamColumn 36 82 44 $ABeam $EBeam $IzelastB
$IDColTransf
#==== Define inelastic elements
element beamWithHinges 300 61 62 $BeamSecTag1 $LpBeam $BeamSecTag1
$LpBeam $EBeam $ABeam
$IzBeam $IDBeamtranf
element beamWithHinges 301 71 72 $BeamSecTag2 $LpBeam $BeamSecTag2
$LpBeam $EBeam $ABeam
$IzBeam $IDBeamtranf
element beamWithHinges 302 81 82 $BeamSecTag3 $LpBeam $BeamSecTag3
$LpBeam $EBeam $ABeam
$IzBeam $IDBeamtranf
# #====Rigid Beams
# #====Pared 1
# equalDOF 21 32 1 2
# #====Pared 2
# equalDOF 22 33 1 2
# #====Pared 3
# equalDOF 23 34 1 2
# #====Frame constrain
# #====Pared 1
# equalDOF 32 42 1 2
# #====Pared 2
# equalDOF 33 43 1 2
# #====Pared 3
# equalDOF 34 44 1 2
# #====Auxiliar Node
# equalDOF 41 411 1 2
# equalDOF 411 421 1 2
# #====Ground
equalDOF 1 31 1
# #====Pared 1
equalDOF 8 32 1
# #====Pared 2
equalDOF 14 33 1
# #====Pared 3
equalDOF 20 34 1
# #====Ground
equalDOF 1 41 1
# #====Pared 1
equalDOF 8 42 1
# #====Pared 2
equalDOF 14 43 1
# #====Pared 3
equalDOF 20 44 1
puts "Model created"
# -----
# Recorder generation
# -----
# ----- Wall recorders
# -----
# -----
# Nodal recorders

recorder Node -file $dataDir/MVLEM_Dtop.out -time -node $IDctrlNodew -
dof 1 disp # Disp Top
recorder Node -file $dataDir/RBasewallllvl1.out -time -node 1 -dof 1 2 3
reaction; #

```

```

support reaction
recorder Node -file $dataDir/RBasewall11vl2.out -time -node 8 -dof 1 2 3
reaction; #
support reaction
recorder Node -file $dataDir/RBasewall11vl3.out -time -node 14 -dof 1 2
3 reaction; #
support reaction
# Panels recorders
# Concrete and steel stress-strain
#=====Level
1=====
recorder Element -file $dataDir/Lvel1_panel1_strain.out -time -ele 1
RCPanel 1 panel_strain
recorder Element -file $dataDir/Lvel1_panel2_strain.out -time -ele 1
RCPanel 2 panel_strain
recorder Element -file $dataDir/Lvel1_panel3_strain.out -time -ele 1
RCPanel 6 panel_strain
recorder Element -file $dataDir/Lvel1_panel4_strain.out -time -ele 1
RCPanel 7 panel_strain
recorder Element -file $dataDir/Lvel1_panel5_strain.out -time -ele 1
RCPanel 8 panel_strain
#=====Level
2=====
recorder Element -file $dataDir/Lvel2_panel1_strain.out -time -ele 8
RCPanel 1 panel_strain
recorder Element -file $dataDir/Lvel2_panel2_strain.out -time -ele 8
RCPanel 2 panel_strain
recorder Element -file $dataDir/Lvel2_panel3_strain.out -time -ele 8
RCPanel 6 panel_strain
recorder Element -file $dataDir/Lvel2_panel4_strain.out -time -ele 8
RCPanel 7 panel_strain
recorder Element -file $dataDir/Lvel2_panel5_strain.out -time -ele 8
RCPanel 8 panel_strain
#=====Level
3=====
recorder Element -file $dataDir/Lvel3_panel1_strain.out -time -ele 14
RCPanel 1 panel_strain
recorder Element -file $dataDir/Lvel3_panel2_strain.out -time -ele 14
RCPanel 2 panel_strain
recorder Element -file $dataDir/Lvel3_panel3_strain.out -time -ele 14
RCPanel 6 panel_strain
recorder Element -file $dataDir/Lvel3_panel4_strain.out -time -ele 14
RCPanel 7 panel_strain
recorder Element -file $dataDir/Lvel3_panel5_strain.out -time -ele 14
RCPanel 8 panel_strain
# Steel stress-strain
#=====Level
1=====
recorder Element -file $dataDir/Lvel1_panel1_stress_steel.out -time -
ele 1 RCPanel 1
panel_stress_steel
recorder Element -file $dataDir/Lvel1_panel2_stress_steel.out -time -
ele 1 RCPanel 2
panel_stress_steel
recorder Element -file $dataDir/Lvel1_panel3_stress_steel.out -time -
ele 1 RCPanel 6
panel_stress_steel
recorder Element -file $dataDir/Lvel1_panel4_stress_steel.out -time -
ele 1 RCPanel 7
panel_stress_steel
recorder Element -file $dataDir/Lvel1_panel5_stress_steel.out -time -
ele 1 RCPanel 8
panel_stress_steel
# Steel stress-strain X-direction
#=====Level
1=====

```

```

recorder Element -file $dataDir/Lvel1_panel1_strain_stress_steelX.out -
time -ele 1 RCPanel 1
strain_stress_steelX
recorder Element -file $dataDir/Lvel1_panel2_strain_stress_steelX.out -
time -ele 1 RCPanel 2
strain_stress_steelX
recorder Element -file $dataDir/Lvel1_panel3_strain_stress_steelX.out -
time -ele 1 RCPanel 6
strain_stress_steelX
recorder Element -file $dataDir/Lvel1_panel4_strain_stress_steelX.out -
time -ele 1 RCPanel 7
strain_stress_steelX
recorder Element -file $dataDir/Lvel1_panel5_strain_stress_steelX.out -
time -ele 1 RCPanel 8
strain_stress_steelX
# Steel stress-strain Y-direction
#=====Level
1=====
recorder Element -file $dataDir/Lvel1_panel1_strain_stress_steelY.out -
time -ele 1 RCPanel 1
strain_stress_steelY
recorder Element -file $dataDir/Lvel1_panel2_strain_stress_steelY.out -
time -ele 1 RCPanel 2
strain_stress_steelY
recorder Element -file $dataDir/Lvel1_panel3_strain_stress_steelY.out -
time -ele 1 RCPanel 6
strain_stress_steelY
recorder Element -file $dataDir/Lvel1_panel4_strain_stress_steelY.out -
time -ele 1 RCPanel 7
strain_stress_steelY
recorder Element -file $dataDir/Lvel1_panel5_strain_stress_steelY.out -
time -ele 1 RCPanel 8
strain_stress_steelY

# ----- Frame recorders
-----
#
-----
-----
# Element recorders
set startEleColm1 31; # Column 1 start
set endEleColm1 321; # Column 1 end
set startEleColm2 41; # Column 2 start
set endEleColm2 421; # Column 2 end
set startEleBe1 61; # Beam 1 start
set endEleBe1 62; # Beam 1 end
set startEleBe2 71; # Beam 2 start
set endEleBe2 72; # Beam 2 end
set startEleBe3 81; # Beam 3 start
set endEleBe3 82; # Beam 3 end
# Nodal recorders
recorder Node -file $dataDir/MVLEM_DtopF.out -time -node $IDctrlNodef -
dof 1 disp # Disp
Top
recorder Node -file $dataDir/RBasewall_$IDReactNode1.out -time -node
$IDReactNode1 -dof 1 2
3 reaction; # support reaction
recorder Node -file $dataDir/RBasewall_$IDReactNode2.out -time -node
$IDReactNode2 -dof 1 2
3 reaction; # support reaction
# Element recorders
#
=====Moments=====
=====
=====

```

```

recorder Element -file $dataDir/Element_100_st.out -time -eleRange
$startEleColm1
$endEleColm1 -ele 100 globalForce; # Column 1
recorder Element -file $dataDir/Element_200_st.out -time -eleRange
$startEleColm2
$endEleColm2 -ele 200 globalForce; # Column 2
recorder Element -file $dataDir/Element_300_st.out -time -eleRange
$startEleBe1 $endEleBe1
-ele 300 globalForce; # Beam 1
recorder Element -file $dataDir/Element_300_all.out -time -ele 300
globalForce;
recorder Element -file $dataDir/Element_301_st.out -time -eleRange
$startEleBe2 $endEleBe2
-ele 301 globalForce; # Beam 2
recorder Element -file $dataDir/Element_302_st.out -time -eleRange
$startEleBe3 $endEleBe3
-ele 302 globalForce; # Beam 3
#
=====Deformations=====
=====
=====
recorder Element -file $dataDir/PH_BeamDeformation2R.out -time -ele 300
301 302 deformation;
recorder Element -file $dataDir/ele1sec1Defo.out -time -ele 100 section
1 deformation
recorder Element -file $dataDir/PH_ColDeformation2R.out -time -ele 100
200 deformation;
#
=====deformation=====
=====
# =====Column
1=====
recorder Element -file $dataDir/ele100sec1deformation.out -time -ele
100 -section 1
deformation
recorder Element -file $dataDir/ele100sec6deformation.out -time -ele
100 -section 6
deformation
# =====Column
2=====

recorder Element -file $dataDir/ele200sec1deformation.out -time -ele
200 -section 1
deformation
recorder Element -file $dataDir/ele200sec6deformation.out -time -ele
200 -section 6
deformation
# =====Beam
1=====
recorder Element -file $dataDir/ele300sec1deformation.out -time -ele
300 -section 1
deformation
recorder Element -file $dataDir/ele300sec6deformation.out -time -ele
300 -section 6
deformation
# =====Beam
2=====
recorder Element -file $dataDir/ele301sec1deformation.out -time -ele
301 -section 1
deformation
recorder Element -file $dataDir/ele301sec6deformation.out -time -ele
301 -section 6
deformation
# =====Beam
3=====

```

```

recorder Element -file $dataDir/ele302sec1deformation.out -time -ele
302 -section 1
deformation
recorder Element -file $dataDir/ele302sec6deformation.out -time -ele
302 -section 6
deformation
#
=====StressStrain=====
=====
# =====Coordinates=====
# =====Column section=====
set y1c 7.5625;
set z1c -7.5625;
set y2c -7.5625;
set z2c -7.5625;
set y3c -7.5625;
set z3c 7.5625;
set y4c 7.5625;
set z4c 7.5625;
set y1ch 10;
set z1ch -10;
set y2ch -10;
set z2ch -10;
set y3ch -10;
set z3ch 10;
set y4ch 10;
set z4ch 10;
set y1 0;
set z1 0;
set y1h 0;
set z1h 0;
# =====Beam section=====
set y1b 9.6875;
set z1b -7.625;
set y2b -9.6875;
set z2b -7.625;
set y3b -9.6875;
set z3b 7.625;
set y4b 9.6875;
set z4b 7.625;
set y1bh 12;
set z1bh -10;
set y2bh -12;
set z2bh -10;
set y3bh -12;
set z3bh 10;
set y4bh 12;
set z4bh 10;

# =====Column
1=====
recorder Element -file $dataDir/ele100sec1stressStrainp1s.out -time -
ele 100 section 1 fiber
$y1c $z1c $IDSteelc stressStrain
recorder Element -file $dataDir/ele100sec1stressStrainp2s.out -time -
ele 100 section 1 fiber
$y2c $z2c $IDSteelc stressStrain
recorder Element -file $dataDir/ele100sec1stressStrainp3s.out -time -
ele 100 section 1 fiber
$y3c $z3c $IDSteelc stressStrain
recorder Element -file $dataDir/ele100sec1stressStrainp4s.out -time -
ele 100 section 1 fiber

```



```

$y4c $z4c $IDSteelc stressStrain
recorder Element -file $dataDir/ele100sec1stressStrainpss.out -time -
ele 100 section 1 fiber
$y1 $z1 $IDSteelc stressStrain
recorder Element -file $dataDir/ele100sec1stressStrainp1.out -time -ele
100 section 1 fiber
$y1ch $z1ch $IDconcCorec stressStrain
recorder Element -file $dataDir/ele100sec1stressStrainp2.out -time -ele
100 section 1 fiber
$y2ch $z2ch $IDconcCorec stressStrain
recorder Element -file $dataDir/ele100sec1stressStrainp3.out -time -ele
100 section 1 fiber
$y3ch $z3ch $IDconcCorec stressStrain
recorder Element -file $dataDir/ele100sec1stressStrainp4.out -time -ele
100 section 1 fiber
$y4ch $z4ch $IDconcCorec stressStrain
recorder Element -file $dataDir/ele100sec1stressStrainps.out -time -ele
100 section 1 fiber
$y1h $z1h $IDconcCorec stressStrain
# ======Column
2=====
recorder Element -file $dataDir/ele200sec1stressStrainp1s.out -time -
ele 200 section 1 fiber
$y1c $z1c $IDSteelc stressStrain
recorder Element -file $dataDir/ele200sec1stressStrainp2s.out -time -
ele 200 section 1 fiber
$y2c $z2c $IDSteelc stressStrain
recorder Element -file $dataDir/ele200sec1stressStrainp3s.out -time -
ele 200 section 1 fiber
$y3c $z3c $IDSteelc stressStrain
recorder Element -file $dataDir/ele200sec1stressStrainp4s.out -time -
ele 200 section 1 fiber
$y4c $z4c $IDSteelc stressStrain
recorder Element -file $dataDir/ele200sec1stressStrainpss.out -time -
ele 200 section 1 fiber
$y1 $z1 $IDSteelc stressStrain
recorder Element -file $dataDir/ele200sec1stressStrainp1.out -time -ele
200 section 1 fiber
$y1ch $z1ch $IDconcCorec stressStrain
recorder Element -file $dataDir/ele200sec1stressStrainp2.out -time -ele
200 section 1 fiber
$y2ch $z2ch $IDconcCorec stressStrain
recorder Element -file $dataDir/ele200sec1stressStrainp3.out -time -ele
200 section 1 fiber
$y3ch $z3ch $IDconcCorec stressStrain
recorder Element -file $dataDir/ele200sec1stressStrainp4.out -time -ele
200 section 1 fiber
$y4ch $z4ch $IDconcCorec stressStrain
recorder Element -file $dataDir/ele200sec1stressStrainps.out -time -ele
200 section 1 fiber
$y1h $z1h $IDconcCorec stressStrain
# ======Beam
1=====
recorder Element -file $dataDir/ele300sec1stressStrainp1s.out -time -
ele 300 section 1 fiber
$y1b $z1b $IDSteelc stressStrain
recorder Element -file $dataDir/ele300sec1stressStrainp2s.out -time -
ele 300 section 1 fiber
$y2b $z2b $IDSteelc stressStrain
recorder Element -file $dataDir/ele300sec1stressStrainp3s.out -time -
ele 300 section 1 fiber
$y3b $z3b $IDSteelc stressStrain
recorder Element -file $dataDir/ele300sec1stressStrainp4s.out -time -
ele 300 section 1 fiber
$y4b $z4b $IDSteelc stressStrain

```

```

recorder Element -file $dataDir/ele300sec1stressStrainpss.out -time -
ele 300 section 1 fiber
$y1 $z1 $IDSteelc stressStrain
recorder Element -file $dataDir/ele300sec1stressStrainp1.out -time -ele
300 section 1 fiber
$y1bh $z1bh $IDconcCore stressStrain
recorder Element -file $dataDir/ele300sec1stressStrainp2.out -time -ele
300 section 1 fiber
$y2bh $z2bh $IDconcCore stressStrain
recorder Element -file $dataDir/ele300sec1stressStrainp3.out -time -ele
300 section 1 fiber
$y3bh $z3bh $IDconcCore stressStrain
recorder Element -file $dataDir/ele300sec1stressStrainp4.out -time -ele
300 section 1 fiber
$y4bh $z4bh $IDconcCore stressStrain
recorder Element -file $dataDir/ele300sec1stressStrainps.out -time -ele
300 section 1 fiber
$y1h $z1h $IDconcCore stressStrain
recorder Element -file $dataDir/ele300sec6stressStrainp1s.out -time -
ele 300 section 6 fiber
$y1b $z1b $IDSteelc stressStrain
recorder Element -file $dataDir/ele300sec6stressStrainp2s.out -time -
ele 300 section 6 fiber
$y2b $z2b $IDSteelc stressStrain
recorder Element -file $dataDir/ele300sec6stressStrainp3s.out -time -
ele 300 section 6 fiber
$y3b $z3b $IDSteelc stressStrain
recorder Element -file $dataDir/ele300sec6stressStrainp4s.out -time -
ele 300 section 6 fiber
$y4b $z4b $IDSteelc stressStrain
recorder Element -file $dataDir/ele300sec6stressStrainpss.out -time -
ele 300 section 6 fiber
$y1 $z1 $IDSteelc stressStrain
recorder Element -file $dataDir/ele300sec6stressStrainp1.out -time -ele
300 section 6 fiber
$y1bh $z1bh $IDconcCore stressStrain
recorder Element -file $dataDir/ele300sec6stressStrainp2.out -time -ele
300 section 6 fiber
$y2bh $z2bh $IDconcCore stressStrain
recorder Element -file $dataDir/ele300sec6stressStrainp3.out -time -ele
300 section 6 fiber
$y3bh $z3bh $IDconcCore stressStrain
recorder Element -file $dataDir/ele300sec6stressStrainp4.out -time -ele
300 section 6 fiber
$y4bh $z4bh $IDconcCore stressStrain
recorder Element -file $dataDir/ele300sec6stressStrainps.out -time -ele
300 section 6 fiber
$y1h $z1h $IDconcCore stressStrain
# =====Beam
2=====
recorder Element -file $dataDir/ele301sec1stressStrainp1s.out -time -
ele 301 section 1 fiber
$y1b $z1b $IDSteelc stressStrain
recorder Element -file $dataDir/ele301sec1stressStrainp2s.out -time -
ele 301 section 1 fiber
$y2b $z2b $IDSteelc stressStrain
recorder Element -file $dataDir/ele301sec1stressStrainp3s.out -time -
ele 301 section 1 fiber
$y3b $z3b $IDSteelc stressStrain
recorder Element -file $dataDir/ele301sec1stressStrainp4s.out -time -
ele 301 section 1 fiber
$y4b $z4b $IDSteelc stressStrain
recorder Element -file $dataDir/ele301sec1stressStrainpss.out -time -
ele 301 section 1 fiber
$y1 $z1 $IDSteelc stressStrain

```

```

recorder Element -file $dataDir/ele301sec1stressStrainp1.out -time -ele
301 section 1 fiber
$y1bh $z1bh $IDconcCore stressStrain
recorder Element -file $dataDir/ele301sec1stressStrainp2.out -time -ele
301 section 1 fiber
$y2bh $z2bh $IDconcCore stressStrain
recorder Element -file $dataDir/ele301sec1stressStrainp3.out -time -ele
301 section 1 fiber
$y3bh $z3bh $IDconcCore stressStrain
recorder Element -file $dataDir/ele301sec1stressStrainp4.out -time -ele
301 section 1 fiber
$y4bh $z4bh $IDconcCore stressStrain
recorder Element -file $dataDir/ele301sec1stressStrainps.out -time -ele
301 section 1 fiber
$y1h $z1h $IDconcCore stressStrain
recorder Element -file $dataDir/ele301sec6stressStrainp1s.out -time -
ele 301 section 6 fiber
$y1b $z1b $IDSteelc stressStrain
recorder Element -file $dataDir/ele301sec6stressStrainp2s.out -time -
ele 301 section 6 fiber
$y2b $z2b $IDSteelc stressStrain
recorder Element -file $dataDir/ele301sec6stressStrainp3s.out -time -
ele 301 section 6 fiber
$y3b $z3b $IDSteelc stressStrain
recorder Element -file $dataDir/ele301sec6stressStrainp4s.out -time -
ele 301 section 6 fiber
$y4b $z4b $IDSteelc stressStrain
recorder Element -file $dataDir/ele301sec6stressStrainpss.out -time -
ele 301 section 6 fiber
$y1 $z1 $IDSteelc stressStrain
recorder Element -file $dataDir/ele301sec6stressStrainp1.out -time -ele
301 section 6 fiber
$y1bh $z1bh $IDconcCore stressStrain
recorder Element -file $dataDir/ele301sec6stressStrainp2.out -time -ele
301 section 6 fiber
$y2bh $z2bh $IDconcCore stressStrain
recorder Element -file $dataDir/ele301sec6stressStrainp3.out -time -ele
301 section 6 fiber
$y3bh $z3bh $IDconcCore stressStrain
recorder Element -file $dataDir/ele301sec6stressStrainp4.out -time -ele
301 section 6 fiber
$y4bh $z4bh $IDconcCore stressStrain
recorder Element -file $dataDir/ele301sec6stressStrainps.out -time -ele
301 section 6 fiber
$y1h $z1h $IDconcCore stressStrain

# =====Beam
3=====
recorder Element -file $dataDir/ele302sec1stressStrainp1s.out -time -
ele 302 section 1 fiber
$y1b $z1b $IDSteelc stressStrain
recorder Element -file $dataDir/ele302sec1stressStrainp2s.out -time -
ele 302 section 1 fiber
$y2b $z2b $IDSteelc stressStrain
recorder Element -file $dataDir/ele302sec1stressStrainp3s.out -time -
ele 302 section 1 fiber
$y3b $z3b $IDSteelc stressStrain
recorder Element -file $dataDir/ele302sec1stressStrainp4s.out -time -
ele 302 section 1 fiber
$y4b $z4b $IDSteelc stressStrain
recorder Element -file $dataDir/ele302sec1stressStrainpss.out -time -
ele 302 section 1 fiber
$y1 $z1 $IDSteelc stressStrain
recorder Element -file $dataDir/ele302sec1stressStrainp1.out -time -ele
302 section 1 fiber
$y1bh $z1bh $IDconcCore stressStrain

```

```

recorder Element -file $dataDir/ele302sec1stressStrainp2.out -time -ele
302 section 1 fiber
$y2bh $z2bh $IDconcCore stressStrain
recorder Element -file $dataDir/ele302sec1stressStrainp3.out -time -ele
302 section 1 fiber
$y3bh $z3bh $IDconcCore stressStrain
recorder Element -file $dataDir/ele302sec1stressStrainp4.out -time -ele
302 section 1 fiber
$y4bh $z4bh $IDconcCore stressStrain
recorder Element -file $dataDir/ele302sec1stressStrainps.out -time -ele
302 section 1 fiber
$y1h $z1h $IDconcCore stressStrain
recorder Element -file $dataDir/ele302sec6stressStrainp1s.out -time -
ele 302 section 6 fiber
$y1b $z1b $IDSteelc stressStrain
recorder Element -file $dataDir/ele302sec6stressStrainp2s.out -time -
ele 302 section 6 fiber
$y2b $z2b $IDSteelc stressStrain
recorder Element -file $dataDir/ele302sec6stressStrainp3s.out -time -
ele 302 section 6 fiber
$y3b $z3b $IDSteelc stressStrain
recorder Element -file $dataDir/ele302sec6stressStrainp4s.out -time -
ele 302 section 6 fiber
$y4b $z4b $IDSteelc stressStrain
recorder Element -file $dataDir/ele302sec6stressStrainpss.out -time -
ele 302 section 6 fiber
$y1 $z1 $IDSteelc stressStrain
recorder Element -file $dataDir/ele302sec6stressStrainp1.out -time -ele
302 section 6 fiber
$y1bh $z1bh $IDconcCore stressStrain
recorder Element -file $dataDir/ele302sec6stressStrainp2.out -time -ele
302 section 6 fiber
$y2bh $z2bh $IDconcCore stressStrain
recorder Element -file $dataDir/ele302sec6stressStrainp3.out -time -ele
302 section 6 fiber
$y3bh $z3bh $IDconcCore stressStrain
recorder Element -file $dataDir/ele302sec6stressStrainp4.out -time -ele
302 section 6 fiber
$y4bh $z4bh $IDconcCore stressStrain
recorder Element -file $dataDir/ele302sec6stressStrainps.out -time -ele
302 section 6 fiber
$y1h $z1h $IDconcCore stressStrain
# -----
# Define Axial Load
# -----
set N [expr 0];
# -----
# Set parameters for displacement controlled analysis
# -----
# vector of displacement-cycle peaks in terms of wall drift ratio
#set iDmax "0.001 0.0025 0.005 0.0075 0.01 0.015 0.02 0.03 0.05 0.08
0.10";
#set Dincr 0.005; # displacement increment for displacement controlled
analysis.
#set CycleType Push; # type of cyclic analysis: Full / Push / Half
#set Ncycles 1; # specify the number of cycles at each peak
#set Dmax 0.10;
set Tol 1.0e-2;
set iPushNode "20";
set LunitTXT "in";
# print element;
# characteristics of pushover analysis
set Dmax [expr 0.1*$H]; # maximum displacement of pushover. push to 10%
drift.

set Dincr [expr 0.001*$H]; # displacement increment. you want this to be
small, but not too

```

```
small to slow analysis  
set numModes 3;  
puts "Model Complete"
```

Appendix 2

In this appendix will be presented the pushover results for all the moment magnitudes for both conditions, with and without considering the aging effects.

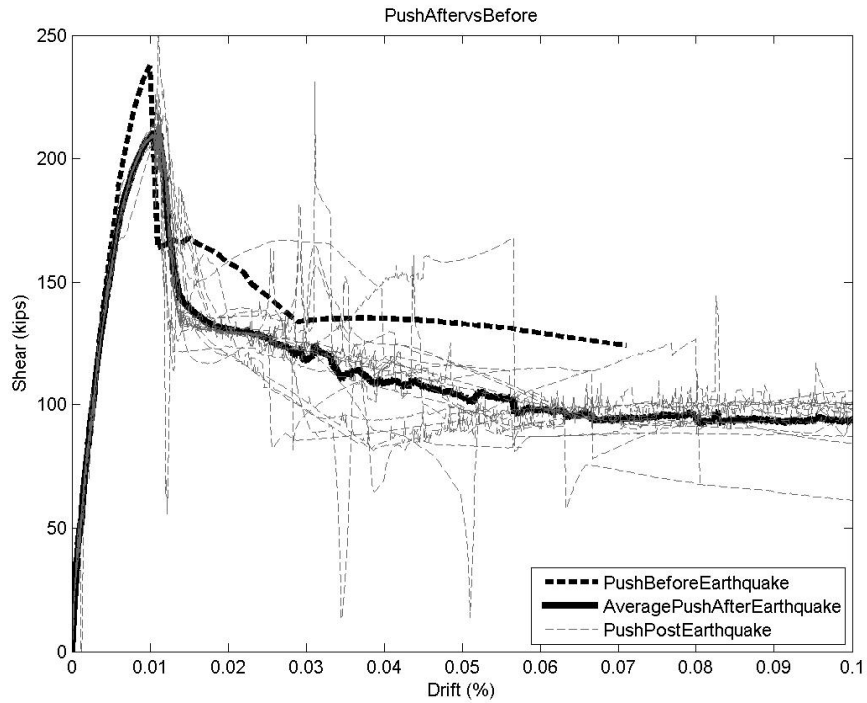


Figure A2.1 Pushover results for moment magnitude 5 without aging effects consideration

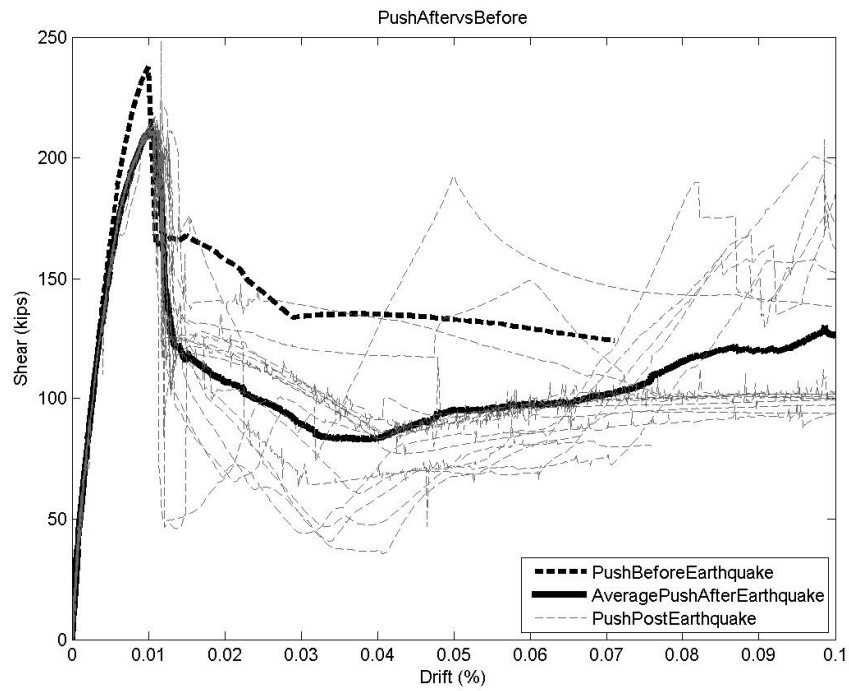


Figure A2.2 Pushover results for moment magnitude 5.5 without aging effects consideration

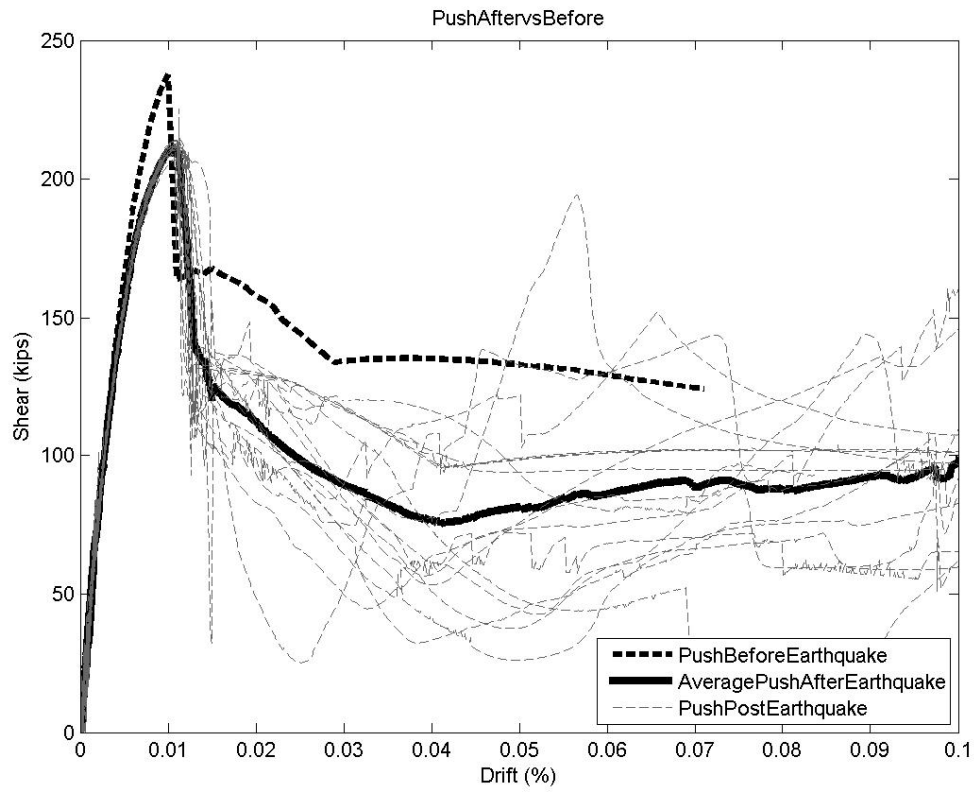


Figure A2.3 Pushover results for moment magnitude 6 without aging effects consideration

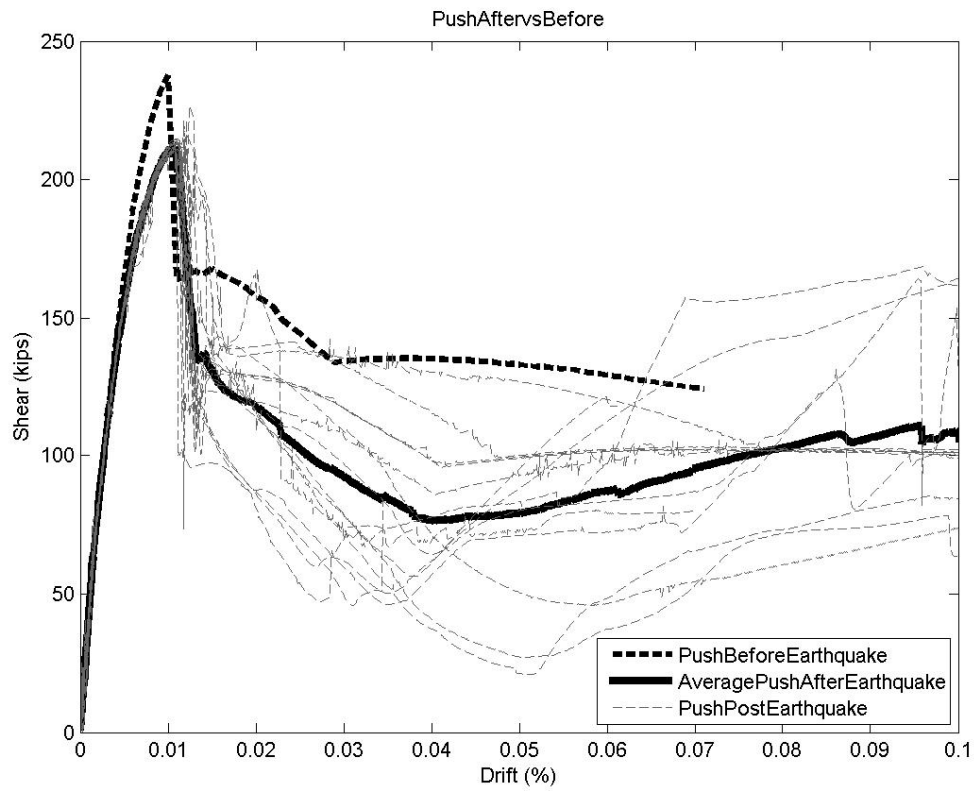


Figure A2.4 Pushover results for moment magnitude 6.5 without aging effects consideration

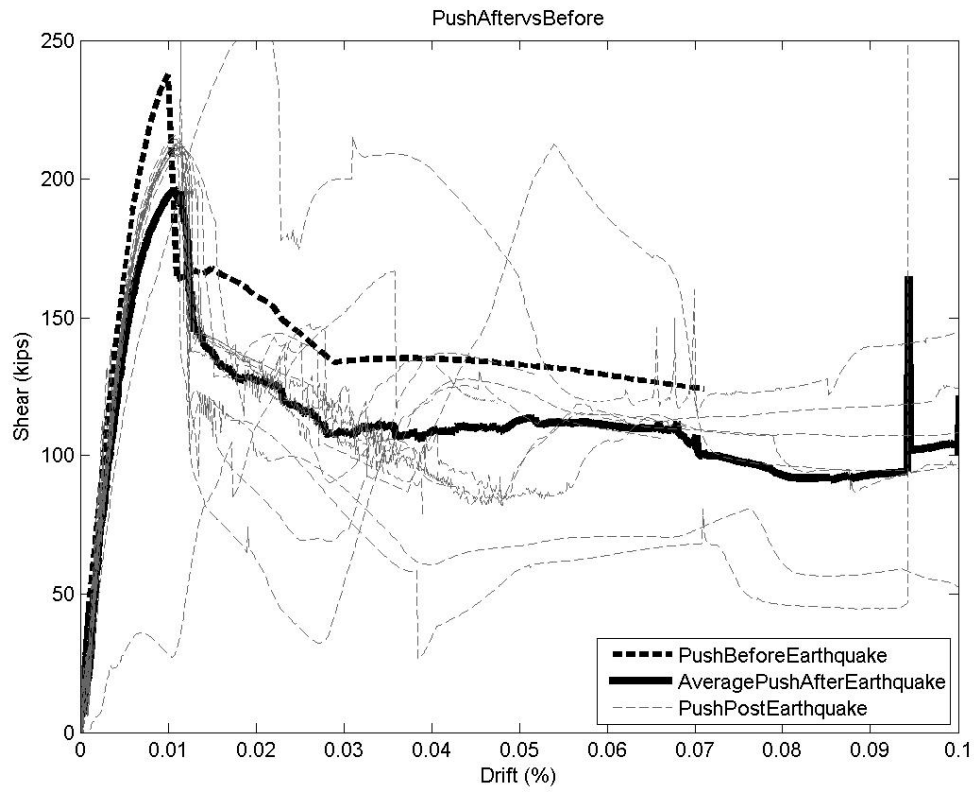


Figure A2.5 Pushover results for moment magnitude 7 without aging effects consideration

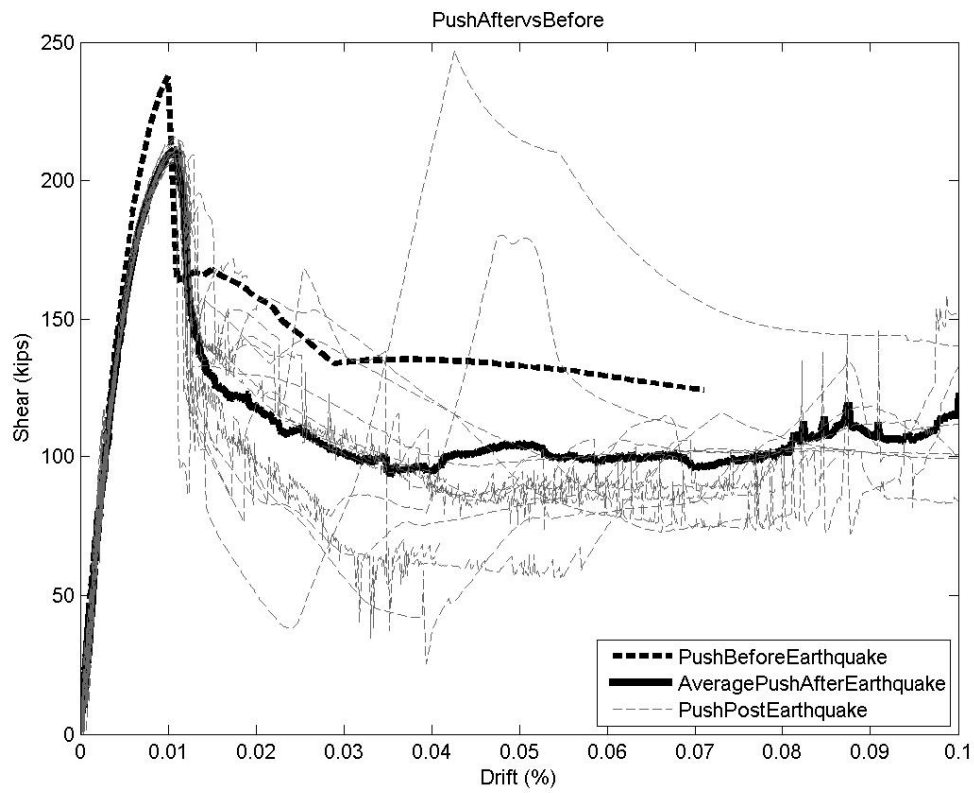


Figure A2.6 Pushover results for moment magnitude 7.5 without aging effects consideration

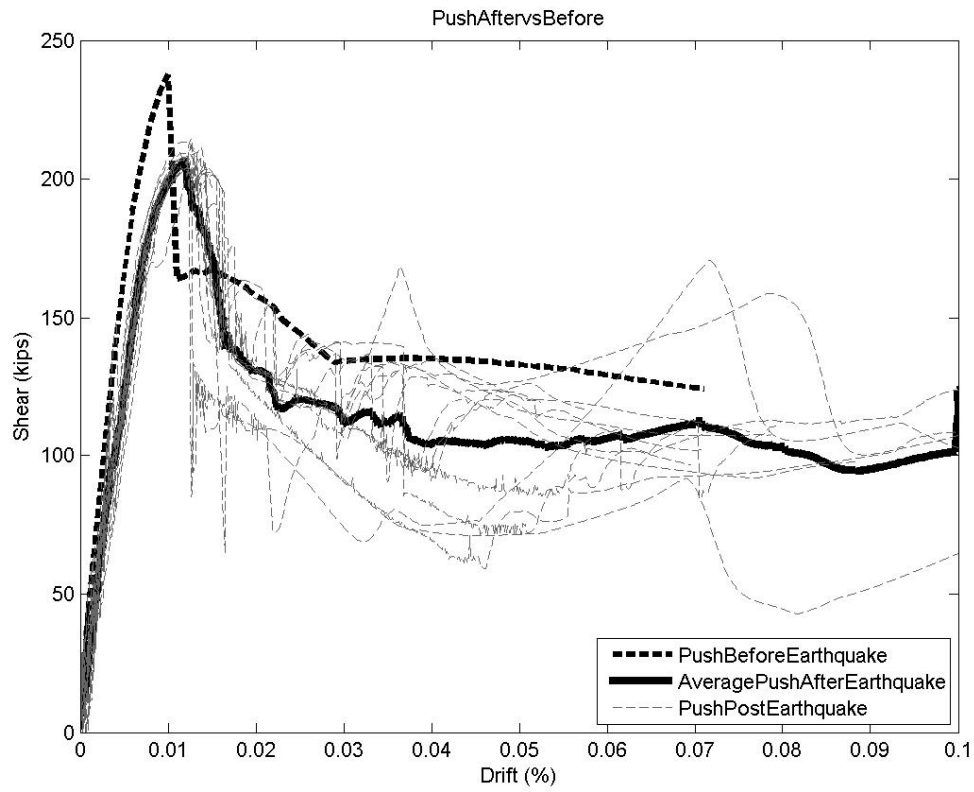


Figure A2.7 Pushover results for moment magnitude 8 without aging effects consideration 1

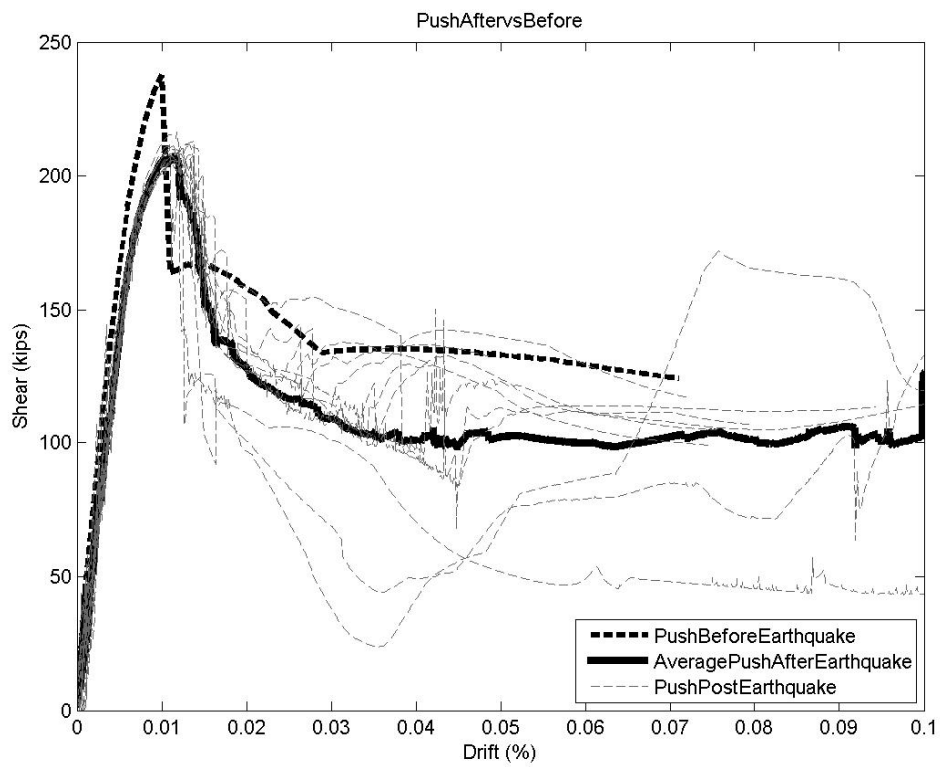


Figure A2.8 Pushover results for moment magnitude 8.5 without aging effects consideration

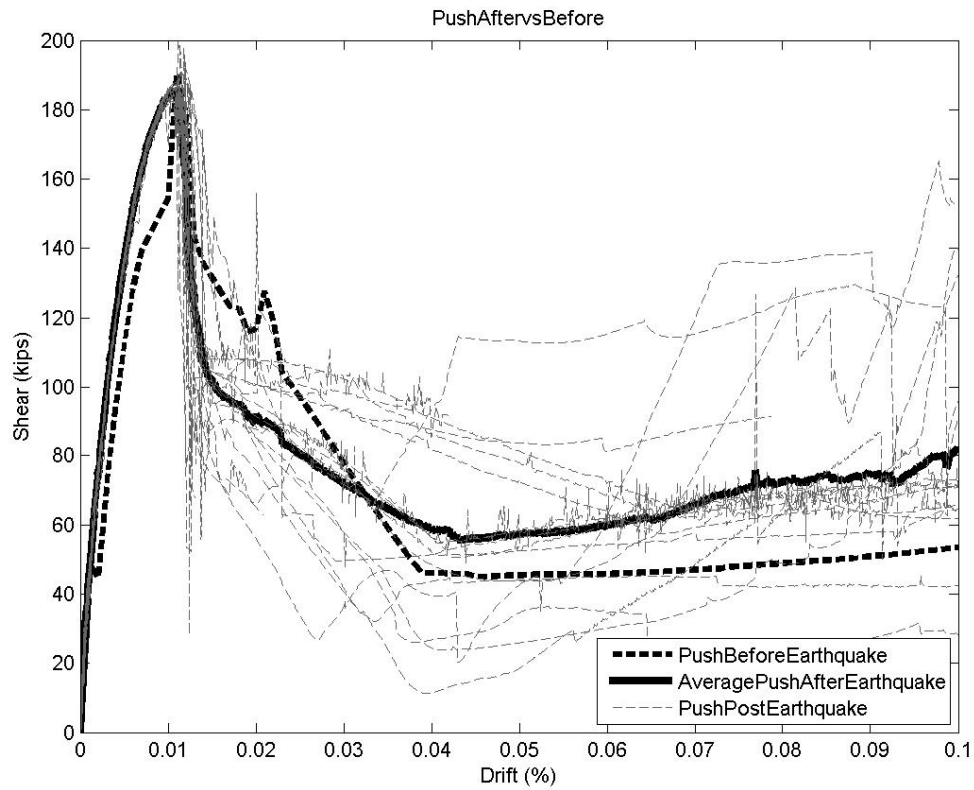


Figure A2.9 Pushover results for moment magnitude 5 with aging effects consideration

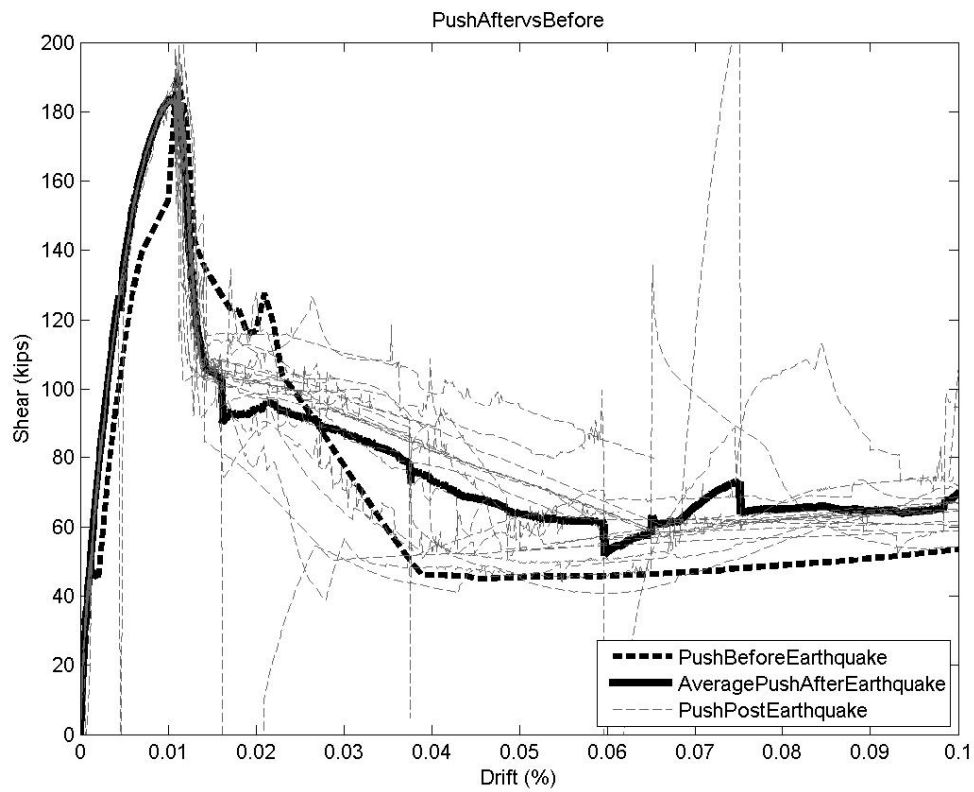


Figure A2.10 Pushover results for moment magnitude 5.5 with aging effects consideration

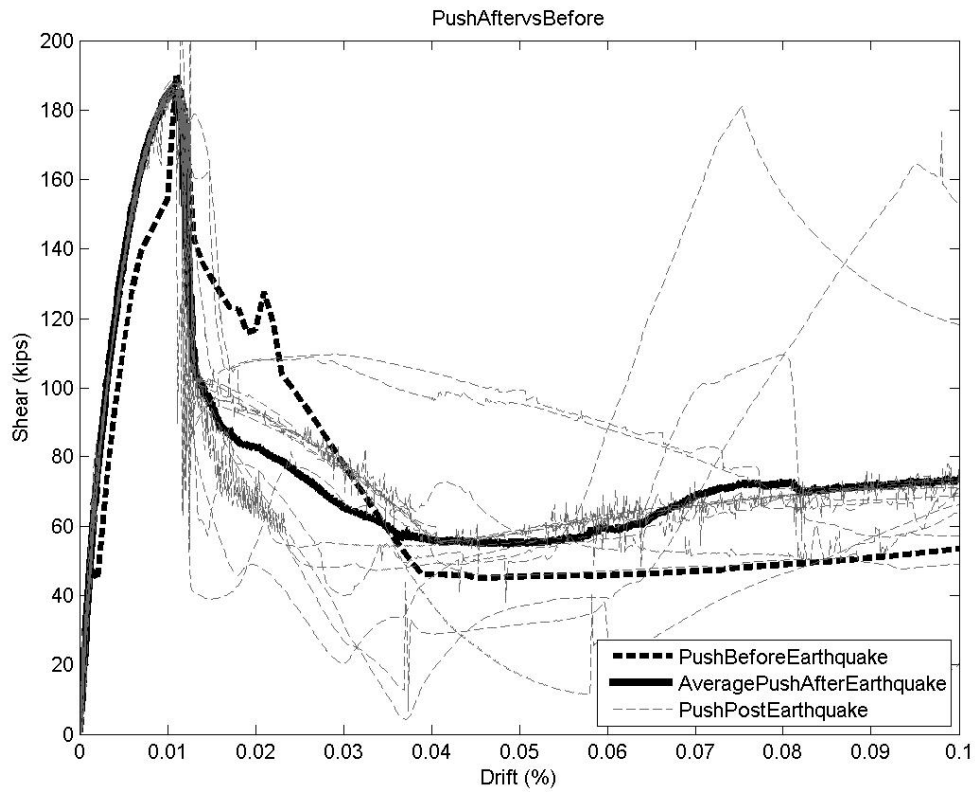


Figure A2.11 Pushover results for moment magnitude 6 with aging effects consideration

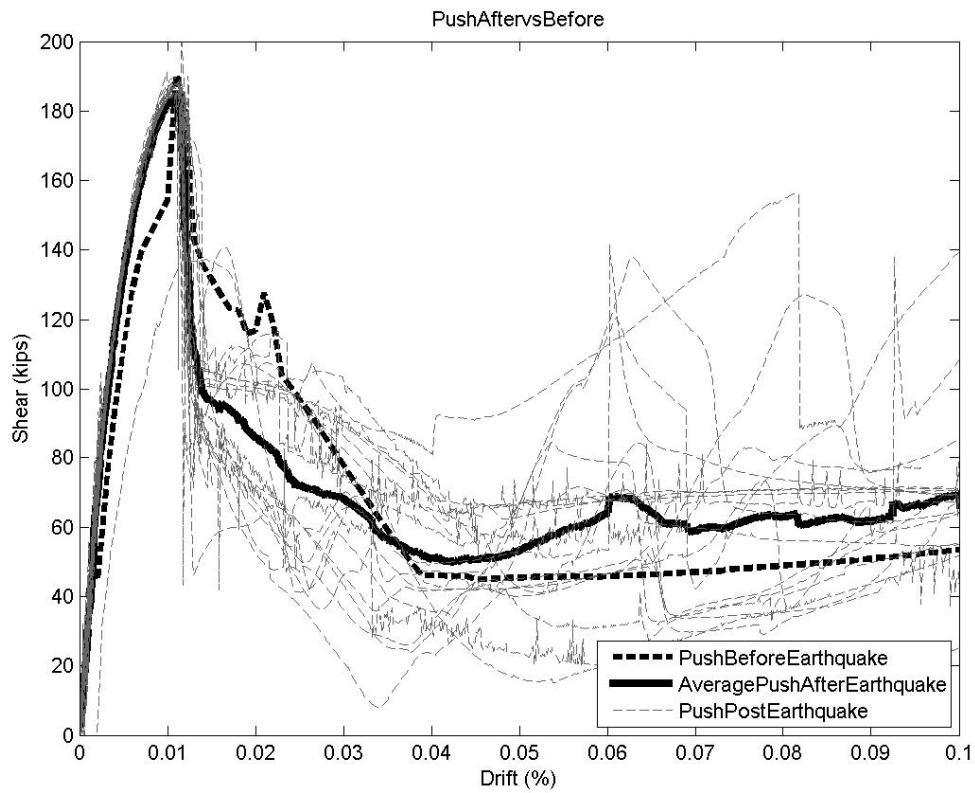


Figure A2.12 Pushover results for moment magnitude 6.5 with aging effects consideration

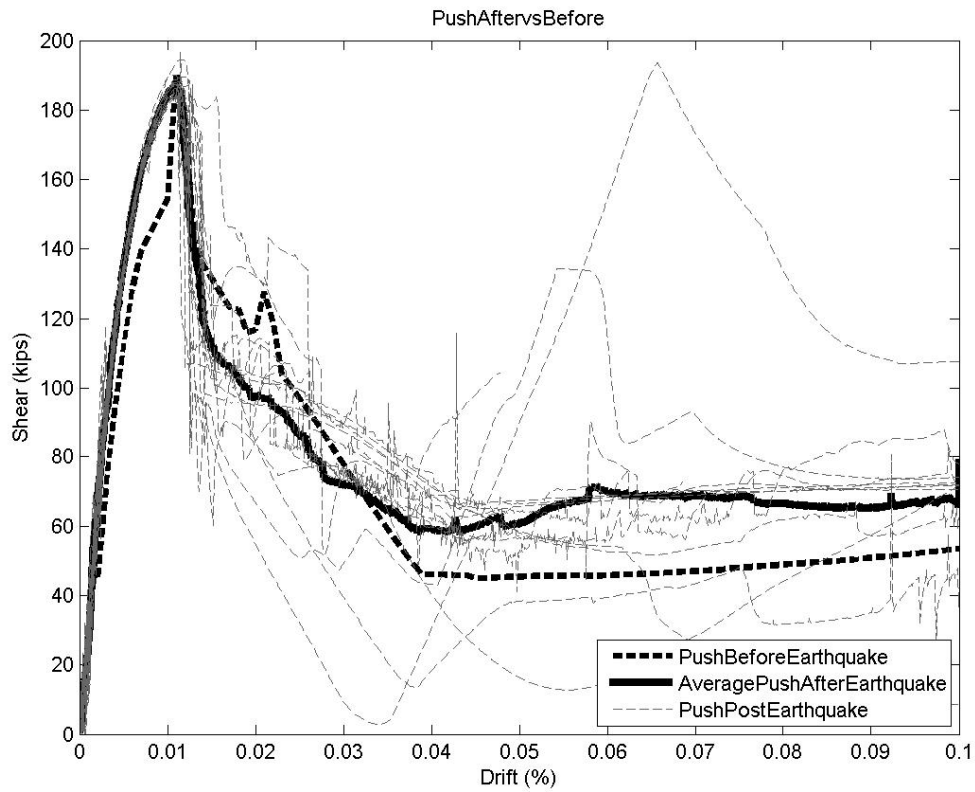


Figure A2.13 Pushover results for moment magnitude 7 with aging effects consideration

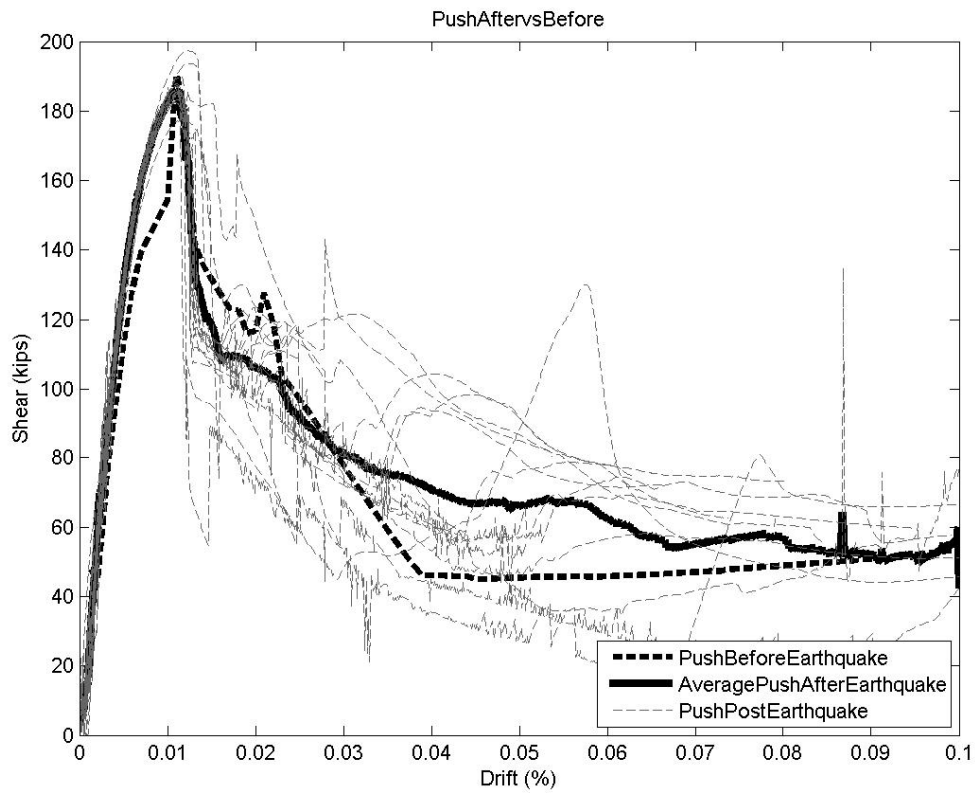


Figure A2.14 Pushover results for moment magnitude 7.5 with aging effects consideration

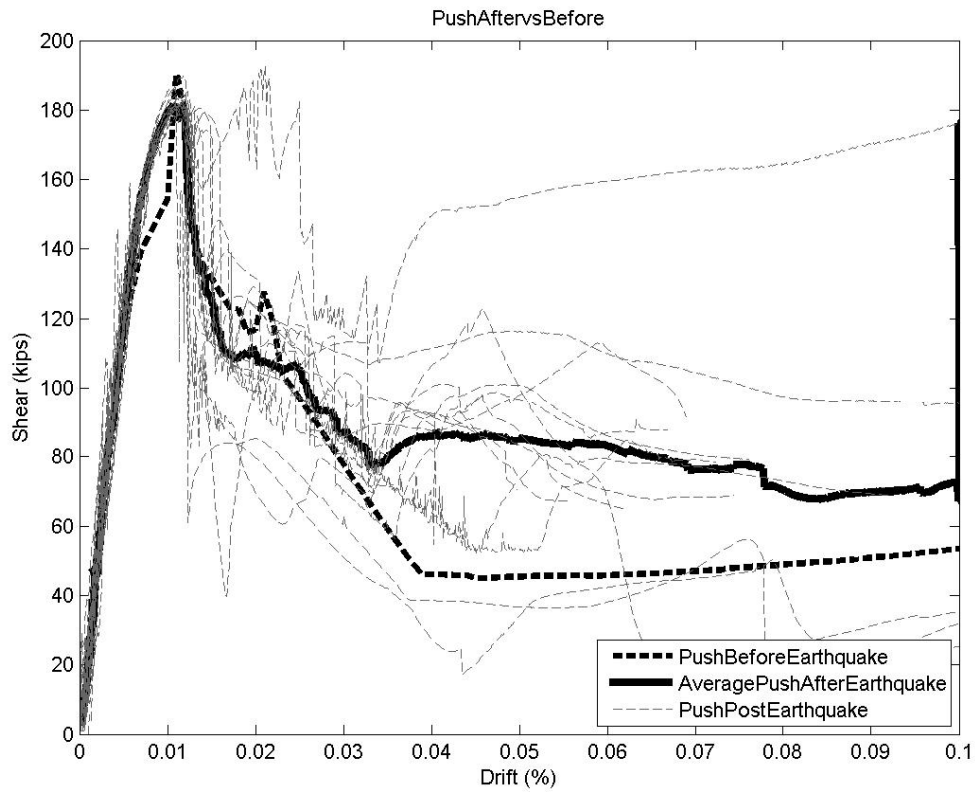


Figure A2.15 Pushover results for moment magnitude 8 with aging effects consideration

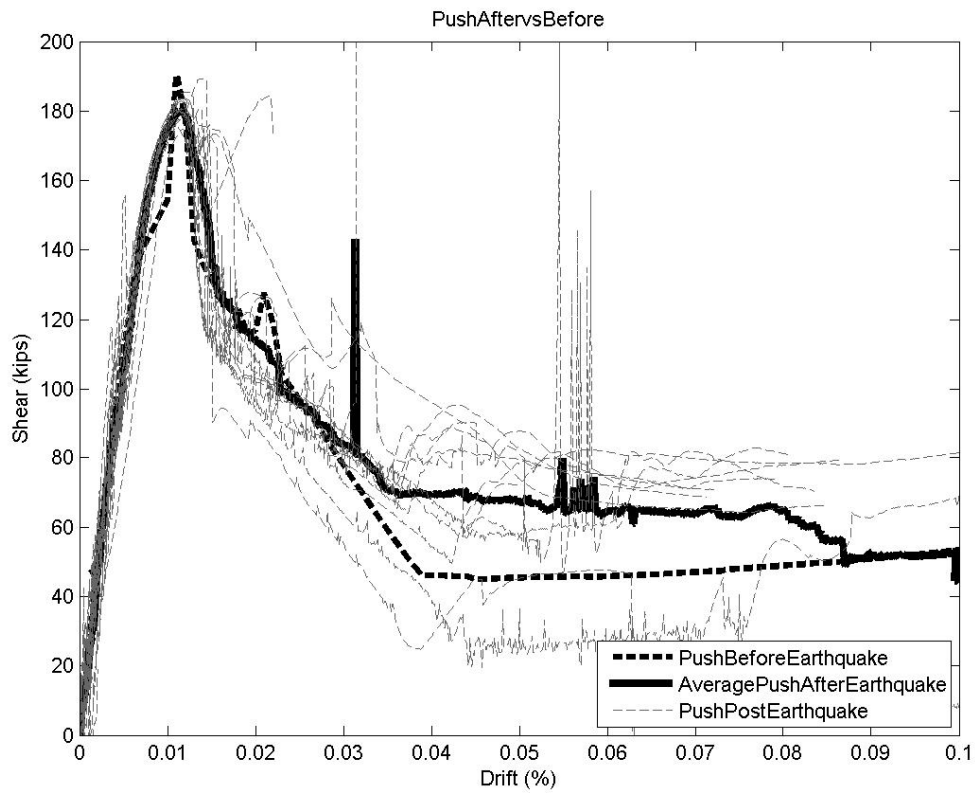


Figure A2.16 Pushover results for moment magnitude 8.5 with aging effects consideration